

**BIOMIMETIC DELIVERY OF REGULATORY T CELL INDUCING FACTORS
TO SUPPRESS CUTANEOUS INFLAMMATION**

by

Stephen Christopher Balmert

B.S. in Bioengineering, University of Pittsburgh, 2010

Submitted to the Graduate Faculty of
Swanson School of Engineering in partial fulfillment
of the requirements for the degree of
Doctor of Philosophy in Bioengineering

University of Pittsburgh

2017

UNIVERSITY OF PITTSBURGH
SWANSON SCHOOL OF ENGINEERING

This dissertation was presented

by

Stephen Christopher Balmert

It was defended on

November 21, 2017

and approved by

Louis D. Falco, Jr., M.D., Ph.D., Professor and Chair,
Departments of Dermatology and Bioengineering

Adrian E. Morelli, M.D., Ph.D., Associate Professor,
Departments of Surgery and Immunology

Yadong Wang, Ph.D., Professor,
Department of Bioengineering

Dissertation Director: Steven R. Little, Ph.D., Professor and Chair,
Departments of Chemical Engineering, Bioengineering, Pharmaceutical Sciences,
Immunology, and Ophthalmology

Copyright © by Stephen Christopher Balmert

2017

BIOMIMETIC DELIVERY OF REGULATORY T CELL INDUCING FACTORS TO SUPPRESS CUTANEOUS INFLAMMATION

Stephen Christopher Balmert, Ph.D.

University of Pittsburgh, 2017

Allergic contact dermatitis (ACD) is a common T-cell-mediated inflammation resulting from repeated contact with allergens (e.g. nickel or poison ivy). Current treatments typically involve topical corticosteroids, which non-specifically and transiently suppress inflammation, but fail to address the underlying allergen-specific immune dysfunction. Here, we present two novel approaches that teach the immune system to tolerate contact allergens by inducing suppressive regulatory T cells (Tregs). Specifically, we leveraged biomimetic delivery systems to modulate the skin draining lymph node (DLN) microenvironment with microparticles (MPs) that release **TR**eg-Inducing (TRI) factors, or the skin microenvironment with microneedle arrays (MNAs) that deliver vitamin D3 analog (MC903) to cultivate Treg-inducing tolerogenic dendritic cells (DCs).

We previously demonstrated that TGF- β 1, rapamycin, and IL-2 (TRI) promote Treg differentiation *in vitro*; however, original TGF- β 1 MPs exhibited an unexpected two-week delay in release, inconsistent with existing models of controlled release. Suspecting electrostatic interactions between cationic TGF- β 1 and negatively charged PLGA MPs were responsible, we characterized the influence of charge on release from PLGA MPs. Release assays revealed inverse correlations between positive charge on encapsulated agents and release rates, and effects of polymer charge density. These results helped us to rationally reformulate TRI MPs using less charged PEG-PLGA to achieve faster release.

In acute murine models of ACD, new TRI MP formulations were injected near sites of allergen exposure to condition the skin DLN. By expanding allergen-specific Tregs and reducing pro-inflammatory effector T cells (Teff), TRI MPs inhibited hypersensitivity responses to subsequent allergen exposure in an allergen-specific manner, effectively preventing or reversing ongoing ACD. Much like TRI MP therapy, intradermal delivery of allergen and MC903 with MNAs also prevented sensitization and inhibited subsequent hypersensitivity responses in naïve and allergic mice by expanding Tregs and reducing Teff. Notably, treatment of human skin explants with MC903 MNA promoted tolerogenic cutaneous microenvironments and caused preferential migration of more tolerogenic DCs, previously shown to support Treg-induction. Collectively, these results suggest that simultaneous introduction of antigen and modulation of local skin or skin DLN with MC903 MNA or TRI MP can induce antigen-specific tolerance, with broad therapeutic applications for other inflammatory disorders, autoimmune diseases, or transplant rejection.

TABLE OF CONTENTS

ACKNOWLEDGMENTS	XVII
COMMON ABBREVIATIONS	XIX
1.0 INTRODUCTION.....	1
1.1 ALLERGIC CONTACT DERMATITIS	1
1.1.1 Clinical Presentation, Prevalence, and Costs	1
1.1.2 Current Treatments and Limitations.....	2
1.2 NATURAL REGULATORS OF INFLAMMATION: TREGS	3
1.2.1 Mechanisms of Treg-Mediated Suppression	4
1.2.2 T-cell Differentiation Requires Integration of Signals from Antigen- Presenting Cells.....	5
1.2.3 Tolerogenic Dendritic Cells (DCs) Promote Treg Differentiation	7
1.2.4 Role of Tregs in ACD.....	8
1.3 EXISTING STRATEGIES TO EXPAND TREGS	9
1.4 BIOMIMETIC DELIVERY MODIFIES THE SKIN MICROENVIRONMENT TO PROMOTE ALLERGEN-SPECIFIC TREGS.....	11
1.4.1 Engineering the Microenvironment of Antigen Presentation (Skin DLN)	13
1.4.2 Engineering the Microenvironment of Antigen Uptake (Skin)	14

1.5	LIMITATIONS OF PRIOR TRI MP FORMULATIONS	15
2.0	AGENT-MATRIX ELECTROSTATIC INTERACTIONS: INFLUENCE ON RELEASE KINETICS	17
2.1	INTRODUCTION.....	17
2.2	MATERIALS AND METHODS	20
2.2.1	Peptide and Biomolecule Selection and Net Charge Predictions.....	20
2.2.2	Microparticle Fabrication	21
2.2.3	Microparticle Characterization.....	22
2.2.4	<i>In Vitro</i> Release Studies	23
2.2.5	Intraparticle pH Measurements	23
2.3	RESULTS	24
2.3.1	Microparticle characteristics	24
2.3.2	Polymer chemistry dictates release kinetics of an uncharged peptide.....	26
2.3.3	Positive peptide charge hinders release from PLGA microparticles	29
2.3.4	Polymer chemistry influences intraparticle pH during degradation.....	32
2.3.5	Release of pH-sensitive peptides depends on intraparticle pH.....	34
2.3.6	Influence of electrostatic interactions on release of larger biomolecules.	38
2.4	DISCUSSION	40
2.5	CONCLUSIONS	49
2.6	IMPLICATIONS FOR DELIVERY OF TREG-INDUCING FACTORS.....	50
3.0	BIOMIMETIC DELIVERY OF TREG-INDUCING FACTORS WITH MICROPARTICLES PROMOTES IMMUNE TOLERANCE AND SUPPRESSES ALLERGIC CONTACT DERMATITIS	52

3.1	MATERIALS AND METHODS	53
3.1.1	Mice	53
3.1.2	Microparticle Fabrication	53
3.1.3	Microparticle Characterization.....	54
3.1.4	Identification of Microparticle in Skin Draining Lymph Nodes after Injection	56
3.1.5	Sequestration of Microparticles at Injection Sites	56
3.1.6	Hapten-Mediated Murine DTH Model.....	57
3.1.7	Protein-Mediated (OVA) Antigen-Specific Murine DTH Model	57
3.1.8	Suppression of Skin DTH with TRI MPs	58
3.1.9	Inhibiting Treg-Mediated Suppression with Anti-GITR or Anti-CD25..	59
3.1.10	Phenotypic Analysis of T-cell Populations in Skin Draining Lymph Nodes by Flow Cytometry	59
3.1.11	<i>In Vitro</i> Suppression Assay	60
3.1.12	Phenotypic Analysis of DCs in Skin Draining Lymph Nodes by Flow Cytometry	61
3.1.13	Functional Analysis of DCs from Skin Draining Lymph Nodes After TRI MP Treatment	61
3.1.14	Cutaneous Histology and Immunohistochemistry	62
3.1.15	Cutaneous Cytokine Expression by qRT-PCR	63
3.1.16	Statistical Analyses.....	63
3.2	RESULTS	64
3.2.1	TRI MPs release TGF- β 1, Rapamycin, and IL-2 for about 1 week.	64

3.2.2	Prophylactic treatment with TRI MPs during hapten sensitization increases the Treg/Teff ratio in skin draining lymph nodes.	66
3.2.3	TRI MP treatment during hapten sensitization suppresses maturation of migratory DCs in skin DLN.	72
3.2.4	TRI MP treatment suppresses T-cell stimulatory function of DCs.	73
3.2.5	Prophylactic treatment with TRI MPs during hapten sensitization suppresses DTH responses to multiple subsequent exposures.	75
3.2.6	Treg-inducing factors must be delivered locally (near the sensitization site), but generate systemic and specific tolerance to contact allergens...	80
3.2.7	TRI MP travel to skin DLN after injection, but therapeutic efficacy does not depend on lymphotropic delivery.	83
3.2.8	In previously sensitized mice, TRI MPs administered at the time of allergen challenge suppress subsequent DTH responses.	86
3.2.9	TRI MPs induce protein-specific Tregs and suppress protein-mediated ACD.	88
3.3	DISCUSSION	92
4.0	CO-DELIVERY OF ALLERGEN AND VITAMIN D3 ANALOG WITH MICRONEEDLE ARRAYS ENGINEERS THE SKIN MICROENVIRONMENT TO PROMOTE ALLERGEN TOLERANCE	98
4.1	INTRODUCTION.....	98
4.2	METHODS	101
4.2.1	Mice	101
4.2.2	Microneedle Array Fabrication.....	101

4.2.3	MNA Characterization.....	103
4.2.4	Murine Models of OVA Delayed Type Hypersensitivity (DTH)	104
4.2.5	Evaluation of Skin Histology by H&E Staining.....	104
4.2.6	Evaluation of Cellular Immune Responses by Flow Cytometry	105
4.2.7	Evaluation of Humoral Immune Responses by ELISA.....	106
4.2.8	Murine Skin Microenvironment Evaluation After Treatment with Topical MC903 or MNAs Containing MC903 and/or DNCB.....	107
4.2.9	Human Skin Explant Cultures with MC903 MNA.....	108
4.2.10	Human Skin Microenvironment Evaluation by qRT-PCR Array	109
4.2.11	Human Skin Migratory Cell Phenotype Analysis by Flow Cytometry..	110
4.2.12	Statistical Analyses.....	110
4.3	RESULTS	111
4.3.1	Characterization of dissolvable tip-loaded MNAs.....	111
4.3.2	Delayed-type hypersensitivity (DTH) responses to different OVA MNA formulations.....	112
4.3.3	Local and systemic T-cell responses to different OVA MNA formulations	116
4.3.4	Prophylactic tolerization with OVA + MC903 MNAs inhibits subsequent OVA sensitization.....	117
4.3.5	Prophylactic tolerization alters cellular and humoral immune responses	120
4.3.6	Tolerization of previously sensitized mice suppresses subsequent DTH responses and alters cellular and humoral immune responses.....	122

4.3.7	MC903 applied topically or with MNAs alters the murine skin microenvironment.....	124
4.3.8	Co-delivery of allergen and MC903 via MNA inhibits allergen-induced expression of pro-inflammatory mediators in murine skin	126
4.3.9	MC903 MNA alter human skin microenvironment	127
4.3.10	MC903 MNAs enhance migration of CD14 ⁺ dermal DCs from human skin	129
4.4	DISCUSSION	131
5.0	FUTURE WORK.....	138
5.1	USING AGENT-POLYMER INTERACTIONS TO IMPROVE RATIONAL DESIGN OF CONTROLLED RELEASE SYSTEMS.....	138
5.2	IMPROVING TRI MP FOR CLINICAL TRANSLATION	139
5.3	EVALUATING TRI MP EFFICACY IN CHRONIC MODELS OF ACD	140
5.4	TESTING MC903 MNA IN MURINE MODELS OF HAPTEN-MEDIATED ACD.....	141
5.5	EVALUATING HUMAN SKIN MICROENVIRONMENT RESPONSES TO ALLERGEN + MC903 MNA.....	142
5.6	INVESTIGATING RESPONSES TO DIFFERENT MODES OF CUTANEOUS DELIVERY OF DIFFERENT TYPES OF ALLERGENS.....	143
6.0	CONCLUSIONS AND BROADER IMPLICATIONS	145
	BIBLIOGRAPHY	147

LIST OF TABLES

Table 2-1. Peptides used for release studies	21
Table 2-2. Average microparticle diameter (μm) based on volume-weighted size distributions of 50,000 particles per formulation	25
Table 2-3. Total peptide loading (ng/mg PLGA) based on 100% cumulative release (mean \pm SD, n=3)	26
Table 2-4. Encapsulation efficiency (%), given theoretical loading of 625 ng/mg PLGA (mean \pm SD, n=3)	26
Table 2-5. Therapeutic peptides and proteins with positive or variable net charge.	49

LIST OF FIGURES

Figure 1-1. T-cell activation and differentiation involves integration of three types of signals from an APC.	6
Figure 1-2. T-cell differentiation is influenced by cytokines secreted by APCs or local cells.....	7
Figure 1-3. Immune responses to contact allergens depend on microenvironment of the skin and/or skin DLN.	13
Figure 2-1. Scanning electron micrographs (SEM) of microparticles.....	25
Figure 2-2. Release kinetics for a neutrally charged peptide depend on PLGA initial molecular weight and end-group chemistry.....	28
Figure 2-3. Proposed mechanism by which peptide charge influences release kinetics.	28
Figure 2-4. Greater net positive charge on a peptide corresponds with slower release kinetics from negatively charged PLGA matrices.	30
Figure 2-5. Correlations between peptide charge and release rates from PLGA microparticles..	32
Figure 2-6. Intraparticle pH and supernatant pH are dynamic and depend on PLGA initial molecular weight and degradation rate.	34
Figure 2-7. Initial burst of pH-dependent peptides is influenced by initial charge, which depends on initial pH of the microenvironment in hydrated microparticles.....	36
Figure 2-8. Magnitude of initial burst is influenced by initial peptide charge.	38

Figure 2-9. PLGA microparticles release more positively charged proteins slower than biomolecules with less positive charge.....	40
Figure 3-1. Microparticle characterization.	65
Figure 3-2. IL-2 and TGF- β 1 released from MPs and detected by ELISAs are bioactive.	66
Figure 3-3. Treatment with TRI MP during DNFB sensitization enhances Treg populations and reduces effector T-cell populations (Teff; Th1 and Tc1) in skin draining lymph nodes (DLN).	68
Figure 3-4. TRI MP treatment expands CD25 ⁺ and CD25 ⁻ Treg populations and alters absolute numbers of Tregs and effector T cells in skin DLN.	69
Figure 3-5. TRI MPs modulate T-cell responses to another chemical hapten (OXA).	69
Figure 3-6. Effects of sustained local delivery and different combinations of TRI MP on Treg (CD4 ⁺ FoxP3 ⁺), Th1 (CD4 ⁺ T-bet ⁺) and Tc1 (CD8 ⁺ T-bet ⁺) populations in DLN four days after sensitizing ears with DNFB.....	71
Figure 3-7. TRI MP treatment during DNFB sensitization suppresses maturation of skin migratory DCs.....	73
Figure 3-8. Treatment with TRI MP plus a bolus of soluble TRI factors impairs stimulatory capacity of DCs in skin DLN.....	74
Figure 3-9. Prophylactic treatment with TRI MP, prior to sensitization, protects skin and suppresses DTH responses to repeated challenges with DNFB.	76
Figure 3-10. TRI MPs suppress inflammatory response to OXA challenge.	77
Figure 3-11. Representative immunofluorescence images of ear sections used for T-cell counts in Figure 3-9.....	78

Figure 3-12. Depletion of CD25 ⁺ Tregs with anti-CD25 (PC-61) modestly impairs TRI MP-mediated suppression of DTH.	80
Figure 3-13. TRI MP injected near sites of skin sensitization can suppress DTH responses to challenge at distal sites.....	82
Figure 3-14. Some TRI MPs arrive in the local skin DLN after injection.....	84
Figure 3-15. TRI MPs do not need to travel to DLN for therapeutic efficacy.	85
Figure 3-16. Treatment of previously sensitized mice with TRI MP at the time of allergen challenge reverses ongoing ACD and suppresses DTH responses to subsequent exposures.	87
Figure 3-17. Treatment with TRI MP prior to OVA sensitization suppresses a protein-specific DTH response.	90
Figure 3-18. TRI MP-induced CD25 ⁺ OT-II T cells suppress proliferation of naïve CD4 ⁺ CD25 ⁻ conventional T cells (T _{conv}).	91
Figure 4-1. Microneedle Array (MNA) geometry and dimensions.	103
Figure 4-2. MNA characterization.....	112
Figure 4-3. Ear swelling responses to Blank, OVA, or OVA _{ETX} MNA in unsensitized and sensitized mice.....	113
Figure 4-4. Characterization of infiltrating leukocyte populations in skin following OVA challenge in sensitized, intolerized mice.....	115
Figure 4-5. Local and systemic T-cell responses to MNAs in unsensitized mice.	117
Figure 4-6. Prophylactic tolerization with OVA + MC903 MNAs prevents OVA sensitization, inhibiting DTH responses to subsequent OVA challenge.	119
Figure 4-7. Prophylactic tolerization with OVA + MC903 MNAs shifts Th1 / Th2 and Treg / Teff ratios in DLN.	120

Figure 4-8. Prophylactic tolerization alters humoral immune response to OVA.	122
Figure 4-9. Tolerization of previously sensitized mice with OVA + MC903 MNAs suppresses subsequent DTH response.....	123
Figure 4-10. Tolerization of previously sensitized mice with OVA + MC903 MNA influences cellular and humoral immune responses.....	124
Figure 4-11. Cutaneous cytokine expression in murine skin is altered by MC903 MNA and differentially regulated by epicutaneously applied MC903.....	125
Figure 4-12. Co-delivery of allergen plus MC903 in MNAs inhibits innate response to allergen in murine skin.....	126
Figure 4-13. MC903 MNAs alter expression of inflammatory immune response genes in human skin explants.....	128
Figure 4-14. MC903 MNAs enhance migration of CD14 ⁺ dermal DCs (DDC) from human skin explants.	130
Figure 5-1. Timelines for future experiments to evaluate (A) duration and (B) durability of TRI MP-induced tolerance.	141
Figure 5-2. MNAs deliver OVA protein to different subsets of skin migratory DCs.	144

ACKNOWLEDGMENTS

I would first like to express my gratitude to my dissertation advisor, Dr. Steven Little, for his invaluable guidance and support throughout my graduate school experience, and also while I was considering my future options as an undergrad. Steve has been a wonderful mentor and has given me the freedom to explore and develop my own projects, as well as the resources to make this work possible. I am also especially grateful to Dr. Louis Falo for offering me a chance to work in his lab and to become a part of his research group. His support and guidance have been tremendous and have helped me to grow as a researcher. I am truly thankful for the opportunity to develop complementary skill sets working in both the Little and Falo Labs. I would also like to thank the other members of my dissertation committee, Dr. Yadong Wang and Dr. Adrian Morelli, for their time and valuable feedback on my thesis. Thanks to the members of the Little Lab for their collaboration and friendship, and especially to Sid Jhunjhunwala for his mentorship during my early years as a grad student and for teaching me many of the techniques that I used throughout my doctoral work. Also, thanks to everyone from the Department of Dermatology. It has been a pleasure working with and learning from all of them over the past several years. I'd also like to acknowledge the tremendous support from the Department of Bioengineering throughout both my undergraduate and graduate careers, and especially Dr. Sanjeev Shroff and Nick Mance for their counsel and assistance navigating the grad program. I am also grateful to the National Science Foundation Graduate Research Fellowship Program (DGE-1247842) for

funding part of my pre-doctoral work. Finally, a huge heartfelt thank you to my incredible friends and family—especially my parents, sister, and Pitt familiee—for their continuous unconditional love and encouragement, and for all of the great memories made on this journey.

COMMON ABBREVIATIONS

ACD – allergic contact dermatitis

APC – antigen-presenting cell

DC – dendritic cell

DLN – draining lymph node

DNCB – 2,4-dinitrochlorobenzene

DNFB – 2,4-dinitrofluorobenzene

DTH – delayed-type hypersensitivity

IL-2 – interleukin-2

LC – Langerhans cell

MHC – major histocompatibility complex

MNA – microneedle array

MP – microparticle

OVA – ovalbumin

PEG – poly(ethylene glycol)

PLGA – poly(lactic-co-glycolic acid)

Tc1 – type 1 cytotoxic T cell (CD8⁺ T-bet⁺)

TCR – T-cell receptor

Teff – effector T cell

TGF-β1 – transforming growth factor-β1

Th1 – type 1 helper T cell (CD4⁺ T-bet⁺)

Th2 – type 2 helper T cell (CD4⁺ GATA-3⁺)

Treg – regulatory T cell (CD4⁺ FoxP3⁺)

Tr1 – type 1 regulatory T cell (CD4⁺ IL-10⁺)

TRI MP – Treg-inducing microparticles

(TGF-β1 MP, Rapamycin MP, & IL-2 MP)

1.0 INTRODUCTION

Aberrant inflammation leading to tissue destruction is responsible for autoimmunity, transplant allograft rejection, and many inflammatory diseases, such as allergic contact dermatitis. These conditions are all characterized by a breakdown in immunological homeostasis, or the balance between pro-inflammatory (effector) and anti-inflammatory (regulatory) arms of the immune system. This chapter discusses allergic contact dermatitis and current treatments, key underlying immunological mechanisms, and some recent experimental approaches to restore homeostasis by enhancing naturally suppressive regulatory T cell populations. Finally, we introduce two novel biomimetic delivery approaches to modify the skin microenvironment, expand allergen-specific Tregs, and treat allergic contact dermatitis.

1.1 ALLERGIC CONTACT DERMATITIS

1.1.1 Clinical Presentation, Prevalence, and Costs

Allergic contact dermatitis (ACD) is one of the most prevalent skin diseases, affecting approximately 15-20 percent of the general population [1]. ACD typically presents as an intensely pruritic rash at the site of contact with one of more than 4,350 potential chemical allergens, including fragrances, metals (e.g. nickel), urushiol oil (poison ivy), topical antibiotics

(e.g. neomycin), and industrial chemicals [2]. Erythematous lesions and weeping blisters appear in acute cases of ACD, while chronic exposure to contact allergens can result in dry, scaly, thickened skin with painful fissures. Chronic ACD, in particular, can have a significant detrimental impact on psychosocial and emotional well being of those afflicted [3, 4]. Direct medical costs associated with ACD have been reported in excess of \$1.6 billion annually in the U.S., not including costs of over-the-counter remedies [5]. As one of the leading work-related illnesses, ACD is also responsible for an estimated \$500 million in indirect costs, associated with lost workdays and reduced productivity due to work restrictions [5].

1.1.2 Current Treatments and Limitations

Whenever possible, identifying and avoiding contact with offending allergens is the best way to manage ACD. In the event of incidental contact with an allergen, topical corticosteroids and/or topical calcineurin inhibitors are typically used to suppress the resulting inflammatory response in the skin [6]. Corticosteroids exhibit broad anti-inflammatory effects on innate and adaptive immune cells (especially neutrophils and macrophages [7]), as well as keratinocytes; however, adverse effects may be associated with prolonged use of moderate to high potency corticosteroids, which is often required for treatment of ACD. Application site side effects include skin atrophy (thinning), telangiectasia (spider veins), photosensitivity, discoloration, and striae [8]. When corticosteroid treatment is unsuccessful or contraindicated, as on sensitive skin of the face and intertriginous regions, topical calcineurin inhibitors, such as tacrolimus or pimecrolimus, may be prescribed. These agents target adaptive immune responses by inhibiting T cell activation, and have fewer local side effects [6], but still fail to reverse the underlying allergen-specific T-cell-mediated immune dysfunction or prevent future allergic reactions.

Additionally, both topical corticosteroids and calcineurin inhibitors can further impair skin barrier function and suppress protective antimicrobial immunity, thereby increasing susceptibility to future allergen exposure, as well as viral and bacterial infections of the skin [9, 10]. For more extensive, severe cases of ACD, systemic antihistamines, corticosteroids, and/or immunosuppressive agents may be required; however, long-term global suppression of the immune system by such agents can leave individuals susceptible to opportunistic infections and increase the risk of cancer [11, 12]. Even with the aforementioned treatments, persistent contact dermatitis occurs in 33-81 percent of individuals [13]. Thus, novel therapeutic approaches to modulate immune responses to contact allergens may improve the treatment of ACD.

1.2 NATURAL REGULATORS OF INFLAMMATION: TREGS

In contrast to current immunosuppressive therapies, our bodies use sophisticated, highly regulated, and highly targeted mechanisms to modulate inflammatory responses. Indeed, the immune system relies on a delicate balance of pro-inflammatory effector cells to protect us from disease-causing pathogens, and anti-inflammatory suppressor cells to prevent excessive or misdirected immune responses that can cause severe tissue damage. Regulatory T cells (Tregs) are subsets of lymphocytes used by the body to suppress and “regulate” immune responses against self and foreign antigens through various contact-dependent and contact-independent mechanisms [14]. CD4⁺ FoxP3⁺ Tregs, which are produced in the thymus or induced *de novo* from naïve T cells in the periphery, constitute approximately 5-15 percent of peripheral CD4⁺ T cells in naïve mice and healthy humans [15]. Tr1 cells (CD4⁺ FoxP3⁻ IL-10⁺) are a similar yet distinct population of suppressive T cells that are exclusively induced in the periphery and also

contribute to immune tolerance [16, 17]. Notably, extensive research indicates that deficiencies in Treg function and quantity leads to augmented immune responses toward self and non-self antigens (e.g. commensal bacteria, allografts, and allergens), causing autoimmunity, chronic inflammatory diseases, and allograft rejection [18]. Numerous studies have also shown that increasing the prevalence and/or function of Tregs can ameliorate the destructive inflammation and re-establish immune tolerance and homeostasis [19].

1.2.1 Mechanisms of Treg-Mediated Suppression

Tregs employ several contact-dependent and contact-independent mechanisms to suppress immune responses (reviewed extensively in [14] and [20]). Tregs can directly suppress, or kill, effector T cells by secreting inhibitory cytokines (e.g. TGF- β 1, IL-10, and IL-35) or cytotoxic proteins (e.g. granzymes and perforin), respectively. Additionally, Tregs can make the local microenvironment less favorable for effector T cell survival and function by sequestering the T-cell mitogen IL-2 via elevated surface expression of high affinity IL-2R α (CD25) [14]. Conversion of pro-inflammatory extracellular ATP to anti-inflammatory adenosine via two ectoenzymes (CD73 and CD39) expressed on the surface of Tregs is another mechanism specifically reported to be important for suppression of ACD [21]. Tregs can also mediate suppression by contact-dependent mechanisms involving APCs. For example, high levels of CTLA-4 expressed on the surface of Tregs acts as a potent negative co-stimulatory signal for APCs (via CD80 and CD86) [14]. Finally, in addition to suppressing effector T cells and APCs, Tregs have been shown to directly inhibit other pro-inflammatory innate immune cells, such as natural killer (NK) cells [22] and neutrophils [23], either directly or indirectly through modifying tissue microenvironments.

1.2.2 T-cell Differentiation Requires Integration of Signals from Antigen-Presenting Cells

Antigen-presenting cells (APCs), such as dendritic cells (DCs), can activate naïve T cells and induce differentiation of either effector or regulatory T cells, depending on integration of three types of signals, summarized in Figure 1-1. Differentiation of naïve CD4⁺ T cells into one of several different types of helper T cells or regulatory T cells depends on a combination of the strength of antigen recognition (signal 1), the presence and nature of co-stimulation (signal 2), and the specific cytokines secreted (signal 3). In particular, T-cell responses are influenced by the avidity of the TCR / peptide-MHC interaction, which depends on both the density of peptide-MHC molecules on the surface of the APC and the affinity of the TCR for a specific peptide-MHC complex [24, 25]. Additionally, the presence or absence of positive and negative co-stimulatory ligands on the APC (summarized in Figure 1-1) can also influence T-cell responses, leading to differentiation and development of memory T cells, or alternative outcomes such as T-cell deletion or anergy [26-28]. Finally, specific cytokines secreted by the APC, or provided in a paracrine fashion by nearby cells, dictate what type of pro-inflammatory helper T cell (e.g. Th1, Th2, etc.) or anti-inflammatory suppressor T cell (e.g. Treg or Tr1) a naïve CD4⁺ T cell will become [17, 29-31]. Different types of CD4⁺ T cells and the cytokines responsible for their differentiation are summarized in Figure 1-2. Finally, differentiation of CD8⁺ T cells into various effector phenotypes, such as IFN- γ -producing Tc1 cells, involves similar mechanisms (reviewed in [32]).

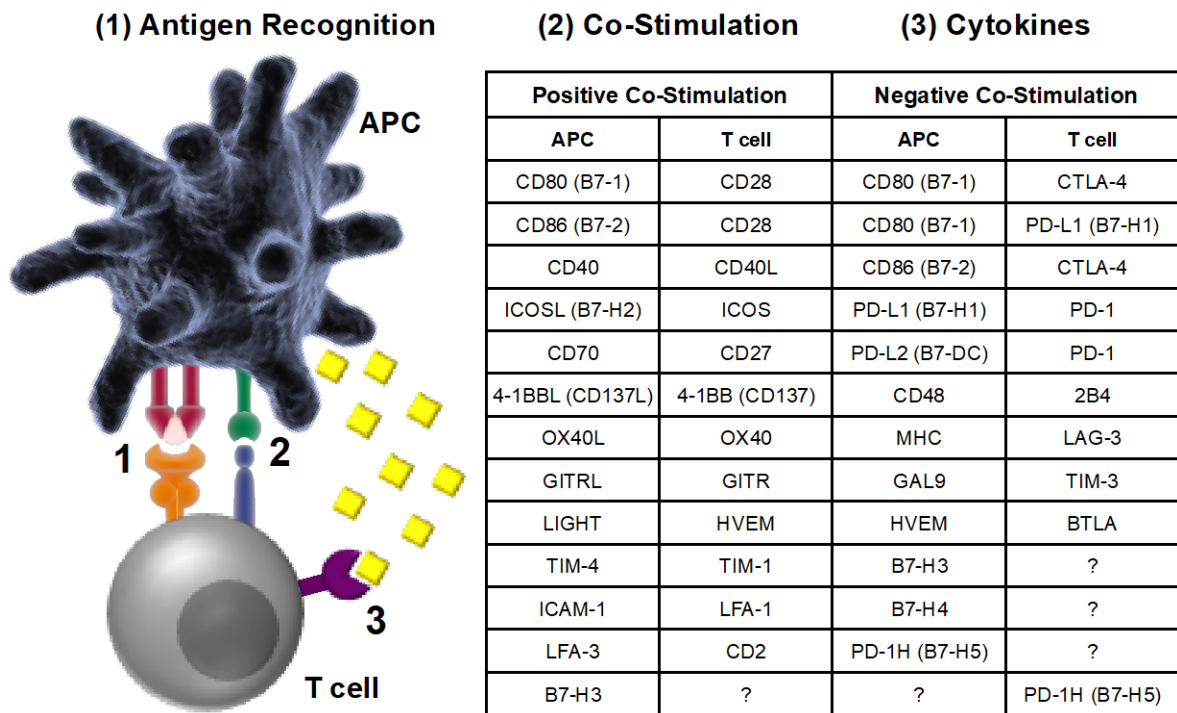


Figure 1-1. T-cell activation and differentiation involves integration of three types of signals from an APC. Antigen recognition (signal 1) occurs when a peptide antigen is presented to the T-cell receptor (TCR) by the major histocompatibility complex (MHC) on the surface of the APC. Co-stimulation (signal 2) is provided by interactions between surface-bound receptor/ligand pairs on the T cell and APC. The table lists several receptor/ligand pairs that provide positive co-stimulatory or negative co-stimulatory (co-inhibitory) signals to the T cell [33, 34]. Finally, cytokine(s) secreted by the APC signal through cytokine receptors on the T-cell (signal 3).

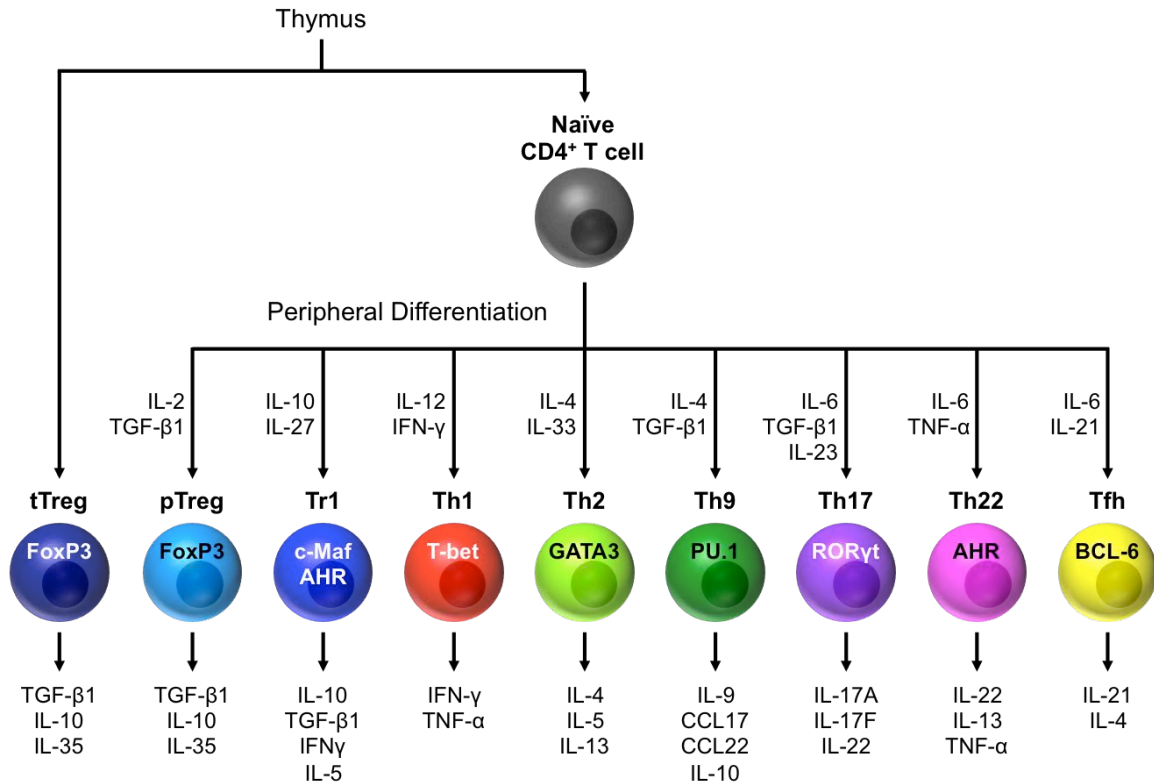


Figure 1-2. T-cell differentiation is influenced by cytokines secreted by APCs or local cells. T-cell development in the thymus leads to mature populations of single positive CD4⁺ or CD8⁺ (not shown) T cells. Following selection, two distinct populations of CD4⁺ T cells emerge: FoxP3⁺ thymic tTreg and FoxP3⁻ conventional naïve T cells. In the periphery, naïve T cells can differentiate into various types of regulatory or effector T cells in response to the indicated cytokines. These T-cell subsets often express distinct master transcription factors (e.g. FoxP3, T-bet, etc.) and have different functions in immunity and tolerance, many of which are mediated by secreted cytokines [17, 29-31].

1.2.3 Tolerogenic Dendritic Cells (DCs) Promote Treg Differentiation

Tolerogenic DCs are a heterogeneous population of DCs with generally anti-inflammatory or suppressive functions that promote immune tolerance. Tolerogenic DCs may occur naturally in response to cues from various tissue microenvironments [35], or may be generated *ex vivo* by various pharmacological treatments (e.g. IL-10, vitamin D3, or rapamycin) [36-38]. While pro-

inflammatory or immunogenic DCs tend to express high levels of MHC (signal 1) and positive co-stimulatory proteins (signal 2), tolerogenic DCs typically express lower levels of MHC and positive co-stimulatory molecules, but higher levels of negative co-stimulatory receptors (see Figure 1-1) [39]. Furthermore, whereas immunogenic DCs secrete various cytokines to induce differentiation of pro-inflammatory effector T cells (see Figure 1-2), tolerogenic DCs secrete anti-inflammatory cytokines and other soluble mediators (e.g. IL-10, TGF- β 1, IDO, and retinoic acid), which promote differentiation of suppressive Tregs or Tr1 cells [40-43].

1.2.4 Role of Tregs in ACD

Unlike immediate, anaphylactic (type I) allergic reactions to foods and bee venom, ACD represents a classic type IV cell-mediated delayed-type hypersensitivity (DTH) response. In ACD, T-cell responses are primed upon first exposure to a contact allergen (sensitization phase), and primed effector T cells are responsible for destructive skin inflammation upon subsequent exposure to the allergen (elicitation phase). These specific mechanisms are reviewed extensively in [44] and [45]. While IFN- γ producing cytotoxic CD8⁺ T cells (Tc1) and helper CD4⁺ T cells (Th1) are predominant effectors of inflammation in DTH responses [45], prior studies have identified pivotal roles of Tregs in the resolution of ACD [45-47]. In the context of ACD, endogenous Tregs have been shown to both control sensitization and resolve inflammation in later stages of the elicitation phase [45, 48, 49]. Notably, depletion of Tregs has been shown to exacerbate and prolong ACD-associated inflammation [48, 50, 51], while systemic infusion of Tregs expanded *ex vivo* significantly reduces skin inflammation [52]. Accordingly, it has been proposed that enriching Treg populations in the body could lead to improvements in treatment strategies for ACD.

1.3 EXISTING STRATEGIES TO EXPAND TREGS

To date, the primary method for expanding Treg populations involves isolation from peripheral blood and *ex vivo* expansion. Drawbacks with such an approach include difficulty isolating pure populations of Tregs, as well as the requirements for GMP facilities and multiple clinic visits for isolation and reinfusion [53-55]. Furthermore, *ex vivo* Treg activation and expansion using microspheres coated with T cell-activating ligands yields less efficient Treg expansion than co-culture with genetically modified APCs, which is considerably more complex, expensive, and time-consuming [53-55]. In addition to infusion of *ex vivo* expanded Tregs, which faces a number of barriers to clinical translation [53-55], several novel strategies have been investigated recently (reviewed in [56] and [57]).

Approaches to selectively expand endogenous Tregs *in vivo* include systemic administration of cytokines (e.g. IL-2 [58]), monoclonal antibodies targeting T-cell surface proteins (e.g. anti-CD4 [59, 60], anti-CD28 [61, 62], anti-TNFR25 [63]), or combinations of factors (e.g. IL-2 plus rapamycin [64] or IL-2/anti-IL-2 complexes [65-68]). Despite promising therapeutic results in various animal models of inflammatory diseases, clinical translation has proven to be difficult. Systemically administered, soluble IL-2 expanded Tregs in some patients with graft-versus-host disease (GVHD) [58]; however, Treg specificity is a concern since activated effector T cells also express IL-2 receptors. In fact, systemic IL-2 is also used clinically to enhance pro-inflammatory anti-tumor immune responses, and vascular leakage syndrome is a potentially life-threatening side effect of systemic IL-2 [69]. In a phase 1 clinical trial, agonistic anti-CD28 caused cytokine storm and catastrophic systemic organ failure in six healthy volunteers [62]. Finally, by expanding existing polyclonal Tregs, these methods are unable to induce Tregs with novel antigen-specificity from the larger pool of naïve T cells. In

other words, if allergen-specific Tregs did not already exist, these methods could not generate allergen-specific Tregs from allergen-specific naïve T cells (a broader repertoire).

In addition to expansion of polyclonal Tregs, antigen-specific Treg populations have been expanded by systemic administration of nanoparticles coated with specific antigens (e.g. peptide-MHCII [70], peptide plus ITE [71], or peptide alone [72]). Similarly, nanoparticles containing peptide or protein antigens and immunomodulatory agents (e.g. antigen plus rapamycin [73]) have been shown to promote development of tolerogenic DCs that induce Tregs. A recent study also demonstrated antigen-specific tolerance in rodent and non-human primate models, following co-administration of unencapsulated therapeutic proteins and rapamycin nanoparticles via intravenous or subcutaneous routes [74]. Most of the aforementioned nanoparticle formulations were injected systemically; however, microparticles containing rapamycin and peptide antigen have also been injected directly into lymph nodes to reprogram the microenvironment in which T-cell polarization occurs [75]. While none of these particle-based treatments have advanced beyond pre-clinical stages yet, allergen-specific immunotherapy (SIT) has been used in the clinic for more than a century to desensitize patients with type I hypersensitivities by generating allergen-specific Tregs [76]. Unfortunately, allergen-SIT requires long-term treatment over a period of months to years, with repeated subcutaneous or oral administration of low doses of protein allergens [76]. Notably, each of the aforementioned methods to generate antigen-specific Tregs uses known protein or peptide antigens, which may not be available in the case of hapten-mediated ACD, since a heterogeneous repertoire of hapten-protein conjugates (neoantigens) forms *in situ*. Thus, novel methods to enhance antigen-specific Tregs, especially for treatment of ACD, are warranted.

1.4 BIOMIMETIC DELIVERY MODIFIES THE SKIN MICROENVIRONMENT TO PROMOTE ALLERGEN-SPECIFIC TREGS

Upon cutaneous antigen exposure, skin-resident dendritic cells (DCs) take up antigen, mature, and migrate to skin draining lymph nodes (DLN) to present antigen to T cells. Information encoded in the local microenvironments, where these processes occur, ultimately dictates whether T cells will become destructive, pro-inflammatory effector T cells (Teff), or tissue-protective Tregs. Typically, innate inflammatory responses to allergens in the skin drive sensitization and Teff-mediated hypersensitivity by inducing maturation and migration of inflammatory DCs (Figure 1-3A) [44]. In contrast, allergen exposure in the absence of pro-inflammatory “danger” signals [77-80], or in the context of tolerogenic signals [81-86], can induce differentiation of tolerogenic DCs and/or Tregs. Accordingly, we hypothesized that using biomimetic delivery systems to engineer the microenvironments in which allergen is processed by DCs, or presented to T cells could lead to allergen-specific tolerance. To test this hypothesis, we developed two complementary approaches to (1) engineer the skin DLN microenvironment with biodegradable microparticles (MPs) that locally sustain release of **TReg-Inducing** (“TRI”) factors (Figure 1-3B), and (2) engineer the skin microenvironment with microneedle arrays (MNAs) that deliver a vitamin D3 analog (MC903) into the skin to cultivate Treg-inducing tolerogenic DCs (Figure 1-3C). These two approaches to allergen-specific Treg induction are examples of biomimetic delivery, as they provide natural (or mimetic) signals to cells in the body with appropriate temporal and spatial context to orchestrate specific cellular responses [87]. In particular, the first approach uses TRI MPs to mimic the secretion of Treg-inducing factors (TGF- β 1 and IL-2) by tolerogenic DCs (or other local cells) during antigen presentation to T cells [40, 88, 89]. Similarly, the second approach involves flooding the skin microenvironment

with an analog of the natural immunosuppressive 1,25-dihydroxyvitamin D₃, which is synthesized in the skin in response to ultraviolet light [83] and helps to maintain immunological homeostasis and peripheral tolerance to benign foreign and self antigens [90, 91].

The induction and expansion of allergen-specific Treg populations *in vivo* represents a shift from the current paradigm of ACD treatment with non-specific topical immunosuppressive agents. In contrast, the two strategies proposed herein harness the body's natural regulators of immune responses (Tregs) for specific suppression of aberrant inflammation. These novel approaches “re-educate” the immune system by conveying immunological context to direct tissue-protective tolerogenic responses to contact allergens, rather than destructive pro-inflammatory ones. Unlike typical anti-inflammatory agents used to quell allergic responses, local modulation of skin and skin DLN milieus during allergen exposure and processing induces Treg-mediated allergen-specific tolerance, which leaves the immune system otherwise intact to detect and neutralize pathogens and malignancies. Efforts by other groups to promote specific immune tolerance—either by expanding Tregs or tolerogenic DCs—have often used infusion of cells manipulated *ex vivo*, or systemic administration of biologic agents that promote activation and proliferation of existing Tregs (as described in Chapter 1.3). In contrast, our biomimetic approaches use “off-the-shelf” acellular delivery systems—described in more detail in the next sections—to directly or indirectly promote local induction of allergen-specific Tregs from larger populations of naïve T cells.

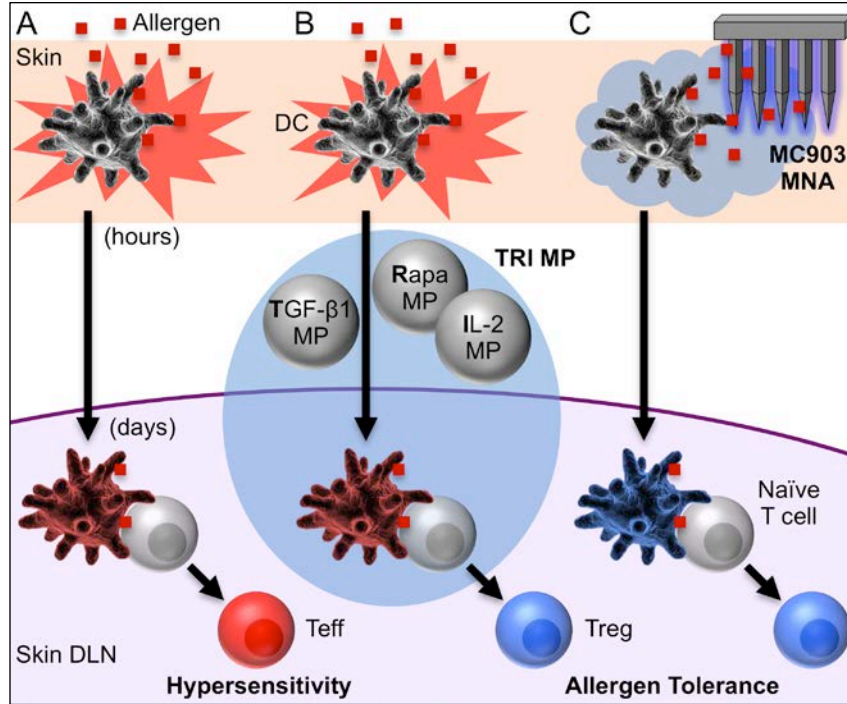


Figure 1-3. Immune responses to contact allergens depend on microenvironment of the skin and/or skin DLN.

(A) Allergens typically promote innate inflammation (red), which triggers migration of pro-inflammatory DCs to skin DLN and differentiation of effector T cells (Teff). (B) TRI MPs injected subcutaneously condition the skin DLN microenvironment to promote Treg differentiation. (C) MC903 MNAs condition the skin microenvironment to provide tolerogenic context (blue) for DCs that take up allergen, migrate to DLN, and induce Treg differentiation.

1.4.1 Engineering the Microenvironment of Antigen Presentation (Skin DLN)

During antigen presentation, specific cytokines secreted by DCs provide immunological context that influences T-cell differentiation (as summarized in Chapter 1.2.2). For example, tolerogenic DCs induce Treg differentiation from naïve $CD4^+$ T cells by secreting factors such as TGF- β 1 and IL-2 [88]. Drawing inspiration from this natural mechanism used by the immune system, our group previously proposed that local delivery of exogenous TGF- β 1 and IL-2 to naïve T cells during antigen presentation by non-tolerogenic DCs would promote Treg induction. Since TGF-

β 1 and IL-2 alone may not prevent effector T cell (Teff) differentiation in a pro-inflammatory milieu (e.g. in skin DLN after allergen exposure), rapamycin (a natural macrolide) was included because of its ability to preferentially suppress generation and proliferation of Teff, while enhancing Treg differentiation [92]. Notably, our group previously demonstrated that this combination of **TR**eg-**I**nducing (“TRI”) factors efficiently generates functionally suppressive Tregs from naïve CD4⁺ T cells activated in culture with artificial APCs (anti-CD3/CD28 coated microbeads [87]) [93, 94]. Furthermore, these TRI factors were also previously encapsulated in biodegradable polymeric MPs to provide sustained release for potential *in vivo* applications (e.g. to induce allergen-specific Tregs and treat ACD) [93].

1.4.2 Engineering the Microenvironment of Antigen Uptake (Skin)

While the approach above attempts to mimic some of the Treg-inducing function of natural tolerogenic DCs, *in vivo* modulation of cutaneous DCs toward tolerogenic phenotypes represents a complementary indirect approach to expand allergen-specific Treg populations. During cutaneous exposure to foreign antigen, cytokines and other factors secreted by keratinocytes and immune cells in the skin provide immunological context that orchestrates maturation and differentiation of resident DCs, which ultimately control T-cell differentiation (as described in Chapter 1.2.2). Thus, introduction of allergens through a skin microenvironment modified to provide tolerogenic context may lead to generation of ACD-suppressing lymphocyte populations, including both classical FoxP3⁺ Tregs and FoxP3⁻ IL-10⁺ Tr1 cells [95].

Modulation of the skin microenvironment was previously reported with ultraviolet (UVB) irradiation, which locally generates several immunosuppressive factors, including 1,25-dihydroxyvitamin D3 [83, 84]. Notably, application of proteins or haptens to UVB-irradiated

skin, or skin pre-treated with topical 1,25-dihydroxyvitamin D3, or synthetic analogs (e.g. MC903), enhanced induction of antigen-specific Tregs and inhibited subsequent delayed-type hypersensitivity (DTH) responses [81, 82, 84-86]. Unfortunately, the complexity of these extensive tolerance induction protocols may limit their translational potential. In particular, epicutaneous allergen application typically follows 3-4 days of treatments with 1,25-dihydroxyvitamin D3, or MC903, and optimal introduction of protein allergens requires barrier layer disruption (e.g. tape-stripping) and occlusive dressings [84, 86]. Each of these components of the treatment regimen introduces potential sources of error, including inconsistent areas of application, variable per area dosing, and excessive or sub-optimal barrier disruption. Dissolvable MNA technology, previously developed by our lab, addresses these limitations by enabling convenient, efficient, and reproducible delivery of multiple proteins and/or drugs into the epidermal and dermal layers of the skin [96-98]. In Chapter 4, we will describe generation of allergen tolerance with MNAs that engineer the skin microenvironment by providing tolerogenic context (MC903) for allergen introduction (Figure 1-3C).

1.5 LIMITATIONS OF PRIOR TRIMMP FORMULATIONS

Mathematical models previously developed by our group allow rational design of biodegradable polymer-based delivery systems to achieve desired release kinetics. In such models, matrix geometry, polymer chemistry, and agent molecular weight dictate the rate of polymer matrix erosion and the degree of erosion needed for egress of encapsulated agents [99-102]. However, because these models neglect electrostatic interactions between encapsulated agents and negatively charged degrading polymer matrices, their utility is limited to neutral or negatively

charged agents. While two of the three TRI factors (rapamycin and IL-2) fit this criterion, the third (TGF- β 1) has considerable positive charge, making its release from PLGA MPs more difficult to control and predict. In fact, the original TGF- β 1 MPs exhibited an unexpected initial lag phase of more than two weeks [93]. In the prior *in vitro* study, this limitation was addressed by pre-incubating TGF- β 1 MPs 18-22 days before adding them to T cell cultures [93]; however, the need to pre-incubate particles before use limits their translational potential. Thus, to extend our rational design capabilities to positively charged factors and gain insight into ways to achieve faster release of positively charged agents, like TGF- β 1, we systematically characterized the influence of electrostatic interactions on kinetics of release from different polymeric matrices. These studies are described in the next chapter.

2.0 AGENT-MATRIX ELECTROSTATIC INTERACTIONS: INFLUENCE ON RELEASE KINETICS*

2.1 INTRODUCTION

The global market for peptide and protein drugs is projected to reach \$179 billion by 2018 [103], and combined sales of 25 FDA-approved peptide therapeutics (<50 amino acids) exceeded \$14 billion in 2011 [104]. Still, the overwhelming potential of therapeutic peptides and proteins has been limited, in part, by short half-life (minutes to hours) and insufficient bioavailability when administered orally. As a result, frequent injections may be needed to deliver sufficient levels of bioactive peptides or proteins, which could exacerbate issues with patient compliance. Controlled release systems, like the TRI MPs presented in this thesis, have the potential to dramatically prolong bioavailability of rapidly cleared drugs (e.g. peptides and proteins) and maintain therapeutic levels for weeks to months with less frequent dosing. In turn, improved patient compliance and therapeutic efficacy could save the U.S. healthcare system upwards of \$100 billion each year [105]—more than the total annual direct costs for treating cancer [106].

A major challenge for developing controlled release formulations is tuning release kinetics to achieve the desired dosing schedule for a given therapeutic agent. As one of the most

* This chapter is adapted from Balmert SC, Zmolek AC, Glowacki AJ, Knab TD, Rothstein SN, Wokpetah JM, Fedorchak MV, and Little SR. Positive charge of “sticky” peptides and proteins impedes release from negatively charged PLGA matrices. *Journal of Materials Chemistry B* (2015) 3:4723-34, with permission from the Royal Society of Chemistry.

common types of controlled release systems, biodegradable polymer matrices are often fabricated as microspheres or microparticles given the ease of loading and minimally invasive implantation through a needle and syringe. These matrices can be fabricated to be practically any size using many common polymers that are commercially available in a variety of molecular weights. In the past twenty-five years, numerous studies have identified key physical properties of such delivery systems that determine their release behavior (reviewed in [99] and [107]). Mathematical models developed by our group and others have enabled predictions of release kinetics based on such factors as matrix geometry, polymer chemistry, and drug/agent molecular weight [101, 102]. Although drug-polymer interactions have been cited as factors affecting release from poly(lactic-co-glycolic acid) (PLGA) microparticles [108], the effects of such interactions on release kinetics have not yet been extensively studied or characterized.

For the past few decades, synthetic biodegradable polymers, such as polyesters (e.g. PLGA), poly(ortho esters), and polyanhydrides, have been used extensively for drug delivery. PLGA is an especially attractive biomaterial for controlled release systems because of its tunable degradation rate, proven biocompatibility, and outstanding history of FDA approval [109]. This includes at least nine microparticle drug delivery formulations currently on the market [110]. Importantly, progressive hydrolytic degradation of polyesters, poly(ortho esters), and polyanhydrides produces increasingly shorter polymer chains with carboxylic acid end groups. In aqueous solution, these carboxylic acid groups dissociate into carboxylate anions, conferring negative charge on the polymers. As a result of this negative charge, which increases over time due to polymer degradation, ionic interactions between PLGA matrices and positively charged (cationic) peptides have been observed [111-113]. A recent study even demonstrated that cationic peptides could be adsorbed to the surface of low molecular weight PLGA microparticles

or thin films for extended delivery via subsequent desorption [114]. Additionally, several groups have demonstrated that positively charged peptides can become acylated in PLGA matrices [115-117]. Acylation reactions between nucleophilic (high pKa) primary amines in peptides (e.g. lysine residues and N-termini) and PLGA ester bonds form new covalent bonds between peptides and PLGA oligomers, resulting in peptide-PLGA adducts [115]. Peptide sorption to PLGA (as by electrostatic interactions) is also believed to be a precursor to peptide acylation [111]. Since many therapeutic proteins, peptides, and small molecule drugs contain positively charged functional groups, better characterization and understanding of the effects of electrostatic interactions and/or acylation reactions between these agents and negatively charged polymers on release kinetics could improve tools for predicting release and designing controlled release systems.

We hypothesized that positively charged peptides (and larger biomolecules) would exhibit a variable degree of “stickiness” to a polymer matrix with negative charge, thereby reducing their diffusion through the polymer matrix and impeding release from microparticles. We further hypothesized that greater positive charge on a peptide would lead to slower release, due to electrostatic interactions and/or acylation. Herein, we demonstrate that release of peptides from PLGA microparticles is, in fact, inversely correlated with the peptides’ net positive charge, which may increase with a decrease in pH of the surrounding microenvironment. We also show that pH of the intraparticle microenvironment, which decreases over time, depends greatly on PLGA initial molecular weight and end-group chemistry. Notably, in some cases, peptide charge may even switch from negative to positive with the drop in pH in degrading PLGA microparticles. Together, these observations allow us to explain previously unintuitive trends in early release behavior for some peptides that release faster from slower degrading (higher initial

intraparticle pH) polymers. Finally, we show that trends identified for charged peptides extend to larger biomolecules, suggesting the results of these studies are relevant to rationale design of controlled release systems for delivery of a broad range of therapeutic proteins, growth factors, cytokines, and oligonucleotides.

2.2 MATERIALS AND METHODS

2.2.1 Peptide and Biomolecule Selection and Net Charge Predictions

Seven peptides, with similar molecular weights and varying positive charge, fluorescently labeled with 5-carboxytetramethyl-rhodamine (5-TAMRA) or HiLyte Fluor 488 (HF488), were obtained from AnaSpec (Fremont, CA) (see Table 2-1). Recombinant murine CCL22 and CCL21 were obtained from R&D Systems (Minneapolis, MN). Ovalbumin labeled with Texas Red was obtained from Life Technologies (Grand Island, NY). STAT3 cyclic decoy oligodeoxynucleotide (ODN) [118] was generously provided by Malabika Sen and Jennifer Grandis (University of Pittsburgh).

Net charge (Z) of peptides and proteins, which is based on the protonation state of amino acid side groups and the C- and N-termini, was calculated as a function of pH, according to:

$$Z = \sum_i N_i \frac{10^{pK_{a_i}}}{10^{pH} + 10^{pK_{a_i}}} - \sum_j N_j \frac{10^{pK_{a_j}}}{10^{pH} + 10^{pK_{a_j}}}$$

where N_i and pK_{a_i} represent the number and pKa values of the N-terminus (9.69) and side chains of cationic amino acid residues: arginine (12.48), lysine (10.53), and histidine (6.00) [119]. N_j and pK_{a_j} represent the number and pKa values of the C-terminus (2.34) and side chains of

anionic residues: aspartic acid (3.86), glutamic acid (4.25), cysteine (8.33), and tyrosine (10.07) [119]. Charge was normalized to the total mass of the peptide or protein. To determine peptide charge as a function of time, we input interpolations of measured intraparticle pH (i.e. pH as a function of time) into the equation above, which represents charge as a function of pH. The interpolations were generated using the piecewise cubic Hermite interpolating polynomial (PCHIP) function in MATLAB (v7.12, The MathWorks, Inc., Natick, MA). Charge predictions for the cyclic oligonucleotide were calculated with the Marvin v14.8 “protonation” plug-in (ChemAxon LLC, Cambridge, MA).

Table 2-1. Peptides used for release studies

<i>Peptide Name</i>	<i>Fluorescent Label & Amino Acid Sequence</i>	<i>MW (kDa)</i>	<i>ID*</i>
CDK7tide	5-TAMRA-YSPTSPSYSPTSPSYSPTSPS	2.59	+0.0
Erktide	5-TAMRA-IPTTPITTTYFFFK	2.09	+0.5
CHK1tide	5-TAMRA-ALKLVRYPSFVITAK	2.12	+1.4
Neurogranin 28-43	5-TAMRA-AAKIQASFRGHMARKK	2.21	+2.7
PCKε peptide substrate	5-TAMRA-ERM RPRKRQGSVRRRV	2.48	+3.1
Casein kinase 1 substrate	5-TAMRA-RRKDLHDDEEDEAMSITA	2.54	CK1sub
Beta-amyloid 1-17	HF488-DAEFRHDSGYEVHHQKL	2.42	BA17

* Identifier used in figures: net charge per mass (kDa^{-1}) at pH 4 for pH-independent peptides, or abbreviated name for pH-dependent peptides.

2.2.2 Microparticle Fabrication

Four poly(D,L-lactic-co-glycolic acid) (PLGA) polymers, with 50:50 lactide:glycolide composition and different molecular weights and end groups, were purchased from Sigma Aldrich (St. Louis, MO; supplier of Evonik RESOMER RG502H, RG504H, and RG502 polymers) and Lakeshore Biomaterials (Birmingham, AL; supplier of Evonik 5050 DLG1A).

Poly(vinyl alcohol) (PVA, 98 mol% hydrolyzed, $M_w = 25,000 \text{ g mol}^{-1}$) was purchased from PolySciences (Warrington, PA).

Microparticles containing one of the eight fluorescently labeled peptides, rmCCL22, or rmCCL21, were fabricated using a double emulsion-evaporation technique, as described previously [120, 121]. Briefly, microparticles were prepared by mixing 200 μL of an aqueous solution containing the respective agent (125 μg of fluorescently labeled peptide, 5 μg of rmCCL22 or rmCCL21, 200 μg of ovalbumin, or 1 mg of STAT3 cyclic decoy ODN) with 200 mg of 50:50 PLGA (DLG1A, RG502H, RG502, or RG504H) dissolved in 4 mL of dichloromethane. This mixture was sonicated (Vibra-Cell VC750; Sonics, Newton, CT) at 25% amplitude for 10 sec to form the first emulsion (water-in-oil, w/o), and then poured into a 2% PVA solution (60 mL) being homogenized (L4RT-A; Silverson, East Longmeadow, MA) at 3000 rpm. Following 1 min of homogenization, the resulting double emulsion (w/o/w) was added to a 1% PVA solution (80 mL) and stirred for 3 h to allow the dichloromethane to evaporate. Freshly formed microparticles were centrifuged (300 g for 5 min at 4 $^{\circ}\text{C}$) and washed 4 times with deionized water (DIW). The microparticles were then re-suspended in DIW (5mL), flash-frozen with liquid nitrogen, and lyophilized (Benchtop 2K Freeze Dryer; VirTis, Gardiner, NY; operating at 80 mTorr).

2.2.3 Microparticle Characterization

Scanning electron micrographs of microparticle surface morphology were obtained using a scanning electron microscope (JSM-6330F; JEOL, Peabody, MA). Size distributions of microparticles were determined using volume impedance measurements on a Beckman Coulter Counter (Multisizer-3; Beckman Coulter, Brea, CA).

2.2.4 *In Vitro* Release Studies

In vitro release behavior for all microparticle formulations was characterized by incubating 10 mg of microparticles in 1 mL of phosphate buffered saline (PBS) on a roto-shaker at 37°C. At regular time intervals, microparticle suspensions were centrifuged, the supernatants were removed, and the microparticles were re-suspended in fresh PBS. Supernatant concentrations of released agents were quantified by fluorescence spectrophotometry (SpectraMax M5; Molecular Devices, Sunnyvale, CA) for fluorescently labeled peptides and ovalbumin, enzyme-linked immunosorbant assay (ELISA; R&D Systems) for CCL22 and CCL21, and Quant-iT dsDNA assay (Life Technologies) for the STAT3 cyclic decoy ODN. Release profiles generated from measured concentrations of peptide, protein, or ODN were normalized to total amounts encapsulated. All release assay experiments were performed in triplicate.

2.2.5 Intraparticle pH Measurements

As described previously [122, 123], hydrogen ion concentration of dissolved PLGA microparticles was measured and converted to average pH of the intraparticle microenvironment, based on the total aqueous volume of hydrated microparticles. Briefly, 10 mg of microparticles were incubated in 1 mL of PBS (pH 7.4) on a roto-shaker at 37°C. At predetermined time points, the microparticle suspensions were centrifuged, and the supernatant was removed. The remaining microparticles and associated aqueous microenvironment were then dissolved in 800 μ L of acetonitrile (ACN) by vigorous vortexing. Tubes were centrifuged a second time to remove any undissolved PLGA, and 800 μ L of this ACN + PBS + PLGA solution was added to 200 μ L of deionized water (DIW) prior to pH measurements with an InLab Routine Pro pH

probe (Mettler Toledo, Columbus, OH). To determine the pH of the microparticles and aqueous microenvironment, we obtained a correlation between the pH of lactic acid monomers in PBS and lactic acid monomers in a mixture of PBS, ACN, and DIW (comparable to the dissolved PLGA microparticles). Based on the measured pH values and total aqueous volume of the hydrated microparticles, average intraparticle pH could be estimated. Supernatant pH was also measured.

2.3 RESULTS

2.3.1 Microparticle characteristics

All microparticles containing peptides were prepared under similar conditions using three uncapped (–COOH acid-terminated) 50:50 PLGA polymers with different average initial molecular weights (7, 15, and 43 kDa), and a fourth ester-capped (–COOCH₃ terminated) 50:50 PLGA (15 kDa). Representative scanning electron micrographs (Figure 2-1) show spherical microparticles with smooth surface morphology, as observed for all formulations. Volume-weighted size distributions of microparticles, measured with a Beckman Coulter Counter, are relatively consistent between batches, with mean diameters of $19.0 \pm 3.4 \mu\text{m}$ (see Table 2-2 for size distributions for each formulation). Total peptide loading was also consistent, with an average encapsulation efficiency of 78 ± 14 percent across all formulations. Total peptide loading and encapsulation efficiencies for individual formulations are presented in Table 2-3 and Table 2-4.

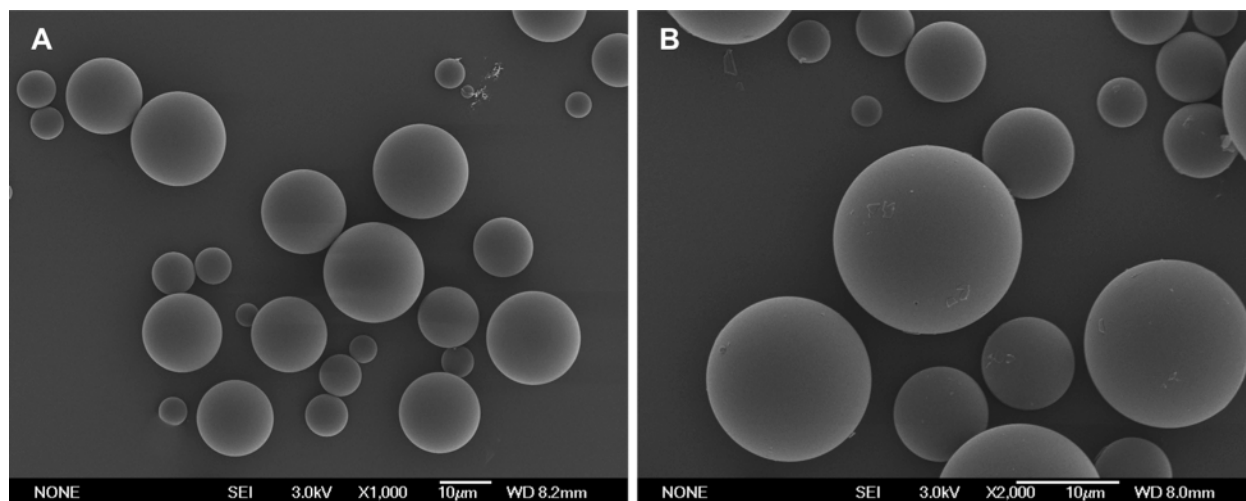


Figure 2-1. Scanning electron micrographs (SEM) of microparticles. Representative images show spherical particles with nonporous surface morphology, characteristic of all microparticle formulations used. (A) 43 kDa PLGA containing $+1.5 \text{ kDa}^{-1}$ peptide at 1000x magnification. (B) 15 kDa PLGA containing $+2.7 \text{ kDa}^{-1}$ peptide at 2000x magnification.

Table 2-2. Average microparticle diameter (μm) based on volume-weighted size distributions of 50,000 particles per formulation

<i>PLGA Polymer</i>	<i>Positively Charged Peptides</i>					<i>Charge Changing Peptides</i>	
	<i>0</i>	<i>+0.5</i>	<i>+1.4</i>	<i>+2.7</i>	<i>+3.1</i>	<i>CK1sub</i>	<i>BA17</i>
7 kDa	20.3±9.3	21.7±12.0	19.5±12.2	21.3±11.9	20.9±9.1	23.5±9.9	
15 kDa	20.3±8.1	19.6±8.6	17.3±6.8	17.4±7.8	22.9±13.6	23.2±9.3	11.3±3.5
43 kDa	23.2±9.3	17.4±7.9	16.8±6.5	21.7±8.9	25.8±14.2	18.9±8.9	
15 kDa-E	20.7±10.9	19.1±8.9	17.4±7.3	14.8±5.1	19.8±9.6	15.7±8.2	14.9±5.6

Table 2-3. Total peptide loading (ng/mg PLGA) based on 100% cumulative release (mean \pm SD, n=3)

<i>PLGA Polymer</i>	<i>Positively Charged Peptides</i>					<i>Charge Changing Peptides</i>	
	<i>0</i>	<i>+0.5</i>	<i>+1.4</i>	<i>+2.7</i>	<i>+3.1</i>	<i>CK1sub</i>	<i>BA17</i>
7 kDa	602 \pm 25	535 \pm 24	575 \pm 27	430 \pm 30	562 \pm 167	417 \pm 9	
15 kDa	597 \pm 37	613 \pm 33	572 \pm 37	590 \pm 38	536 \pm 58	467 \pm 19	440 \pm 13
43 kDa	603 \pm 13	513 \pm 22	497 \pm 25	524 \pm 11	472 \pm 32	342 \pm 5	
15 kDa-E	434 \pm 42	442 \pm 29	325 \pm 7	504 \pm 46	537 \pm 29	458 \pm 22	362 \pm 20

Table 2-4. Encapsulation efficiency (%), given theoretical loading of 625 ng/mg PLGA (mean \pm SD, n=3)

<i>PLGA Polymer</i>	<i>Positively Charged Peptides</i>					<i>Charge Changing Peptides</i>	
	<i>0</i>	<i>+0.5</i>	<i>+1.4</i>	<i>+2.7</i>	<i>+3.1</i>	<i>CK1sub</i>	<i>BA17</i>
7 kDa	96 \pm 4	86 \pm 4	92 \pm 4	69 \pm 5	90 \pm 27	67 \pm 1	
15 kDa	95 \pm 6	98 \pm 5	91 \pm 6	94 \pm 6	86 \pm 9	75 \pm 3	70 \pm 2
43 kDa	97 \pm 2	82 \pm 4	80 \pm 4	84 \pm 2	76 \pm 10	55 \pm 1	
15 kDa-E	69 \pm 7	71 \pm 5	52 \pm 1	81 \pm 7	86 \pm 5	73 \pm 4	58 \pm 3

2.3.2 Polymer chemistry dictates release kinetics of an uncharged peptide

To establish a baseline for peptide release behavior with minimal electrostatic interactions and acylation reactions between the peptide and polymer matrix, a fluorescently labeled peptide with an amino acid sequence that yielded net neutral charge across a range of pH values was used. This peptide also lacked primary amine groups, which are common targets of acylation (i.e. no lysine residues, and N-terminus capped by 5-TAMRA fluorophore). This uncharged hydrophilic peptide was encapsulated in microparticles comprised of acid-terminated 50:50 PLGA with three different initial molecular weights (7 kDa, 15 kDa, and 43 kDa), and an ester-terminated (capped) 15 kDa PLGA (“15 kDa-E”). Ester-capped PLGA initially lacks carboxylic acid end

groups, is more hydrophobic, and thus degrades more slowly [124]. *In vitro* release assays for each formulation demonstrated a substantial effect of polymer molecular weight on release kinetics (Figure 2-2). For the lowest molecular weight (7 kDa) PLGA microparticles, release appeared to follow first-order kinetics with no initial delay in release, since the low molecular weight regions of the polymer matrix were already sufficiently permeable to the encapsulated peptide at the start of incubation. First-order release kinetics of the neutral peptide were progressively delayed with increasing PLGA molecular weight, resulting in initial lag phases of approximately 10 and 20 days for the 15 and 43 kDa PLGA, respectively. Due to less mobile higher molecular weight polymer chains [101], these matrices were initially less permeable to the encapsulated peptide. Therefore, the PLGA polymers degraded with minimal release (lag phase) until regions with sufficiently low molecular weight (permeable to the peptide) formed and bulk release could begin [101]. We also observed a substantial increase in lag phase duration and decrease in the rate of subsequent release for the slower degrading ester-capped 15 kDa PLGA. Complete release of the neutral peptide occurred within 13, 37, 46, and 58 days of incubation for uncapped 7, 15, and 43 kDa PLGA and ester-capped 15 kDa PLGA, respectively (Figure 2-2). These results indicate that with minimal electrostatic interactions and/or acylation reactions between a peptide and polymer matrix, polymer molecular weight and end-group chemistry control release kinetics, presumably by influencing the rate of matrix erosion and formation of interconnected porous networks through which encapsulated peptide can egress (Figure 2-3, top) [102].

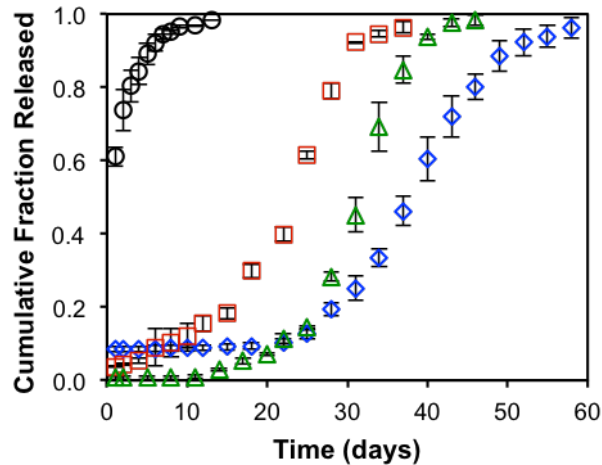


Figure 2-2. Release kinetics for a neutrally charged peptide depend on PLGA initial molecular weight and end-group chemistry. Comparative in vitro release profiles for a 2.6 kDa peptide with net neutral charge, encapsulated in microparticles with different PLGA molecular weights and end groups: 7 kDa (circles), 15 kDa (squares), 43 kDa (triangles), and ester-capped 15 kDa (diamonds).

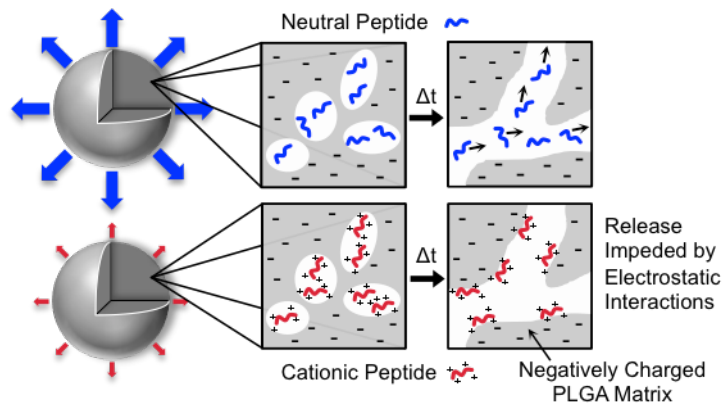


Figure 2-3. Proposed mechanism by which peptide charge influences release kinetics. Polymer degradation and matrix erosion over time form increasingly interconnected pores. Unlike neutral (uncharged) peptides, cationic peptides may stick to the polymer matrix via electrostatic interactions and/or acylation, thereby impeding release.

2.3.3 Positive peptide charge hinders release from PLGA microparticles

For positively charged peptides, we hypothesized that electrostatic interactions and/or acylation reactions with a negatively charged polymer matrix would essentially restrict diffusion of the peptides through the degrading matrix and impede release from microparticles (Figure 2-3, bottom). We further hypothesized that greater positive charge on a peptide would correspond to slower release. In order to test the effects of peptide charge on release kinetics, we identified four fluorescently labeled peptides with positive net charges that were consistent across a range of pH values (Figure 2-4A). These hydrophilic peptides also had similar molecular weights (2.1-2.6 kDa) to that of the neutral peptide (2.6 kDa), to eliminate any confounding effects of peptide size on release [101]. These peptides were encapsulated in microparticles comprised of each of the four aforementioned PLGA polymers, and *in vitro* release assays were conducted, as for the neutral peptide.

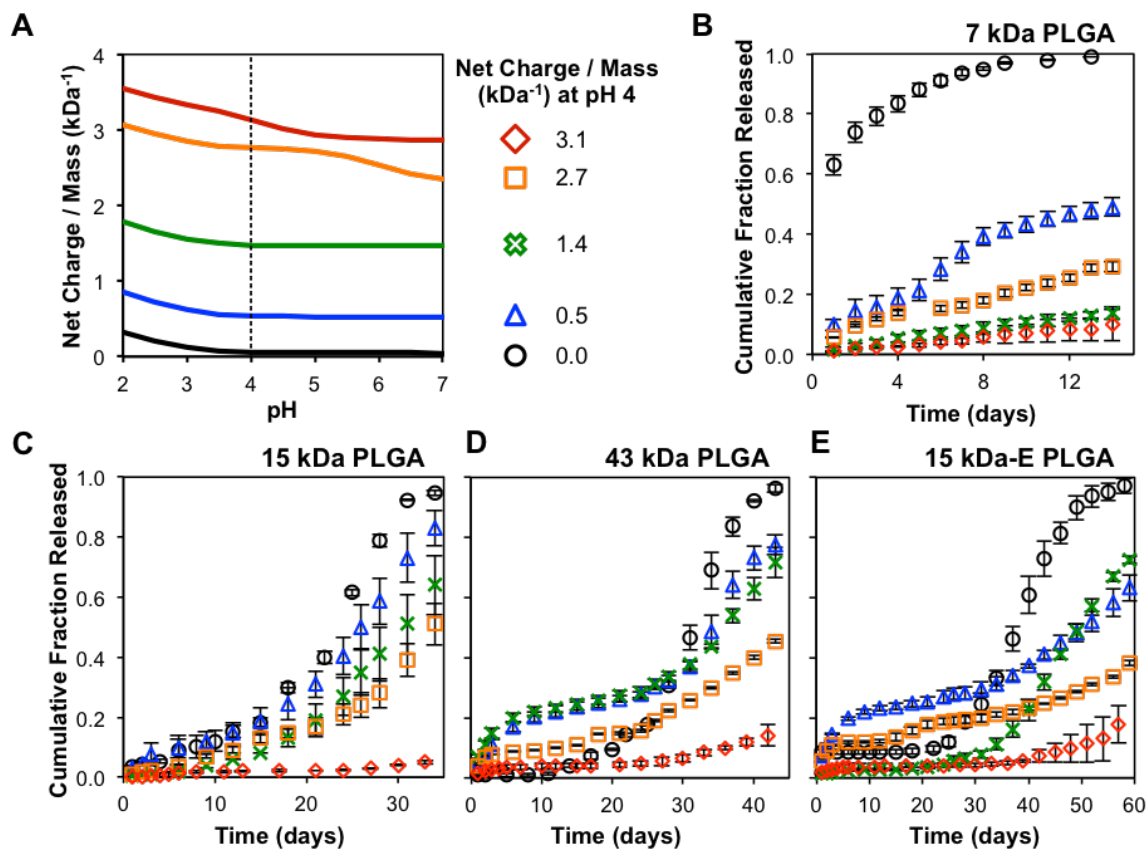


Figure 2-4. Greater net positive charge on a peptide corresponds with slower release kinetics from negatively charged PLGA matrices. (A) Calculated net charge per mass, as a function of pH, for five peptides with similar molecular weights (2.3 ± 0.2 kDa). (B-E) *In vitro* release kinetics for those five peptides, encapsulated in microparticles with different PLGA molecular weights and end-groups: (B) 7 kDa, (C) 15 kDa, (D) 43 kDa, (E) ester-capped 15 kDa-E. Release profiles are truncated at time points corresponding to complete release for the neutral peptide (black circles).

Compared to the neutral peptide, positively charged peptides released more slowly from all PLGA polymers (Figure 2-4B-E). For the peptide with the greatest net positive charge per mass ($+3.1 \text{ kDa}^{-1}$), release was most significantly impeded. In fact, less than 20 percent of the encapsulated cationic ($+3.1 \text{ kDa}^{-1}$) peptide was released by the time at which microparticles had degraded sufficiently to release nearly 100 percent of the neutral peptide. For each formulation,

nearly 100 percent of the total peptide encapsulated was eventually detected; however, for comparison, release profiles graphed in Figure 2-4 were cut off when the neutral peptide had completely released. As shown in Figure 2-2, complete release of the neutral peptide ranged from approximately two weeks for the 7 kDa PLGA to more than 8 weeks for the ester-capped 15 kDa PLGA microparticles. Notably, we observed inverse correlations between peptide charge and release rate for each polymer formulation (summarized in Figure 2-5). These trends are especially consistent for each of the uncapped PLGA polymers; however, release from the ester-capped PLGA appears to be somewhat less dependent on peptide charge. This may be due to the fact that with minimal electrostatic interactions or acylation, the maximum rate of release from the slower degrading ester-capped PLGA is less than that for the uncapped polymers (3.8% vs. 6.6-6.9% of total peptide encapsulated per day). Counter to the trends described above, the +0.5 kDa⁻¹ and +1.4 kDa⁻¹ peptides released slightly faster than the neutral peptide from 43 kDa and/or ester-capped 15 kDa PLGA microparticles, during days 3-9 (Figure 2-4D-E). These minor anomalies may be attributed to a combination of factors, including slight differences in particle size, peptide size, peptide loading, or peptide distribution within the microparticles. Additionally, since the neutral peptide is somewhat less hydrophilic than the positively charged peptides, it may exhibit greater hydrophobic interactions with the more hydrophobic (higher molecular weight or ester-capped) PLGA microparticles. Overall, the results of these release studies demonstrate that the amount of positive charge on peptides can influence their release kinetics dramatically, regardless of polymer formulation, and greater peptide charge contributes to slower release.

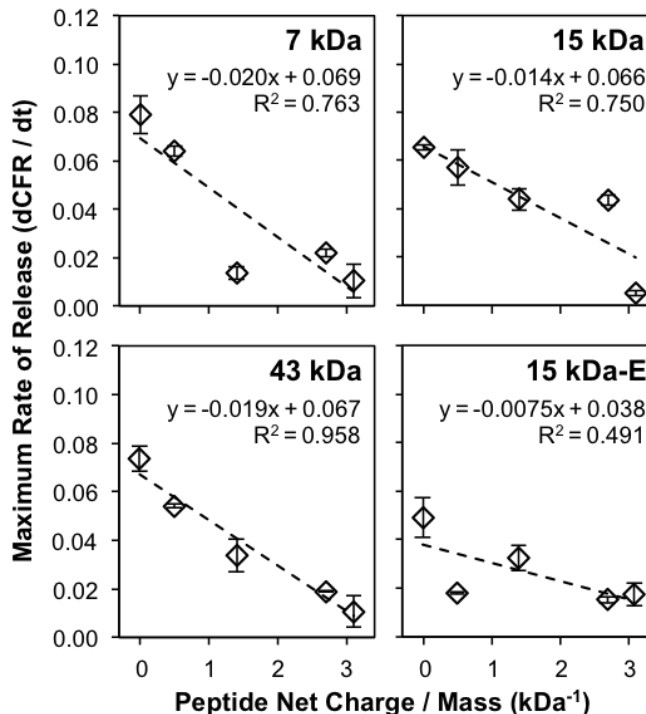


Figure 2-5. Correlations between peptide charge and release rates from PLGA microparticles. Data represent maximum release rates for each microparticle formulation in Figure 2-4, grouped by polymer molecular weight. The maximum rate of release (i.e. the maximum $d(\text{Cumulative Fraction Released})/dt$, or $d\text{CFR}/dt$) typically follows the lag phase, and any initial burst is not considered. $d\text{CFR}/dt = 0.1$ corresponds to a rate of 10 percent of total release per day.

2.3.4 Polymer chemistry influences intraparticle pH during degradation

Previous studies have noted that pH within degrading PLGA microparticles is acidic and dynamic, decreasing over time as more carboxylic acid end groups are produced by progressive hydrolysis of the PLGA backbone [107, 123, 125]; however, the effects of polymer initial molecular weight and end-group chemistry on intraparticle pH have not been examined. Changes in pH during particle degradation, or differences in intraparticle pH among polymer formulations, would have nominal effects on net charge of the aforementioned five peptides

(Figure 2-4A) since they are composed of uncharged and basic residues (positive at $\text{pH} < 7$). However, for peptides with a greater frequency of both acidic and basic residues, net charge would vary greatly depending on the pH of the surrounding microenvironment (for $\text{pH} < 7$), and could even switch from negative to positive as pH drops. More acidic intraparticle pH could also catalyze peptide acylation reactions [115].

In order to determine the dynamic charge of such peptides, we first measured bulk intraparticle pH of four different PLGA microparticle formulations incubating in PBS for up to three weeks (Figure 2-6A). Comparison of intraparticle pH in the different microparticles illustrates the dramatic impact of PLGA initial molecular weight and end group chemistry on the evolution of intraparticle pH . For microparticles made of higher molecular weight or ester-capped PLGA, intraparticle pH was higher initially and decreased more gradually. Average initial intraparticle pH (after 1 hour of incubation in PBS) was 6.0 and 5.9 for the 43 kDa and ester-capped 15 kDa PLGA microparticles, compared to 4.5 and 3.6 for the lower molecular weight, uncapped polymers (7 and 15 kDa). Intraparticle pH of the 7 kDa PLGA microparticles dropped considerably to 3.3 by day 3 and gradually decreased to a minimum of 2.2 by day 12. The 15 kDa PLGA microparticles exhibited a similar decrease in pH to a minimum of 2.4 by day 18. In contrast, microparticles comprised of 43 kDa or ester-capped 15 kDa PLGA polymers had more moderate drops in intraparticle pH to 3.2 or 3.4 by day 21 (Figure 2-6A). Lower intraparticle pH for 7 and 15 kDa PLGA microparticles was accompanied by marked decreases in supernatant pH to 3.5 (7 kDa, day 12) and 4.1 (15 kDa, day 18) (Figure 2-6B). In contrast, supernatant pH for the 43 kDa and ester-capped 15 kDa PLGA microparticles never dropped below 5.7 or 6.4, respectively, after 21 days (Figure 2-6B). Collectively, the intraparticle pH measurements suggest that agents encapsulated in PLGA microparticles with different polymer

chemistry (molecular weight and end-groups) would experience microenvironments with different pH.

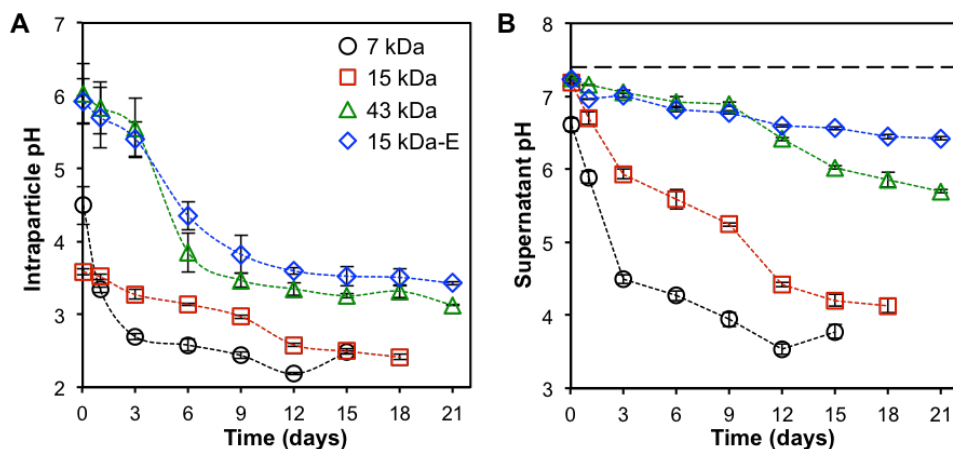


Figure 2-6. Intraparticle pH and supernatant pH are dynamic and depend on PLGA initial molecular weight and degradation rate. (A) Intraparticle pH measurements for microparticles made of 7 kDa (black circles), 15 kDa (red squares), 43 kDa (green triangles), or ester-capped 15 kDa-E PLGA (blue diamonds). (B) Corresponding measured supernatant pH for the microparticle formulations. Dashed line at pH 7.4 represents the pH of PBS. Data represent mean \pm SD for 3-6 independent samples.

2.3.5 Release of pH-sensitive peptides depends on intraparticle pH

To investigate the effects of pH-dependent peptide charge on release kinetics, we identified a fluorescently labeled peptide (“CK1sub”) with a low isoelectric point (pI 4.16) that falls within the range of intraparticle pH observed in degrading PLGA microparticles (Figure 2-6A). Net charge of this peptide—and others that contain abundant acidic (Asp, Glu) and basic (Arg, Lys, His) amino acid residues—depends greatly on pH, and transitions from negative to positive as pH drops below its isoelectric point (Figure 2-7A). Based on intraparticle pH measurements (Figure 2-6A) and CK1sub’s pH-dependent charge (Figure 2-7A), we were able to estimate its net charge over time in the various polymer formulations. Notably, the lower initial intraparticle

pH for uncapped 15 kDa PLGA microparticles, relative to ester-capped 15 kDa PLGA microparticles (Figure 2-6A), contributed to striking differences in peptide charge during the initial week of release (Figure 2-7B). Specifically, initial net charge of the CK1sub peptide was predicted to be positive in uncapped PLGA (Figure 2-7B, red), due to the lower initial intraparticle pH, but negative in ester-capped PLGA (Figure 2-7B, blue), due to the higher initial pH. Accordingly, we hypothesized that CK1sub would exhibit greater early release from ester-capped PLGA than from uncapped PLGA, due to fewer electrostatic interactions with the polymer matrix. As predicted, release profiles indicated accelerated early release kinetics and greater initial burst from ester-capped PLGA when compared to uncapped PLGA (Figure 2-7C). This result was consistent with our hypothesis, but could otherwise appear to be counterintuitive under the expectation that the more hydrophobic, slower degrading, ester-capped polymer would produce slower release [126]. Similar results for another pH-dependent peptide (beta-amyloid “BA17”) with a low isoelectric point (pI 5.75) corroborate the trends in release we observed for CK1sub: BA17 also exhibited greater initial burst from ester-capped vs. uncapped PLGA (Figure 2-7).

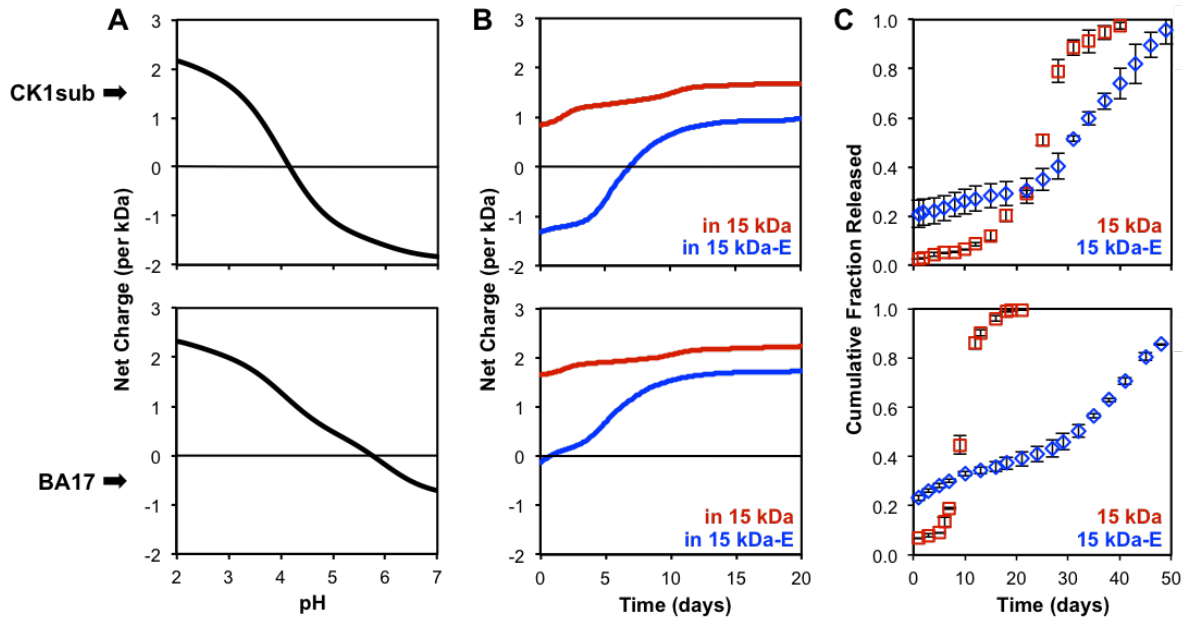


Figure 2-7. Initial burst of pH-dependent peptides is influenced by initial charge, which depends on initial pH of the microenvironment in hydrated microparticles. (A) Net charge as a function of pH (normalized to peptide mass) for CK1sub and BA17 peptides, which have low isoelectric points ($pI < 6$) and pH-dependent charge. (B) Temporally dynamic net charge estimates for peptides encapsulated in uncapped (red) or ester-capped (blue) 15 kDa PLGA microparticles. Charge predictions are based on intraparticle pH measurements and pH-dependent peptide charge. (C) Cumulative release profiles for peptides encapsulated in uncapped (red squares) or ester-capped (blue diamonds) 15 kDa PLGA microparticles, showing greater early release from ester-capped PLGA microparticles.

For all peptides studied (pH dependent and independent), we observed distinct inverse correlations between initial burst (fraction released within the first 24 hours) and initial peptide charge within certain PLGA matrices (Figure 2-8). When encapsulated in 7 kDa or ester-capped 15 kDa PLGA microparticles, peptides with negative initial net charge (Figure 2-8, data points in grey regions) exhibited greater burst release than those with positive net charge. This suggests that initial burst of positively charged peptides is inhibited by electrostatic interactions with these polymer matrices. Since the initial intraparticle pH for uncapped 15 kDa PLGA microparticles (pH 3.6, Figure 2-6A) was below the isoelectric points of all peptides (see Figure 2-4A and

Figure 2-7A), none of these peptides were negatively charged when encapsulated in these microparticles. This includes the pH-dependent peptides (BA17 and CK1sub, identified by arrows in Figure 2-8), which though negatively charged in the ester-capped 15 kDa PLGA microparticles, were positively charged in uncapped 15 kDa PLGA microparticles. Consequently, minimal initial burst of all peptides from uncapped 15 kDa PLGA microparticles can be attributed to electrostatic interactions with the polymer matrix. On the other hand, minimal initial burst of all peptides from 43 kDa PLGA microparticles (Figure 2-8), including those with negative or neutral initial charge, suggests that peptides are retained in these microparticles by physical barriers (i.e. a less permeable matrix). This result is consistent with previous reports that initial burst is influenced by polymer molecular weight, with less initial burst from higher molecular weight polymers [126]. In fact, for negatively charged peptides, burst release decreased with increasing polymer molecular weight, or decreasing matrix permeability (Figure 2-8, left to right). Specifically, initial burst of negatively charged peptides was 60-80%, 20-30%, and <10% for uncapped 7 kDa, ester-capped 15 kDa, and uncapped 43 kDa PLGA microparticles, respectively (Figure 2-8). Taken together, these results suggest that burst release depends on both electrostatic interactions and matrix permeability, and negatively charged peptides exhibit significantly greater initial burst than positively charged peptides, from polymer matrices with sufficient initial permeability.

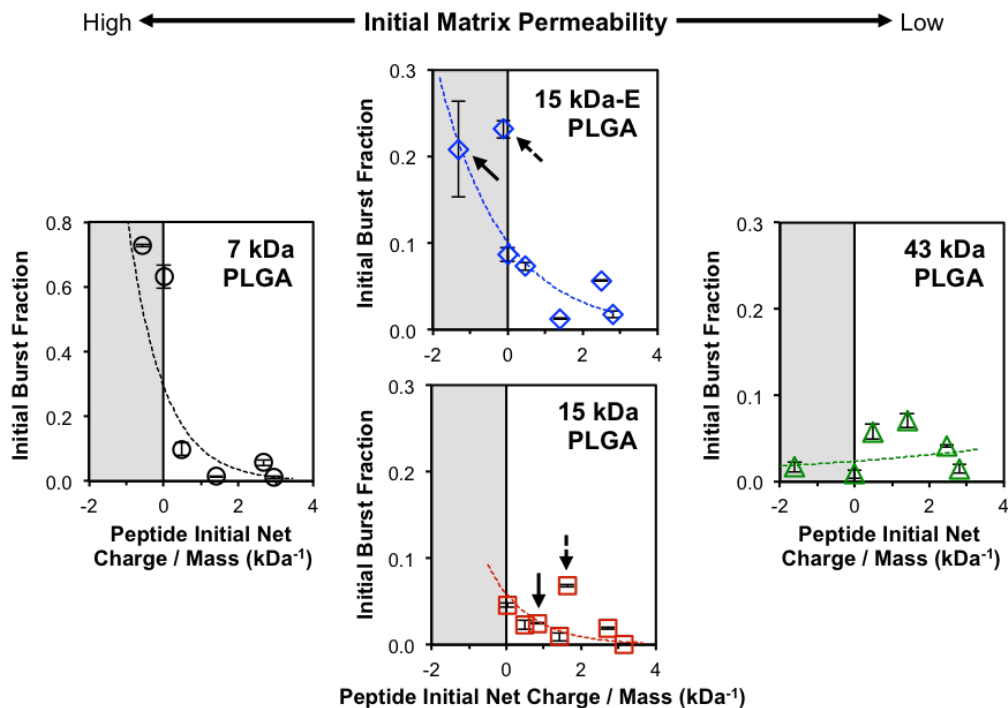


Figure 2-8. Magnitude of initial burst is influenced by initial peptide charge. Peptide release in the first 24 hours (initial burst) is presented as a fraction of total peptide encapsulated for all controlled release formulations, including those for positively charged peptides (from **Figure 2-4**) and pH-dependent peptides (from **Figure 2-7**). Each peptide's initial net charge is estimated using initial intraparticle pH measurements and the peptide's charge vs. pH relationship. Arrows identify pH-dependent CK1sub (solid) and BA17 (dashed) peptides, which are positively charged in uncapped 15 kDa PLGA (red), but negatively charged in ester-capped 15 kDa PLGA (blue). Peptides in the grey regions would have minimal electrostatic interactions with the negatively charged PLGA matrix, but may be retained physically by less permeable matrices associated with higher molecular weight polymers [114, 126].

2.3.6 Influence of electrostatic interactions on release of larger biomolecules

To determine whether the effects of electrostatic interactions and/or acylation reactions between positively charged agents and negatively charged PLGA microparticles extend to larger biomolecules, we examined release kinetics of several therapeutically relevant proteins and oligonucleotides (8 to 43 kDa molecular weight). Specifically, we compared release kinetics of

proteins with greater positive charge density (CCL21, CCL22, and TGF- β 1) to release kinetics of two less positively charged proteins (ovalbumin and IL-2), or an oligodeoxynucleotide (ODN; STAT3 cyclic decoy [118]) with net negative charge. For each of the six biomolecules, net charge (per mass) across a range of intraparticle pH (2 to 7) is presented in Figure 2-9A. CCL21, CCL22, and TGF- β 1, with high isoelectric points (pI 8.2-10.4), are positively charged at any intraparticle pH. In contrast, ovalbumin and IL-2 (pI 5.0 and 4.7) have net charge that shifts from negative to neutral to positive with a drop in intraparticle pH. Even at pH 2, CCL21 and CCL22 have approximately twice the positive charge per mass as ovalbumin and IL-2 (Figure 2-9A).

When encapsulated in 7 kDa PLGA microparticles, positively charged CCL22 released considerably slower than neutral/negative ovalbumin (Figure 2-9B), even though CCL22 is five times smaller than ovalbumin. Similarly, when encapsulated in 15 kDa PLGA microparticles, positively charged TGF- β 1 released substantially slower than ovalbumin (Figure 2-9C), again despite the fact that TGF- β 1 is smaller than ovalbumin. Even in the case of initially porous microparticles, which may have faster release kinetics due to greater accessibility of the encapsulated agent to the release media [127], positive charge on an encapsulated biomolecule seemed to considerably decrease the release rate. For example, release of IL-2 from porous 15 kDa PLGA microparticles was substantially faster than release of CCL22 from similar microparticles (Figure 2-9D). For both formulations, comparable porosity was achieved by adjusting the osmolality between the inner and outer aqueous phases of the double emulsions (+30 mM ions in inner aqueous phase) [120, 121]. Notably, 73% of IL-2 released in an initial burst, compared to only 14% of CCL22. Finally, release of CCL21 was substantially slower than that of a STAT3 cyclic decoy ODN from nonporous 15 kDa PLGA microparticles (Figure 2-9E). Taken together, these four examples suggest that charge density on larger biomolecules can also

contribute to release kinetics, with slower release of more positively charged biomolecules from similar PLGA microparticles.

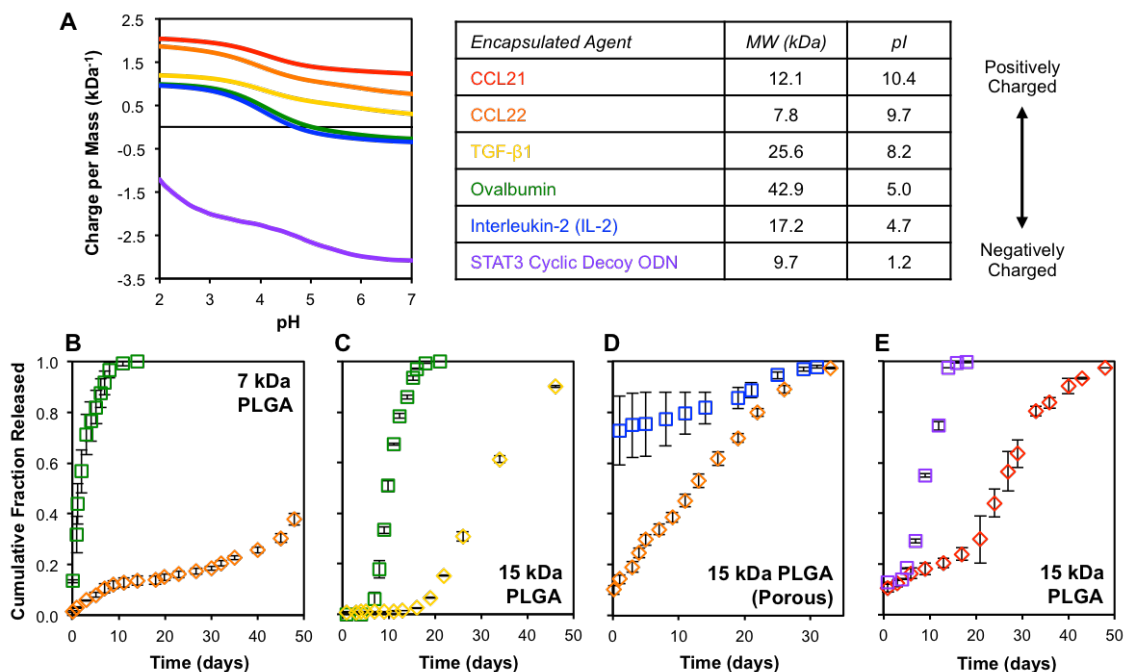


Figure 2-9. PLGA microparticles release more positively charged proteins slower than biomolecules with less positive charge. (A) Plot of net charge density as a function of pH for each protein or oligodeoxynucleotide (ODN), and table showing agent molecular weight (MW) and isoelectric point (pI). (B-E) Cumulative release profiles for (B) ovalbumin vs. CCL22, (C) ovalbumin [128] vs. TGF- β 1 [121], (D) IL-2 [121] vs. CCL22 [120], and (E) STAT3 ODN vs. CCL21. For each comparison, both biomolecules were encapsulated in comparable PLGA microparticle formulations, fabricated from the indicated PLGA. Microparticles were non-porous, unless otherwise indicated.

2.4 DISCUSSION

For agents encapsulated within a biodegradable polymer matrix, both physical barriers to diffusion (i.e. impermeable regions of surrounding polymer) and electrostatic or covalent interactions between the agent and matrix may contribute to sustained release kinetics.

Numerous previous studies have identified key properties of polymer matrices that influence release behavior (reviewed in [99] and [107]), and mathematical models have been used to predict release kinetics based on such factors, which include matrix geometry, polymer chemistry, and molecular weight of the encapsulated agent [101, 102]. Such parameters dictate the timeframe of matrix erosion and the extent of erosion needed for an encapsulated agent to diffuse out of the matrix, based on the molecular weight of the agent. For example, a matrix comprised of higher molecular weight and/or slower degrading PLGA generally takes longer to become sufficiently permeable for release (as in Figure 2-2), and larger encapsulated agents (e.g. acylated peptide-PLGA adducts or fluorescently labeled peptides, relative to unlabeled native peptides) generally require formation of larger interconnected pores. Electrostatic interactions and acylation reactions between cationic therapeutic agents and negatively charged polymeric delivery systems have also been cited as factors affecting release kinetics [108, 115, 116]. A few studies have even shown that adsorption/desorption of certain cationic proteins or peptides to/from the surfaces of PLGA constructs depends on negative charge density of the polymers. For example, the amount of BMP-2 (positively charged growth factor) adsorbed to the surface of porous PLGA microparticles was directly related to the negative charge density of the PLGA polymer [129]. Furthermore, “release” (i.e. desorption) of BMP-2 was most prolonged through the use of low molecular weight, acid-terminated PLGA, which had the greatest negative charge density [129]. Another recent study showed that therapeutic cationic peptides could be sustainably “released” from the surface of low molecular weight, acid-terminated PLGA microparticles and films for more than two weeks [114]. In both of these studies, the PLGA constructs were soaked in

solutions of a particular cationic protein or peptide, so sustained “release” was entirely due to prolonged surface desorption resulting from agent-polymer electrostatic interactions. Additionally, these studies investigated the effects of polymer matrix charge density on “release,” rather than the influence of the amount of positive charge on the peptide or protein [114, 129].

Accordingly, in the studies presented in this chapter, we investigated the influence of peptide charge on release kinetics from a given PLGA formulation. Here, the peptides were encapsulated within PLGA microparticles by a common emulsion-solvent evaporation method, instead of being sorbed to the surface of pre-fabricated PLGA constructs. Compared to surface sorption, encapsulation of peptides within PLGA microparticles generally enables release for longer periods of time (depending on the polymer), and may better protect peptides from enzymatic degradation *in vivo* [130, 131]. Encapsulation, as opposed to surface sorption, also means that release kinetics would be influenced both by erosion of the surrounding polymer matrix and by peptide-polymer electrostatic interactions. Specifically, as a polymer matrix becomes sufficiently porous and diffusion is no longer physically constrained, we hypothesized that release would be hindered by peptide-polymer interactions, in proportion to the positive charge (per mass) of the peptide. Indeed, we observed striking inverse correlations between net positive charge on a peptide and release rates (following the lag phase) from all polymers, including high molecular weight and ester-capped PLGAs (Figure 2-4 and Figure 2-5). Notably, since peptide release was detected by fluorescence, native peptide and acylated peptide-PLGA adducts in release media are not differentiated (as by HPLC-MS [115]). Therefore, this study does not specifically distinguish between contributions of

electrostatic interactions and peptide acylation to slower release kinetics for more positively charged peptides.

Attention to electrostatic or covalent interactions between charged peptides and polymers could also give key insight into new strategies to achieve desired release kinetics. For instance, whereas fast release of uncharged agents would traditionally be achieved with fast degrading, acid-terminated, low molecular weight polymers (as in Figure 2-2), such polymers substantially delay release of positively charged agents (as in Figure 2-4B and Figure 2-9B), due to agent-polymer interactions. Therefore, faster release of cationic peptides and proteins might be accomplished instead by using very low molecule weight ester-capped PLGA. Although ester-capped PLGA degrades more slowly than uncapped PLGA of similar molecular weight [124], it would exhibit less negative charge, and thus reduced interactions with cationic agents. Furthermore, rapid bulk erosion of the polymer matrix, due to the low initial molecular weight, would translate to fewer physical barriers to egress of encapsulated agents. Despite the fact that PLGA has a proven track record with the FDA, and is therefore widely used, alternate biodegradable polymers with neutral or positive charge (e.g. polyketals [132], polyphosphazenes [133], or poly(β amino esters) [122]) may actually be used to enable faster release of cationic agents, or more sustained release of anionic agents. Finally, co-encapsulation of excipients that would neutralize electrostatic interactions between PLGA and cationic peptides may accelerate release kinetics. For example, inorganic divalent cations (e.g. Ca^{2+} or Mn^{2+}) have been shown to reduce adsorption of a cationic peptide on the surface of acid-terminated PLGA, as well as subsequent acylation reactions [111, 117]. Alternatively, polyanionic excipients (e.g. chondroitin sulfate [134]) that complex

with cationic peptides could also reduce peptide-polymer electrostatic interactions and permit faster release by masking the positive charge of the peptide.

While the aforementioned approaches to tune release kinetics involve altering properties of the delivery system, correlations between agent charge and release kinetics could also motivate novel ways to control release by modifying the encapsulated agent itself. Desired release kinetics for a given agent are traditionally attained by selecting a polymer with a particular combination of initial molecular weight, hydrophobicity (end-group chemistry), and lactide to glycolide ratio. Unfortunately, polymers chosen for preferable release rates may not have ideal physical properties for the intended application. Since the amount of positive charge on a peptide influences its rate of release from each polymer (Figure 2-4 and Figure 2-5), chemical modification of therapeutic agents to increase or reduce positive charge could prolong or accelerate release from any polymer chosen for its physical properties. For peptides and proteins, various chemical modifications (acetylation, methylation, PEGylation, aminoalkylation, etc.) have been used to increase half-life, or alter bioavailability, bioactivity, and solubility. Addition or deletion of charged amino acids (without altering protein function), or modification of charged residues can eliminate or enhance positive or negative charge (and acylation targets, such as primary amine groups), and the degree of modification can be controlled by reagent stoichiometry [135]. Just as chemical modification of proteins has been used to study effects of protein surface charge on self-assembly with gold nanoparticles [136], modification of peptides and proteins may also be used to tune release kinetics from a given polymer.

In contrast to invariant net charge of some cationic peptides, net charge of some peptides with low isoelectric points is a function of the pH of the local microenvironment (Figure 2-7A). Previous studies have noted inverse relationships between “acid number” (a measure of carboxylic acid content of a polymer) and PLGA molecular weight or end-group chemistry [129, 137]. Here, we show that initial polymer chemistry also dictates evolution of bulk intraparticle pH during microparticle degradation (Figure 2-6A). Specifically, higher molecular weight (43 kDa) and ester-capped PLGA microparticles have higher initial intraparticle pH and more gradual decreases in pH than lower molecular weight uncapped PLGA (Figure 2-6A). Importantly, pH within microparticles degrading *in vivo* may differ from that measured *in vitro*, due to differences in external volume, buffering capacity of interstitial fluid, and the presence of enzymes that contribute to PLGA degradation *in vivo*. Still, understanding the dynamic intraparticle microclimate enables estimates of peptide charge, which in turn could explain unconventional release kinetics. For example, without peptide-polymer interactions, we would expect faster release and greater initial burst from more hydrophilic uncapped PLGA, due to faster hydration and degradation [126]. Instead, some peptides have greater early release from ester-capped PLGA microparticles (Figure 2-7), likely due to higher intraparticle pH and resultant less positive peptide charge. Since acylated peptide adducts form over the course of particle degradation, and not during particle fabrication [116], initial burst release may not be influenced by peptide acylation; however, faster evolution of more acidic intraparticle pH in some PLGA microparticles (Figure 2-6) may promote greater acylation and contribute to slower release at later time points, since acylation reactions are catalyzed by acidic pH [115].

It is worth noting that measurements of bulk intraparticle pH may overestimate acidity near the particle surface, since radial pH gradients exist in microparticles [125, 138, 139]. This could translate into slight overestimates of net charge for pH-dependent peptides (Figure 2-7B), especially near the surface of microparticles. Microclimate pH near the particle surface is, however, likely still lower than external supernatant pH, since continuous ester hydrolysis generates tethered carboxylic acid groups at the matrix surface faster than associated protons can diffuse away with buffer salt counterions. This is evidenced by the presence of radial pH gradients in well-hydrated matrices, which would be permeable to buffer salts from external media [125, 138, 139]. Additionally, since peptides are initially sorbed to dry PLGA matrix (before hydration), pre-sorbed peptides may compete with incoming buffer salts for the protons associated with tethered carboxylic acid groups on the matrix.

Differences in early release from uncapped and ester-capped PLGA microparticles (Figure 2-7C) could also be attributed in part to competing electrostatic interactions within a single peptide, between multiple peptides, or between a peptide and the PLGA matrix. In a somewhat less acidic microclimate, the pH-dependent peptides would contain both unprotonated acidic residues (negatively charged) and protonated basic residues (positively charged). Negative or neutral *net* charge (due to more acidic residues) could mask the fact that positively charged residues may interact electrostatically with negatively charged residues from the same or nearby peptides, or with the negatively charged PLGA matrix. In a matrix with less negative charge density (e.g. ester-capped PLGA), electrostatic interactions among peptides might dominate, whereas in a matrix with greater negative charge density (e.g. uncapped PLGA),

electrostatic interactions between peptides and the matrix might be dominant. This competition for electrostatic interactions could contribute to faster release of CK1sub peptide from ester-terminated PLGA, relative to uncapped PLGA (Figure 2-7C). In terms of cationic peptides with few acidic residues (e.g. +3.1/kDa peptide), less intra- and inter-peptide electrostatic interactions may allow peptide-PLGA interactions to dominate, resulting in impeded release even from ester-capped PLGA with less negative charge density (Figure 2-4E).

Admittedly, peptide-polymer electrostatic interactions are not the only factor that influences early release kinetics. For example, greater initial burst for peptides with initial negative charge from low molecular weight 7 kDa PLGA microparticles and minimal burst of those peptides from 43 kDa PLGA microparticles (Figure 2-8) may be attributed to greater matrix permeability of microparticles made of the lower molecular weight 7 kDa PLGA. This notion is consistent with a previous report indicating that peptides can penetrate hydrophilic (acid-terminated), low molecular weight PLGA to a much greater extent than higher molecular weight PLGA, which lacks sufficiently mobilized polymer chains [114]. It is also supported by our observation of initial higher intraparticle pH and lower supernatant pH for 7 kDa, relative to 15 kDa, PLGA microparticles (Figure 2-6), which indicates a substantial number of acidic PLGA polymer chains may be able to diffuse out of the 7 kDa PLGA microparticles upon hydration. We expect this is due to the lower initial molecular weight PLGA having more polymer chains below the critical molecular weight for water solubility (~1050 Da [140]).

In the past decade, research (by our lab and others) has focused on controlled delivery of chemokines, cytokines, protein antigens, and growth factors from polymeric

microparticles and scaffolds, with numerous therapeutic applications [120, 121, 128, 130, 141, 142]. Notably, many of these proteins have significant positive charge at varying intraparticle pH (Figure 2-9A and Table 2-5), which could contribute to impeded release from negatively charged polymeric delivery systems. Comparisons of release kinetics for several proteins and oligonucleotides with different net charge profiles (Figure 2-9) suggest that, as with smaller peptides, release of larger biomolecules is impacted by electrostatic interactions. Specifically, a high degree of net positive charge on proteins (e.g. CCL21, CCL22, and TGF- β 1) considerably slows their release, even from porous microparticles, which have pre-established pathways for release of even large encapsulated agents. In contrast, proteins and oligonucleotides with less positive charge or negative charge tend to release faster from microparticles with similar formulation characteristics. Overall, our observations of early release kinetics for peptides and release of larger biomolecules are consistent with anecdotal reports of greater initial burst for proteins with lower isoelectric points (i.e. those that could have initial net negative charge within some PLGA microparticles). For example, Lee et al. noted 20-50 percent initial burst of insulin (pI 5.4), compared to less than 10 percent initial burst for VEGF (pI 8.5), both encapsulated in 10 kDa PLGA microparticles [143]. Therefore, we expect examination of protein charge vs. pH relationships and prediction of dynamic intraparticle pH will lead to better design of formulations to achieve desired release kinetics for a wide variety of peptide and protein therapeutics, including those in Table 2-5. Furthermore, agent-polymer charge interactions may have an even greater impact on release of positively charged small molecule drugs, which may have greater charge density (e.g. gentamicin +10.5/kDa, metformin +15.5/kDa, or olanzapine +6.1/kDa at pH 3). The

small size of these drugs would allow them to diffuse more freely through a given polymer matrix, so considerable positive charge density could have a more striking impact on impeding release. Finally, drug analogs with added positive charge may enable more sustained release of small molecules, for which even very high molecular weight, slow degrading polymers may not serve to sufficiently sustain release.

Table 2-5. Therapeutic peptides and proteins with positive or variable net charge.

<i>Protein / Peptide</i>	<i>NCBI / Drug Bank Accession (residues)</i>	<i>M_w (kDa)</i>	<i>pI</i>	<i>Charge per kDa</i>	
				<i>pH 5</i>	<i>pH 3</i>
CXCL10 (IP-10)	P02778 (22-98)	8.6	10.7	+1.38	+1.95
CXCL12 (SDF1 α)	P48061 (22-89)	8.0	10.3	+1.42	+1.87
bFGF	P09038 (143-288)	16.4	9.9	+0.88	+1.64
PDGF-BB (dimer)	P01127 (82-190)	24.6	9.3	+0.83	+1.51
TGF- β 1 (dimer)	P01137 (279-390)	25.6	8.2	+0.59	+1.13
BMP-2 (dimer)	P12643 (283-396)	25.8	7.9	+0.67	+1.41
IL-12p40	P29460 (23-328)	34.7	5.3	+0.07	+1.13
GM-CSF	P04141 (18-144)	14.5	5.0	0.00	+0.97
EGF	P01133 (971-1023)	6.2	4.6	-0.20	+1.02
Exenatide	DB01276	4.2	4.5	-0.30	+0.91
Enfuvirtide	DB00109	4.5	4.1	-0.70	+0.62
Thymalfasin	DB04900	3.1	4.0	-1.27	+1.14

2.5 CONCLUSIONS

We have identified pronounced, inverse correlations between positive net charge on peptides and the rates of release from PLGA microparticles. Our empirical measurements of intraparticle pH demonstrate considerable influence of PLGA chemistry, with less acidic microenvironments present in higher molecular weight or ester-capped PLGA microparticles. Such information

enabled estimates of peptide charge in degrading PLGA microparticles, which suggest that initial net charge of certain peptides (with low isoelectric points) may be negative in ester-capped PLGA, but positive in uncapped PLGA. This could explain the otherwise counterintuitive, faster early release from the slower degrading ester-capped PLGA microparticles, relative to faster degrading uncapped PLGA microparticles. By demonstrating that our results with model peptides extend to larger biomolecules (proteins and oligonucleotides), we underscore the importance and broad relevance of agent-polymer charge interactions to the field of controlled release. Finally, we expect that these trends between biomolecule charge and release kinetics will improve future design of controlled release formulations for a wide range of therapeutically relevant peptides and proteins, and may be incorporated into mathematical models of controlled release to improve their predictive capacity.

2.6 IMPLICATIONS FOR DELIVERY OF TREG-INDUCING FACTORS

As mentioned in Chapter 1.4.1, our lab previously demonstrated *in vitro* Treg induction using TRI MPs, which sustain release of TGF- β 1 (a positively charged protein), rapamycin (a small molecule), and IL-2 (a negatively charged protein) [121]. Results of studies presented in this chapter suggest that the initial two-week lag in release of TGF- β 1 [121], which was unexpected given existing predictive models of release from biodegradable PLGA MPs [99, 101, 102], may be attributed to protein-polymer electrostatic interactions. Based on our previous understanding of factors affecting release kinetics (independent of charge), re-formulating TGF- β 1 MPs to eliminate the lag phase would have involved using a lower molecular weight PLGA; however, since TGF- β 1 is cationic, the lessons from this chapter indicate that a lower molecular weight

polymer would likely lead to more electrostatic interactions and slower release kinetics. Therefore, we instead used a blend of ester-terminated PLGA and PEG-PLGA di-block copolymer to increase the hydrophilicity and rate of hydration, while also decreasing electrostatic interactions between the particle matrix and encapsulated TGF- β 1. The next chapter describes these new PEG-PLGA TRI MP formulations and their therapeutic application in acute murine models of allergic contact dermatitis.

3.0 BIOMIMETIC DELIVERY OF TREG-INDUCING FACTORS WITH MICROPARTICLES PROMOTES IMMUNE TOLERANCE AND SUPPRESSES ALLERGIC CONTACT DERMATITIS †

As discussed in Chapter 1.1.2, corticosteroids typically used to treat allergic contact dermatitis (ACD) act transiently and non-specifically, but ultimately fail to address the underlying allergen-specific adaptive immune responses or prevent future allergic reactions [6]. In this chapter, we present the first of two approaches to “re-educate” the immune system by conveying immunological context that directs tissue-protective tolerogenic responses to contact allergens, rather than destructive pro-inflammatory ones. Specifically, this therapeutic approach involves using **TReg-Inducing** “TRI” microparticles (MPs) to condition the local skin draining lymph node (DLN) microenvironment to promote induction of allergen-specific Tregs in murine models of ACD. These TRI MPs, which partially mimic the Treg-inducing function of tolerogenic DCs by providing sustained release of TGF- β 1 and IL-2 (and rapamycin), are similar to formulations previously shown by our group to induce Treg differentiation *in vitro* [121]. With insight from the studies in Chapter 2 [144], the current MP formulations were engineered to provide short-term (~1 week) sustained release of all three factors, and eliminate the extended lag-phase of the original TGF- β 1 MPs that required pre-incubation before use [121]. Here, we demonstrate that

† This chapter is adapted from Balmert SC, Donahue C, Vu JR, Falo LD, and Little SR. In vivo induction of regulatory T cells promotes allergen tolerance and suppresses allergic contact dermatitis. *Journal of Controlled Release* (2017) 261:223-33, with permission from Elsevier.

these new TRI MPs expand Treg populations and reduce effector T-cell populations in acute murine models of hapten- and protein-mediated ACD. Furthermore, *in vivo* Treg-induction with TRI MPs effectively suppresses delayed-type hypersensitivity (DTH) responses and protects skin from subsequent allergen exposures.

3.1 MATERIALS AND METHODS

3.1.1 Mice

Female C57BL/6 and congenic CD45.1 B6 (B6.SJL-*Ptprc*^a *Pepc*^b/BoyJ) mice were purchased from The Jackson Laboratory (Bar Harbor, ME) and used at 8-12 weeks of age. OVA TCR-transgenic B6 Rag1^{-/-} OT-I (B6.129S7-Rag1^{tm1Mom} Tg(TcraTcrb)1100Mjb) and B6 Rag2^{-/-} OT-II (B6.129S6-Rag2^{tm1Fwa} Tg(TcraTcrb)425Cbn) mice were purchased from Taconic (Rensselaer, NY). All mice were maintained under specific pathogen-free conditions at the University of Pittsburgh, and experiments were conducted in accordance with institutional animal care and use committee guidelines.

3.1.2 Microparticle Fabrication

Poly(ethylene glycol)-poly(lactic-co-glycolic acid) (PEG-PLGA) microparticles (MPs) were fabricated using an emulsion-solvent evaporation method [93]. A 2.5% (wt/vol) polymer solution was prepared by dissolving 40 mg mPEG-PLGA (5 kDa PEG:20 kDa PLGA; PolySciTech, West Lafayette, IN) and 160 mg ester-capped PLGA (14 kDa for IL-2 MP and

Rapa MP or 40 kDa for TGF- β 1 MP, 50:50 LA:GA; Sigma Aldrich, St. Louis, MO) in 8 mL dichloromethane. For IL-2 and TGF- β 1 MPs, 5 μ g of recombinant protein (rmIL-2 from R&D Systems, Minneapolis, MN; or rhTGF- β 1 from PeproTech, Rocky Hill, NJ) was dissolved in 200 μ L deionized water (diH₂O), added to the organic polymer phase, and sonicated at 25% amplitude for 10 sec (Vibra-Cell, Newton, CT). For Rapa MPs, 1.5 mg rapamycin (Alfa Aesar, Ward Hill, MA) was dissolved in 150 μ L DMSO and added to the polymer phase without sonication. The resulting primary emulsion (solution for rapamycin) was transferred to 60 mL of 2% (wt/vol) poly(vinyl alcohol) (PVA, MW ~25 kDa, 98% hydrolyzed; Polysciences, Warrington, PA) in diH₂O and homogenized (L4RT-1; Silverson, East Longmeadow, MA) on ice at 10,000 rpm for 1 min. The resulting double or single emulsion was then added to 80 mL of 1% PVA, and stirred (600 rpm) for 3 hours on ice to allow the dichloromethane to evaporate. Subsequently, MPs were centrifuged (3000 g, 8 min, 4°C), washed 4 times in diH₂O to remove residual PVA, re-suspended in 10 mL diH₂O, flash frozen, and lyophilized for 72 hrs (Virtis Benchtop K freeze dryer, Gardiner, NY).

3.1.3 Microparticle Characterization

Surface characterization of MPs was conducted using a scanning electron microscope (JSM-6330F; JEOL, Peabody, MA), and particle size distributions were determined by volume impedance measurements using a Multisizer-3 (Beckman Coulter, Brea, CA). For IL-2 or TGF- β 1 release assays, 5 mg MPs were suspended in 1 mL PBS with 1% bovine serum albumin, and incubated at 37°C with end-over-end rotation. Supernatant release media was sampled and replaced daily, and IL-2 or TGF- β 1 quantified by ELISAs (R&D Systems). For rapamycin release assays, 5 mg MPs were suspended in 1 mL PBS with 0.2% Tween80 (to maintain sink

conditions [145]), and rapamycin concentrations in supernatant were determined by spectrophotometry (absorbance at 278 nm). Total loading of IL-2 and TGF- β 1 was determined using a two-phase extraction method with surfactant [146]. Briefly, 5 mg MPs were dissolved in 0.5 mL dichloromethane and cytokines extracted three times into 0.25 mL volumes of PBS + 0.1% sodium dodecyl sulfate (SDS; Sigma). Cytokine concentrations in the pooled aqueous phases were determined by ELISAs, and used to calculate total encapsulation. Rapamycin loading was determined by dissolving 5 mg Rapa MPs in acetonitrile and measuring absorbance (278 nm) of the resulting solution. Acetonitrile spiked with rapamycin was used to generate a standard curve. Encapsulation efficiencies are expressed as ratios of actual to theoretical loading.

Bioactivity of encapsulated IL-2 and TGF- β 1 was assessed by IL-2-induced proliferation of HT-2 cells, or TGF- β 1-mediated inhibition of IL-4-induced HT-2 proliferation [147]. HT-2 cells were maintained in RPMI-1640 supplemented with 10% fetal bovine serum (FBS; Atlanta Biologicals, Atlanta, GA), 10 mM Hepes (Lonza, Walkersville, MD), 2 mM L-glutamine (Gibco by Life Technologies, Thermo Fisher), 1 mM sodium pyruvate (Sigma), 1X antibiotic-antimycotic solution (Sigma), 1X non-essential amino acids (NEAA; Lonza), and 55 μ M 2-mercaptoethanol (Gibco). For HT-2 expansion, media also contained 10 ng/mL rmIL-2. To assay encapsulated IL-2 and TGF- β 1, 10 mg MPs were incubated at 37°C in 1 mL supplemented RPMI, and release samples taken at 24 and 48 hours. IL-2 and TGF- β 1 concentrations in the release samples were determined by ELISAs. Unencapsulated, stock cytokines and release samples were serially diluted in supplemented RPMI, and added to 96-well flat-bottom plates (100 μ L / well). HT-2 cells in the log-phase of growth (2 days after last sub-culture) were washed three times, re-suspended in supplemented media without IL-2, and added to each well

(100 μ L, 2×10^4 cells / well). For the TGF- β 1 assay, all wells also contained 7.5 ng/mL rmIL-4 (PeproTech). HT-2 cells were cultured for 48 hours at 37°C and 5% CO₂, and cell proliferation measured with a colorimetric MTS assay (CellTiter 96 AQueous One Solution Cell Proliferation Assay; Promega, Madison, WI).

3.1.4 Identification of Microparticle in Skin Draining Lymph Nodes after Injection

To enable detection in skin DLN, MPs were fluorescently labeled by encapsulating TRITC-dextran (1 mg per 200 mg polymer; Sigma Aldrich), or by incorporating FITC-labeled PLGA (45 mg per 200 mg total polymer; Mw = 31.6 kDa; 0.78 μ g FITC per mg PLGA; PolySciTech). Fluorescent MPs were suspended in sterile PBS and injected subcutaneously at the base of ears of mice. Mice were euthanized, and DLN were excised and flash frozen in Optimal Cutting Temperature (OCT) compound (Fisher Scientific, Pittsburgh, PA) 90 minutes or 48 hours post-injection. Frozen DLN were cryosectioned and mounted in aqueous media for fluorescent microscopy imaging. Some sections were stained with DAPI and Alexa Fluor 647-labeled antibodies specific for DCs (CD11c, N418; BioLegend, San Diego, CA). Lymph node sections were imaged with an epifluorescence microscope (Olympus Provis AX-70; Center Valley, PA).

3.1.5 Sequestration of Microparticles at Injection Sites

To test the importance of lymphotropic microparticle trafficking for TRI MP therapeutic efficacy, microparticles were sequestered at sites of injection using a thermoresponsive hydrogel. Specifically, MPs were suspended in a 10 wt% solution of poly(N-isopropylacrylamide) (pNIPAM; Sigma Aldrich) in PBS for injection. This pNIPAM solution transitions from a liquid

at room temperature to a solid hydrogel above 32 °C [148], thereby sequestering MPs upon injection in mice (37 °C).

3.1.6 Hapten-Mediated Murine DTH Model

Two chemical haptens, 2,4-dinitrofluorobenzene (DNFB) and 4-Ethoxymethylene-2-phenyl-2-oxazolin-5-one (oxazolone, OXA) were purchased from Sigma Aldrich and dissolved in acetone and olive oil (4:1 v/v). C57BL/6 mice were sensitized by topical application of 20 µL of 0.5% DNFB (or 1.0% OXA) to the dorsal size of both ears. Alternatively, 50 µL of 0.5% DNFB was applied to the shaved abdomen for sensitization. To elicit a DTH response, mice were challenged 10 days post-sensitization (5 days if sensitized on abdomen) with 20 µL of 0.5% DNFB (or 1.0% OXA) applied to both ears. For the re-challenge experiment, mice were challenged with DNFB a second time 10 days after the first challenge. Ear thickness was measured immediately prior to challenge (or re-challenge) and 24, 48, 72, and 96 hours post-challenge using an engineer's spring-loaded micrometer (Mitutoyo, Aurora, IL). Increases in ear thickness (i.e. ear swelling), relative to the baseline measurements, were indicative of inflammation.

3.1.7 Protein-Mediated (OVA) Antigen-Specific Murine DTH Model

OVA-specific CD8⁺ and CD4⁺ T cells were isolated from spleens of OT-I and OT-II mice (CD45.2⁺) and adoptively transferred to congenic CD45.1 B6 mice by tail vein injection (5x10⁶ OT-I and 5x10⁶ OT-II cells per mouse). One day later, the mice were sensitized to ovalbumin (OVA) by transdermal application of dissolvable microneedle arrays (MNAs), each containing

100 µg OVA (Grade V, Sigma Aldrich), to both ears. The carboxymethyl cellulose-based MNAs were fabricated according to the spin-casting method described in [98]. To elicit a DTH response, mice were challenged 5 days post-sensitization by applying an OVA (100 µg) MNA to the right ear. A blank (empty) MNA was applied to the left ear to control for any swelling caused by MNA application itself. Ear thickness was measured prior to the OVA challenge, and at 24, 48, 72, and 96 hours post-challenge, and data presented as differences between OVA MNA-treated and contralateral Blank MNA-treated ears.

3.1.8 Suppression of Skin DTH with TRI MPs

Mice received subcutaneous MP injections at the base of each ear two days before hapten sensitization, or immediately prior to OVA sensitization. For treatment of previously sensitized mice, TRI MP were injected at the base of each ear immediately prior to DNFB challenge. For some experiments, MPs were injected intradermally at the abdomen. Each injection (2 per mouse) contained a total of 8 mg “Blank” (empty) or TRI MPs in 150 µL sterile PBS. TRI MPs included a mix of 2.2 mg IL-2 MPs, 4.3 mg TGF-β1 MPs, and 1.5 mg Rapa MPs. For the OVA-specific DTH model, some mice were treated with TRI MPs supplemented with soluble (unencapsulated) Treg-inducing factors (50 ng IL-2, 75 ng TGF-β1, and 10 µg rapamycin per injection; 2 per mouse). Additional controls for some experiments included soluble TRI, as well as individual TRI MP formulations or combinations of two TRI MPs (e.g. IL-2 MP + TGF-β1 MP). For these treatments, the total mass of MPs was kept constant by supplementing with Blank MPs.

3.1.9 Inhibiting Treg-Mediated Suppression with Anti-GITR or Anti-CD25

To inhibit effects of Treg-mediated suppression on effector T cells, a monoclonal antibody specific for glucocorticoid-induced TNFR-related protein (GITR, clone DTA-1; BioXcell, West Lebanon, NH) was injected intraperitoneally (0.5 mg per mouse) 3 days prior to DNFB challenge. Alternatively, anti-CD25 (clone PC-61.5.3; BioXcell) was injected intraperitoneally (0.5 mg per mouse) 3 days prior to DNFB challenge to deplete CD25⁺ Tregs.

3.1.10 Phenotypic Analysis of T-cell Populations in Skin Draining Lymph Nodes by Flow Cytometry

Four days after sensitization with DNFB or OVA, ear-draining cervical lymph nodes (or non-draining inguinal lymph nodes) were harvested, passed through 70 μ m filters to create single cell suspensions, stained for T-cell markers, and analyzed with a flow cytometer (LSR-II; BD Biosciences, San Jose, CA). Lymphocytes were also counted with a hemocytometer to determine total cells per lymph node. Cells were stained with fluorescently labeled antibodies purchased from BD Biosciences, eBioscience (San Diego, CA), or BioLegend (San Diego, CA). To identify Treg, Th1, and Tc1 populations, lymphocytes were blocked with anti-CD16/32 (2.4G2; BD) and stained for CD4 (RM4-5; eBio), CD8b (H35-17.2; eBio), CD25 (PC61; BD), FoxP3 (FJK-16s; eBio), and T-bet (O4-46; BD). Adoptively transferred OVA-specific T cells were identified by staining for CD45.2 (104; BD). For further Treg phenotypic analysis, cells were also stained for CTLA-4 (CD152, UC10-4B9; eBio), LAP (TGF- β 1, TW7-16B4; BioLegend), CD39 (Duha59; BioLegend), and GITR (DTA-1; eBio). FlowJo (Tree Star,

Ashland, OR) software was used for analysis, and population gates were set based on isotype, single-stain, and fluorescence minus one controls.

3.1.11 *In Vitro* Suppression Assay

OT-II cells were adoptively transferred to CD45.1 B6 mice (5×10^6 cells / recipient) one day prior to sensitization of ears with OVA MNA and local injection of TRI MP and soluble factors. Four days post-sensitization, DLN from five mice were harvested under sterile conditions, passed through 70 μm filters to create a single cell suspension, and stained with fixable viability dye (eBioscience) and antibodies for CD45.2, CD4, and CD25. Live CD45.2⁺ CD4⁺ CD25⁺ cells (CD25⁺ OT-II) were isolated by FACS sorting (FACS Aria; BD Biosciences). Conventional T cells (Tconv; CD4⁺ CD25⁻) were isolated from the spleen of a naïve CD45.1 B6 mouse using a CD4⁺CD25⁺ Regulatory T Cell Isolation Kit (Miltenyi Biotec, San Diego, CA), and labeled with 5 μM CFSE (Vybrant CFDA SE Cell Tracer Kit; Invitrogen, Thermo Fisher). Suppression assays were performed in 96-well round-bottom plates in 200 μL supplemented RPMI per well. Tconv (5×10^4 cells / well) were cultured with anti-CD3/CD28-coated beads for stimulation (5×10^4 beads / well; Dynabeads Mouse T-Activator; Life Technologies, Thermo Fisher) and different quantities of CD25⁺ OT-II cells. After 3 days, cells were stained with fixable viability dye and antibodies for CD45.2 and CD4. Proliferation of Tconv (live CD45.2⁻ CD4⁺ cells), as indicated by CFSE-dilution, was analyzed by flow cytometry (LSR Fortessa; BD Biosciences).

3.1.12 Phenotypic Analysis of DCs in Skin Draining Lymph Nodes by Flow Cytometry

Four days after sensitization with DNFB, ear-draining cervical lymph nodes were harvested, passed through 70 µm filters to create single cell suspensions, stained for DC phenotypic and maturation markers, and analyzed with a flow cytometer (LSR-II). Cells were also counted with a hemocytometer to determine total cells per lymph node. Cells were blocked with anti-CD16/32 (2.4G2; BD) and stained with fluorescently labeled antibodies: CD11c (HL3; BD), I-A^b (AF6-120.1; BD), CD80 (16-10A1; BioLegend), and CD86 (GL1; BD). FlowJo software was used for analysis, and population gates were set based on isotype, single-stain, and fluorescence minus one controls.

3.1.13 Functional Analysis of DCs from Skin Draining Lymph Nodes After TRI MP

Treatment

Forty-eight hours after application of OVA (100 µg) MNAs to both ears of mice and injection of Blank MP or TRI MP plus soluble TRI at the base of each ear, ear-draining cervical lymph nodes were isolated and cultured in serum-free RPMI 1640 (HyClone, Fisher Scientific) with Collagenase D (1 mg/mL; Roche, Sigma Aldrich), and incubated 45 minutes at 37°C. DLN were then passed through 70 µm filters and washed with sterile MACS buffer. CD11c⁺ DCs were isolated from each DLN by positive-selection, using CD11c MicroBeads UltraPure with MS Columns and an OctoMACS Separator (Miltenyi Biotec, San Diego, CA). The purity of some sorted cells from each DLN was assessed by flow cytometry, with staining for CD11c (HL3; BD) and I-A^b (AF6-120.1; BD). After selection, 2x10⁴ CD11c⁺ DCs were plated with 2x10⁵ OT-I or OT-II T cells in a 96-well round-bottom plate. Prior to culture, T cells were stained with

5(6)-carboxyfluorescein diacetate succinimidyl ester (5 nM CFSE, CellTrace Cell Proliferation Kit; Thermo Fisher Scientific, Pittsburgh, PA). T cells cultured without DCs were used as unstimulated controls. After 3 days, flow cytometry analysis of CFSE-dilution was used to quantify T-cell proliferation. Cells were also stained for CD3 (17A2; eBio) and CD4 (RM4-5; eBio) or CD8a (53-6.7; BD).

3.1.14 Cutaneous Histology and Immunohistochemistry

Ears from mice sacrificed 4 days after DNFB (or OVA) challenge or re-challenge were excised and flash frozen in OCT compound. Skin cross-sections (7 μ m thick) were stained with hematoxylin and eosin and imaged with a Nikon Eclipse E400 microscope. For fluorescent immunohistochemistry (IHC), 10 μ m thick sections were fixed with 96% ethanol, blocked with PBS containing 5% donkey serum and 1% Tween20, and treated with a streptavidin/biotin blocking kit (Vector Labs, Burlingame, CA). Blocked sections were incubated overnight at 4°C with primary antibodies: biotin-FoxP3 (FJK-16s; eBio), biotin-CD8a (53-6.7, eBio), or CD3 (SP7, monoclonal rabbit IgG; Thermo Scientific, Waltham, MA). Sections were then incubated with Cy3-streptavidin (Jackson ImmunoResearch Laboratories, West Grove, PA) or Alexa Fluor 555 donkey anti-rabbit IgG (Thermo Scientific) for 1 hour at room temperature, counterstained with DAPI, and fixed with 2% paraformaldehyde. Slides were imaged with an epifluorescence microscope (Olympus Provis AX-70; Center Valley, PA). For histology and IHC, ears from naïve mice were used as controls.

3.1.15 Cutaneous Cytokine Expression by qRT-PCR

Two days after DNFB challenge, total RNA was extracted from excised ear tissue using TRI-reagent (Molecular Research Center, Cincinnati, OH), according to the manufacturer's instructions, and quantified using a NanoDrop 2000 (Thermo Scientific). For each reverse transcriptase assay, 2 µg RNA was converted to cDNA using a QuantiTect Reverse Transcription Kit (Qiagen, Valencia, CA). Quantitative real-time PCR was then performed using VeriQuest Probe qPCR Mastermix (Affymetrix, Santa Clara, CA), according to the manufacturer's instructions, with 5' nuclease PrimeTime qPCR assays (Integrated DNA Technologies, Coralville, IA) specific for IFN γ , IL-1 β , TNF, and β -glucuronidase (GUSB, endogenous control). Duplex reactions (target gene + GUSB) were run and analyzed on a StepOnePlus Real-Time PCR System (Applied Biosystems, Carlsbad, CA). Relative fold changes of IFN γ , IL-1 β , and TNF expression were calculated and normalized based on the $2^{-\Delta\Delta C_t}$ method, with naïve ear skin as the untreated control.

3.1.16 Statistical Analyses

Statistical analyses were performed with GraphPad Prism v6 (San Diego, CA). For cytokine bioactivity assays, ED₅₀ values were determined by nonlinear 4- or 5-parameter logistic regression. Data from experiments with multiple treatment groups were analyzed by one-way ANOVA, followed by Tukey's post-hoc testing. For experiments with only two groups, two-tailed independent t-tests were used. Ear thickness measurements from multiple time points were analyzed by two-way mixed ANOVA, followed by post-hoc testing of treatment effect with

a Sidak correction. Differences were considered significant if $p < 0.05$. Data represent mean \pm SD, except for ear thickness measurements, which are mean \pm SEM.

3.2 RESULTS

3.2.1 TRI MPs release TGF- β 1, Rapamycin, and IL-2 for about 1 week.

We previously reported encapsulation and sustained release of Treg-inducing factors from biodegradable PLGA MPs [93]. For the current study, particle formulations were re-engineered to achieve faster release kinetics (i.e. greater release within the first week), which is more suitable for short-term immunomodulation during acute immune responses, such as allergen sensitization. Accordingly, we encapsulated the Treg-inducing factors in MPs composed of a blend of ester-terminated poly(lactic-co-glycolic acid) (PLGA) and poly(ethylene glycol) (PEG)-PLGA diblock copolymer. New formulations contained PEG (4 wt%, MW ~5 kDa), which helped to augment early release by enhancing the hydration rate and matrix swelling [149], and ester-terminated PLGA, which served to reduce electrostatic interactions with positively charged amino acid residues [144].

Surface morphology and particle size distributions were consistent for all formulations, regardless of whether they were fabricated using a single emulsion (Rapa MP) or double emulsion protocol (IL-2 MP and TGF- β 1 MP). A representative scanning electron micrograph (Figure 3-1A) shows spherical particles with somewhat irregular surface morphology, consistent with that reported for other PEG-coated MPs [150]. Particle size distributions (Figure 3-1B) are also consistent across all formulations, with volume-average diameters of $1.78 \pm 0.92 \mu\text{m}$ (TGF-

β 1 MP), $1.77 \pm 0.89 \mu\text{m}$ (Rapa MP), and $1.73 \pm 0.90 \mu\text{m}$ (IL-2 MP). Total loading of TGF- β 1, rapamycin, and IL-2 were $12.64 \pm 0.97 \text{ ng}$, $5.53 \pm 0.04 \mu\text{g}$, and $16.92 \pm 1.11 \text{ ng per mg MP}$, respectively. Given theoretical loading of $25 \text{ ng TGF-}\beta$ 1, $7.5 \mu\text{g rapamycin}$, or $25 \text{ ng IL-2 per mg MP}$, encapsulation efficiencies for TGF- β 1, rapamycin, and IL-2 were $50.6 \pm 3.9 \%$, $73.8 \pm 0.5 \%$, and $67.7 \pm 4.4 \%$, respectively. PEG-PLGA MPs provide sustained release of each factor over a period of approximately one week (Figure 3-1C). For Rapa MP, $95.7 \pm 3.8 \%$ of total encapsulated drug was released within 7 days; however, for TGF- β 1 and IL-2 MPs, only $23.5 \pm 3.6 \%$ and $30.2 \pm 3.7 \%$ of total encapsulated cytokines were released in the first week. Release assays for IL-2 and TGF- β 1 MPs were carried out to 22 days, and no cytokine release was detected between days 8 and 22 (not shown), consistent with a lag phase. Finally, bioactivity of IL-2 and TGF- β 1 released from MPs and detected by ELISAs was comparable to that of unencapsulated cytokines, as determined by HT-2 cell-based bioassays (Figure 3-2).

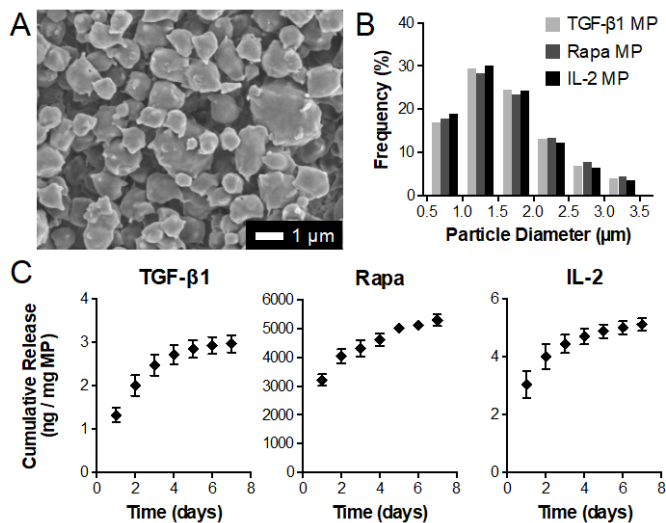


Figure 3-1. Microparticle characterization. (A) Representative scanning electron micrograph showing surface morphology of PEG-PLGA MPs (5000x magnification). (B) Number-weighted size distributions for IL-2, TGF- β 1, and Rapamycin (Rapa) MPs, determined by volume impedance measurements of 50,000 particles. (C) Cumulative

release profiles for IL-2, TGF- β 1, and Rapa formulations (N=3-6). *In vitro* release was measured for MPs incubating at 37°C in PBS with 1% BSA for IL-2 and TGF- β 1, or PBS with 0.2% Tween-80 for Rapa.

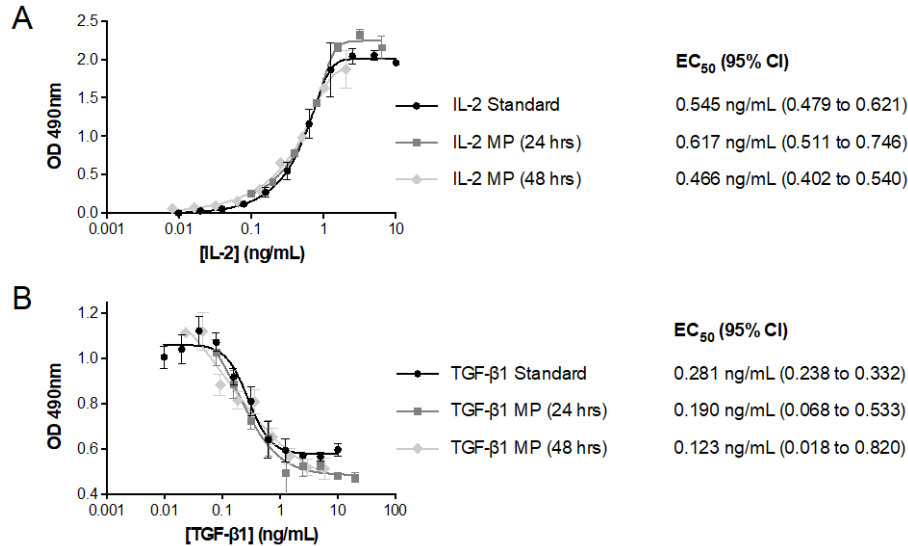


Figure 3-2. IL-2 and TGF- β 1 released from MPs and detected by ELISAs are bioactive. (A) IL-2 released from MPs induces proliferation of HT-2 cells with potency and efficacy comparable to unencapsulated IL-2 standard. (B) TGF- β 1 released from MPs inhibits IL-4-induced proliferation of HT-2 cells with potency and efficacy comparable to unencapsulated TGF- β 1 standard. For both bioassays, MPs were incubated in complete RPMI media, release samples taken at 24 and 48 hours, and cytokine concentrations determined by ELISA. Total proliferation of HT-2 cells after 48 hours of culture with cytokines was measured by MTS assay, and half-maximal effective concentrations (EC₅₀) determined by nonlinear regression on dose-response curves. Data are representative of release samples from two different batches of MPs per cytokine, and HT-2 cultures were performed in triplicate.

3.2.2 Prophylactic treatment with TRI MPs during hapten sensitization increases the Treg/Teff ratio in skin draining lymph nodes.

We previously demonstrated that TRI MP induce differentiation of naïve CD4⁺ T cells to CD4⁺ FoxP3⁺ regulatory T cells (Tregs) *in vitro* in the presence of T-cell activating microbeads [93].

To determine whether our new TRI MP formulations could promote Treg differentiation and enhance Treg populations *in vivo*, TRI MP were injected subcutaneously at the base of the ears two days prior to sensitization of the ears with 2,4-dinitrofluorobenzene (DNFB), a small molecule hapten and model contact allergen. Naïve mice, sensitized but untreated mice (DNFB only), and sensitized mice treated with Blank MP served as controls. Flow cytometry analysis on DLN from four days post-sensitization revealed significant effects of DNFB and TRI MPs on T-cell populations. Relative to naïve mice, sensitized mice (with or without Blank MP) had significantly greater Treg, Th1, and Tc1 frequencies and numbers in the DLN (Figure 3-3A and Figure 3-4). Notably, TRI MP treatment dramatically enhanced the frequency and absolute number of CD4⁺ FoxP3⁺ Tregs (including both CD25⁺ and CD25⁻ Treg subsets), relative to sensitized controls (Figure 3-3A and Figure 3-4). Tregs from TRI MP-treated mice expressed several characteristic markers important for suppressive function, including CD25 (IL-2R α), CTLA-4 (Cytotoxic T-Lymphocyte Antigen-4), GITR (Glucocorticoid-Induced TNFR-Related protein), LAP (Latency Associated Peptide, pro-TGF- β 1), and CD39 (ectonucleotidase that generates anti-inflammatory adenosine) [14]. Furthermore, expression of CTLA-4, GITR, and LAP was slightly greater on Tregs from TRI MP-treated mice, relative to naïve Tregs (Figure 3-3D). In addition to expanding Treg populations, TRI MP treatment led to decreases in frequencies and numbers of proinflammatory CD4⁺ T-bet⁺ Th1 and CD8⁺ T-bet⁺ Tc1 effector T cells (Teff) (Figure 3-3A and Figure 3-4B). Concurrent enhancement of Treg populations and reduction of Teff populations contributed to a dramatic increase in the Treg/Teff ratio in TRI MP-treated mice, relative to naïve and sensitized controls (Figure 3-3B). Despite shifts in T-cell sub-populations, total numbers of lymphocytes in DLN were consistent across all sensitized groups, and significantly greater than in DLN from naïve mice (Figure 3-3C). Finally, we

observed similar trends in T-cell populations using a second model hapten, oxazolone (OXA). Specifically, treatment with TRI MPs prior to topical application of OXA, nearly doubled the Treg/Teff ratio in skin DLN by expanding Treg and suppressing Th1 and Tc1 populations (Figure 3-5). These data suggest that our approach to *in vivo* modulation of T cell responses during allergen sensitization is not restricted to a particular hapten, and could potentially be extended to a variety of other allergens.

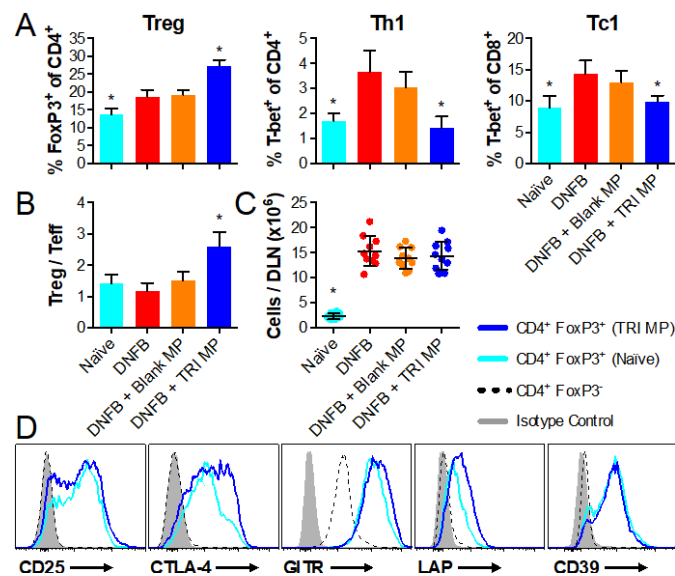


Figure 3-3. Treatment with TRI MP during DNFB sensitization enhances Treg populations and reduces effector T-cell populations (Teff; Th1 and Tc1) in skin draining lymph nodes (DLN). Sustained release TRI MP were injected 2 days prior to sensitization and DLN were isolated and analyzed by flow cytometry four days post-sensitization. Naïve (unsensitized) mice were used as a control. (A) Relative frequencies of Treg (CD4⁺ FoxP3⁺), Th1 (CD4⁺ T-bet⁺), and Tc1 (CD8⁺ T-bet⁺) populations in DLN. (B) Ratios of anti-inflammatory Treg to pro-inflammatory Teff in DLN. (C) Total cells per DLN as counted with a hemocytometer. (D) Representative histograms showing expression of characteristic Treg markers by CD4⁺ FoxP3⁺ Tregs from DLN of TRI MP treated or naïve mice. CD4⁺ FoxP3⁻ T cells and isotype controls are also shown. Significant differences, relative to DNFB sensitized control, are indicated by *p < 0.001 (N=8-20).

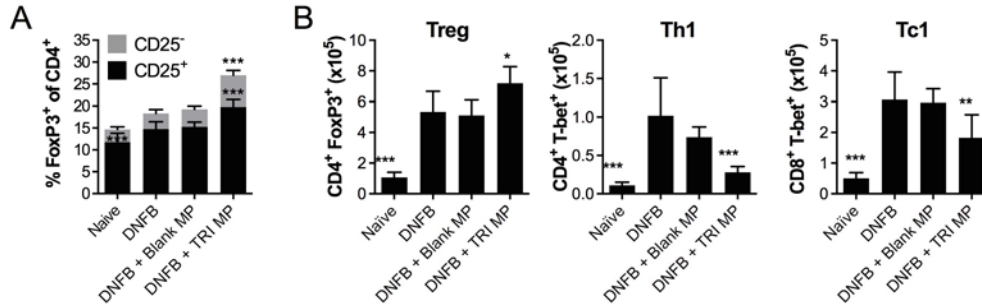


Figure 3-4. TRI MP treatment expands CD25⁺ and CD25⁻ Treg populations and alters absolute numbers of Tregs and effector T cells in skin DLN. (A) Treatment with TRI MPs during DNFB sensitization expands both CD25⁺ (black) and CD25⁻ (grey) populations of CD4⁺ FoxP3⁺ Tregs in skin DLN four days post-sensitization. Overall Treg frequencies (% FoxP3⁺ CD25^{+/-} of CD4⁺) are also presented in Figure 3-3A. (B) TRI MPs also increase absolute numbers of Tregs and decrease absolute numbers of Th1 and Tc1 cells in skin DLN. Numbers are cells per DLN. Significant differences, relative to DNFB alone, are indicated by *p < 0.05, **p < 0.001, ***p < 0.0001 (N_{Treg} ≥ 14; N_{abs} = 5-10 for absolute numbers).

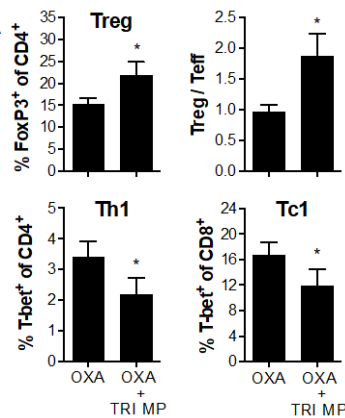


Figure 3-5. TRI MPs modulate T-cell responses to another chemical hapten (OXA). Frequencies of T-cell subsets in skin DLN at 4 days post-sensitization with OXA. Treg / Teff is the ratio of Treg to Th1 and Tc1 populations. Significant differences indicated by *p < 0.05 (N=5).

To investigate the importance of sustained delivery of Treg-inducing factors during the sensitization phase, some mice were treated with a single local bolus of soluble TRI (TGF-β1,

Rapamycin, and IL-2 without MPs). Unlike treatment with sustained release TRI MPs, soluble TRI injected one or two days before sensitization (as with MP treatments) did not affect Treg or effector T-cell populations (Figure 3-6A). Interestingly, local injection of soluble TRI at the time of sensitization (day 0), or 1 to 3 days after sensitization, reduced Th1 and Tc1 frequencies, but failed to expand Treg populations (Figure 3-6A). This suggests that these mediators must be present at the time of antigen exposure, and that Treg induction requires their sustained presence throughout antigen presentation.

Finally, while IL-2 and TGF- β 1 are essential for Treg induction [151], and addition of rapamycin significantly enhanced Treg-induction efficiency *in vitro* [93], we wanted to determine whether delivery of all three factors was essential to enhance Treg populations and suppress Th1 and Tc1 populations *in vivo*. Treatment with different combinations of TRI MP revealed that all three factors were in fact required to significantly enhance Treg frequencies and reduce Th1 and Tc1 frequencies (Figure 3-6C). The combination of TGF- β 1 MP and Rapa MP also increased Treg frequencies and reduced Th1 frequencies, but did not have a significant effect on Tc1 frequencies (Figure 3-6C). Together, these data suggest that sustained delivery of all three Treg-inducing factors is capable of enhancing Treg populations and reducing Th1 and Tc1 populations.

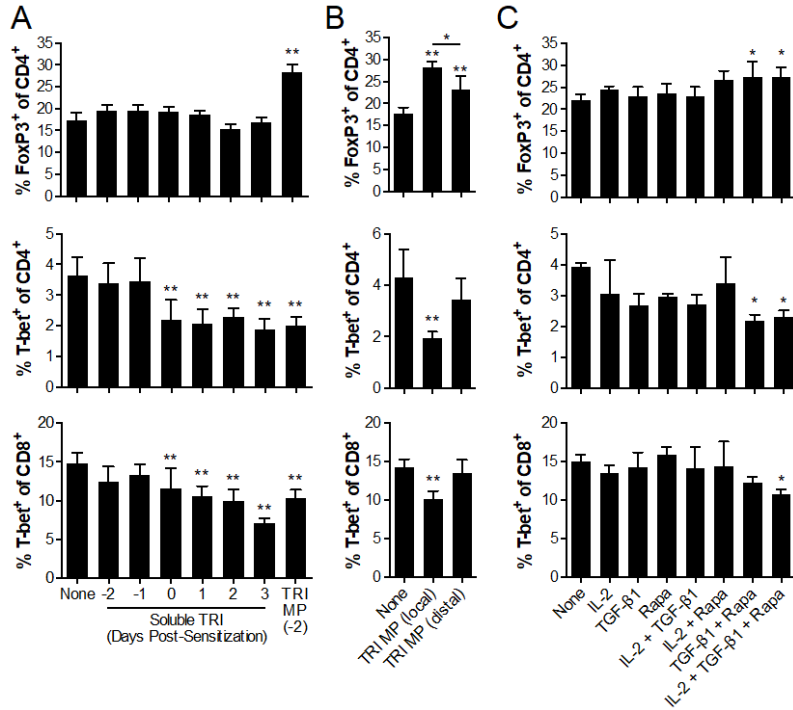


Figure 3-6. Effects of sustained local delivery and different combinations of TRI MP on Treg (CD4⁺ FoxP3⁺), Th1 (CD4⁺ T-bet⁺) and Tc1 (CD8⁺ T-bet⁺) populations in DLN four days after sensitizing ears with DNFB. (A) Two days prior to sensitization, TRI MP were injected near the sensitization site (base of ears). Alternatively, a bolus of soluble TRI (IL-2, TGF-β1, and Rapa w/o MPs) was injected at the base of the ears at the indicated time point with respect to sensitization (N≥5). (B) TRI MP were injected at the base of the ears (local) or at the abdomen (distal) two days prior to sensitization (N=7). (C) Mice were treated with different combinations of TRI MP two days prior to DNFB sensitization (N=3). Total mass of injected particles was kept constant by supplementing single or double particle combinations with Blank MP. *p < 0.05 or **p < 0.001 vs. DNFB alone (Treatment: “None”).

3.2.3 TRI MP treatment during hapten sensitization suppresses maturation of migratory DCs in skin DLN.

In addition to direct effects on T-cell differentiation, TGF- β 1 and rapamycin can directly influence the phenotype of DCs [43]. Specifically, DCs cultured with rapamycin and/or TGF- β 1, in soluble form or encapsulated in MPs, exhibited lower expression of MHC-II, co-stimulatory molecules (CD80 and CD86), and pro-inflammatory cytokines (IL-12) [145, 152-154]. Such DCs were also less able to stimulate allogeneic T-cell proliferation [145, 152-154], though rapamycin conditioned DCs did support Treg proliferation [153]. Given these reported effects of TRI factors on DCs, we examined the phenotype of skin migratory DCs (CD11c⁺ MHC-II^{high}) and lymph node resident DCs (CD11c^{high} MHC-II^{int}) in DLN after treatment with TRI MPs and sensitization with DNFB. Sensitization increased migration of skin DCs to DLN, and MPs had no effect on absolute numbers of migratory DCs in the DLN (Figure 3-7B). Sensitization also induced maturation of skin migratory DCs, as evidenced by enhanced expression of co-stimulatory CD80 and CD86 (Figure 3-7C-D). Interestingly, treatment with TRI MPs significantly inhibited DNFB-induced expression of CD80 and CD86 on migratory DCs (Figure 3-7C-D), but did not alter expression on lymph node resident DCs (data not shown). Unexpectedly, Blank MPs also seemed to reduce expression of CD80 and CD86 on migratory DCs, though to a lesser extent than TRI MPs (Figure 3-7C-D). This may reflect inclusion of cells that migrated to the skin DLN after ingesting Blank MPs, instead of in response to DNFB exposure; however, this phenomenon will require further investigation. Ultimately, these results suggest that the effects of TRI MPs on T-cell populations (seen in Figure 3-3) could also potentially be mediated indirectly through effects on DCs.

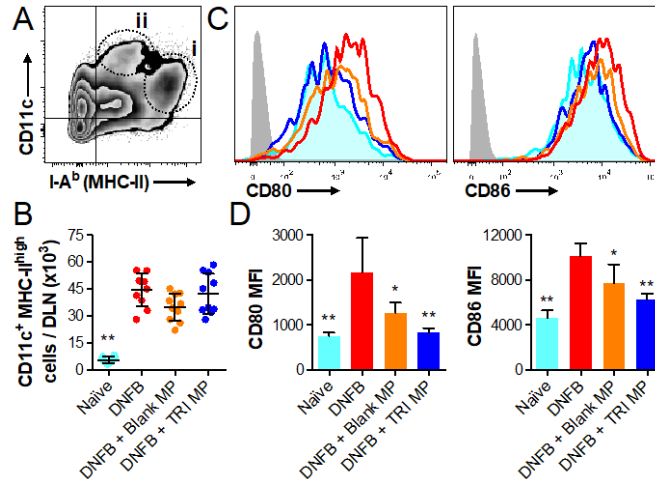


Figure 3-7. TRI MP treatment during DNFB sensitization suppresses maturation of skin migratory DCs. TRI MPs or Blank MPs were injected 2 days prior to sensitization with DNFB, and DLN were isolated and analyzed by flow cytometry four days post-sensitization. Naïve mice were used as a control. (A) Representative flow cytometry plot shows gating for (i) skin migratory DCs (CD11c⁺ MHC-II^{high}) and (ii) lymph node resident DCs (CD11c^{high} MHC-II^{int}). (B) Absolute numbers of migratory DCs in skin DLN, as determined by flow cytometry and total cell counts with a hemocytometer (N=10). (C) Fluorescence intensity histograms for co-stimulatory molecules CD80 and CD86, which are up-regulated upon DC maturation. Colors correspond to experimental groups identified in B and D, and grey histograms are isotype controls. (D) Median fluorescence intensity (MFI) for CD80 and CD86 (N=5, representative of two independent experiments). Significant differences, relative to DNFB sensitized controls, are indicated by * p<0.05 and ** p<0.001.

3.2.4 TRI MP treatment suppresses T-cell stimulatory function of DCs.

To assess the stimulatory function of DCs following TRI MP treatment, CD11c⁺ DCs were isolated from skin DLN of mice 48 hours after application of OVA MNA and treatment with TRI MP plus soluble TRI factors or Blank MP. These DCs were then co-cultured with CFSE-labeled, OVA-specific TCR transgenic OT-I and OT-II T cells, in order to evaluate their function in the absence of TRI MP-induced Tregs, which could suppress T-cell proliferation. Positive

selection with MACS columns yielded an average of 84% CD11c⁺ cells, which included similar sized populations of migratory DCs (CD11c^{high} MHC-II^{int}) and lymph node resident DCs (CD11c⁺ MHC-II^{high}) (Figure 3-8A-B). Notably, compared to DCs from Blank MP treated mice, those from mice treated with TRI MP plus soluble TRI induced significantly less proliferation of OT-I and OT-II T cells, as evidenced by fewer CFSE^{low} T cells (Figure 3-8C-E). These results suggest that TRI MPs (with additional soluble TRI factors) can suppress the T-cell stimulatory function of DCs independent of Treg-mediated suppression.

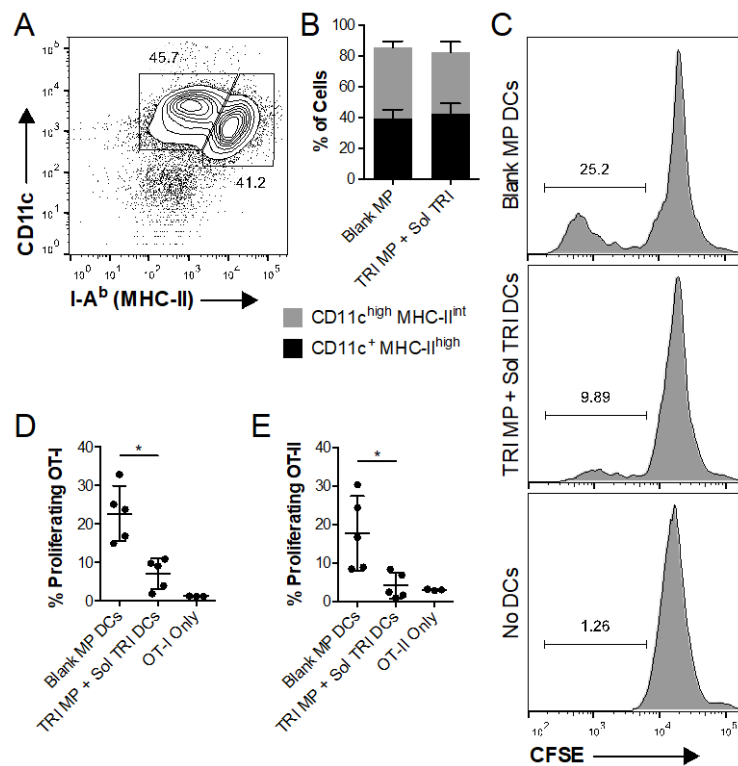


Figure 3-8. Treatment with TRI MP plus a bolus of soluble TRI factors impairs stimulatory capacity of DCs in skin DLN. Blank MP or TRI MP + Soluble TRI were injected at the base of ears of mice immediately before application of OVA (100 µg) MNA to ears. After 48 hours, CD11c⁺ cells were isolated from skin DLN by MACS, and co-cultured with CFSE-labeled OT-I or OT-II T cells (1:10 DC:T cell). (A) Representative flow cytometry analysis of cells after CD11c isolation. (B) Percentages of lymph node resident DCs (CD11c^{high} MHC-II^{int}) and skin migratory DCs (CD11c⁺ MHC-II^{high}) based on gating in (A). (C) Representative CFSE dilution (proliferation) of CD3⁺ CD8⁺ cells (OT-I T cells) after 3 days co-culture with DCs. Gates indicate percent proliferating (CFSE^{low})

cells. (D-E) Frequencies of proliferating OT-I (D) and OT-II (E) T cells, as identified by CFSE dilution. Significant differences are indicated by * $p < 0.05$ (N=5).

3.2.5 Prophylactic treatment with TRI MPs during hapten sensitization suppresses DTH responses to multiple subsequent exposures.

Since TRI MPs expanded suppressive Treg populations and reduced pro-inflammatory Th1 and Tc1 populations after sensitization, we hypothesized that TRI MP treatment would suppress DTH responses to subsequent allergen exposure (challenge). To test this hypothesis, mice treated with TRI MP and sensitized to DNFB were challenged by re-painting the ears with DNFB 10 days after sensitization (see experimental timeline in Figure 3-9A). DNFB sensitized mice (with or without Blank MP) served as controls. Ear swelling responses, indicative of cutaneous inflammation, were measured after DNFB challenge. Notably, TRI MP treatment significantly reduced ear swelling compared to sensitized controls (Figure 3-9B). Furthermore, tolerance induced by TRI MP treatment was persistent enough to suppress the hypersensitivity response to a second allergen challenge (“re-challenge”) 10 days after the first (Figure 3-9C). Importantly, this effect was generalized, as TRI MP treatment was also able to suppress DTH responses to a second model hapten, OXA, in OXA-sensitized mice (Figure 3-10), suggesting that *in vivo* expansion of Treg populations with TRI MP may be a viable therapeutic approach for a variety of contact allergens.

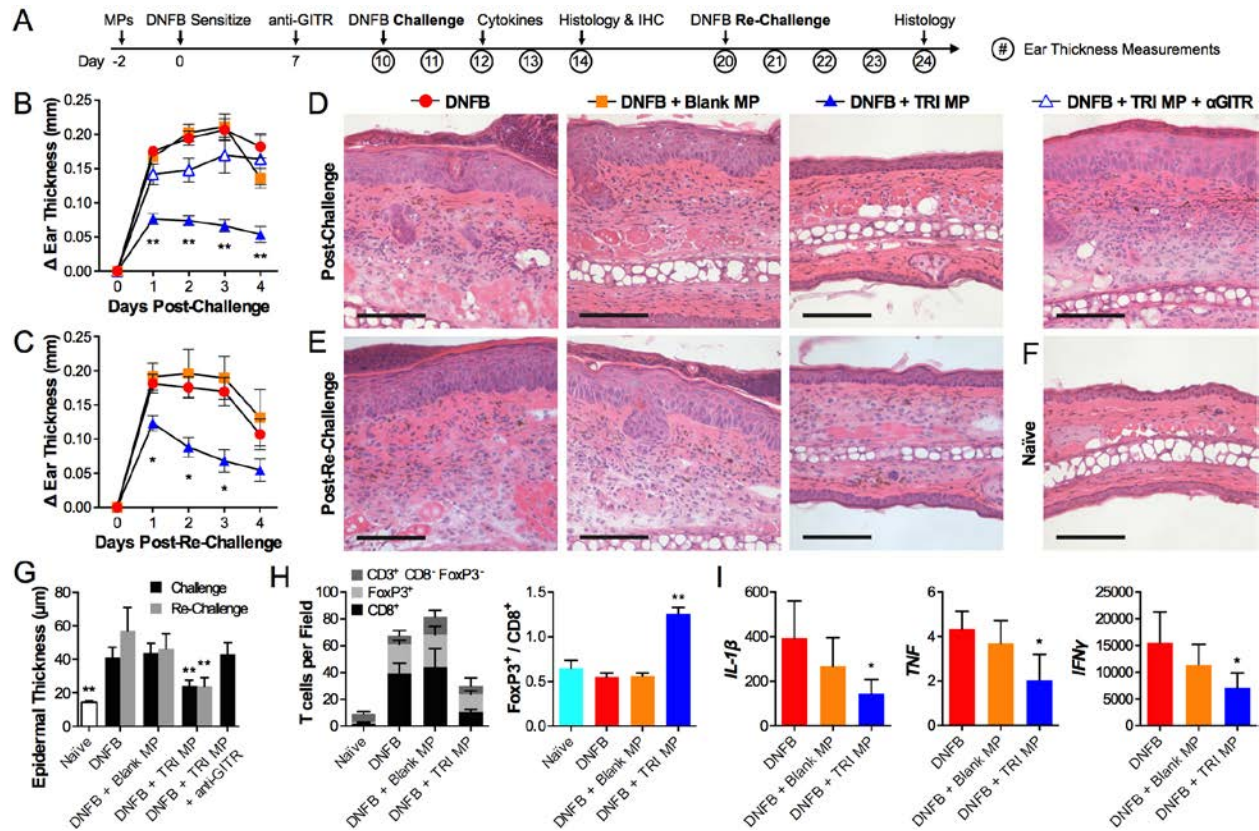


Figure 3-9. Prophylactic treatment with TRI MP, prior to sensitization, protects skin and suppresses DTH responses to repeated challenges with DNFB. (A) Experimental timeline. (B-C) Increases in ear thickness (swelling) after (B) DNFB challenge (N=20, N=5 for anti-GITR) or (C) re-challenge (N=6-7), relative to pre-challenge or pre-re-challenge thickness. (D-F) Representative ear skin histology (H&E) from 4 days post-challenge (D) or re-challenge (E), or from naïve ears not exposed to DNFB (F). DNFB was applied to the dorsal side of ears (top of images). Scale bars are 100 µm. (G) Average epidermal thickness as measured from histology images as in (D-F) (N=5-8). (H) T-cell counts in skin sections from 4 days post-challenge. Representative immunofluorescence images (fields) used for cell counts are presented in Figure 3-11 (N=5). A high FoxP3⁺ / CD8⁺ T-cell ratio is indicative of a more tolerogenic microenvironment. (I) Expression of pro-inflammatory cytokines in skin tissue 48 hours post-challenge (N=5). mRNA was quantified by qRT-PCR, and expression is relative to naïve skin (2^{-ΔΔCt}). Significant differences, relative to DNFB alone, are indicated by *p<0.05 or **p<0.001.

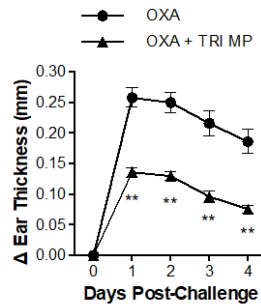


Figure 3-10. TRI MPs suppress inflammatory response to OXA challenge. Increases in ear thickness (swelling) relative to baseline (pre-challenge) measurements. Significant differences indicated by * $p < 0.05$ or ** $p < 0.001$ (N=5).

In addition to macroscopic differences in ear swelling, histological evaluation of ear skin from four days after DNFB challenge or re-challenge revealed remarkable differences in skin morphology from TRI MP treated mice, compared to sensitized controls (Figure 3-9D,E). After DNFB challenge or re-challenge, skin from sensitized controls showed acanthosis (epidermal hyperplasia), hyperkeratosis (thickening of the stratum corneum), some spongiosis (intercellular edema between keratinocytes), and lymphocyte infiltrates in the epidermis and dermis (Figure 3-9D,E). These features are consistent with subacute allergic dermatitis [155]. Notably, TRI MP treatment reduced acanthosis, hyperkeratosis, spongiosis, and cellular infiltrates (Figure 3-9D,E), resulting in skin that looked more like naïve skin histologically (Figure 3-9F). Quantification of epidermal thickness also confirmed that TRI MP treatment significantly reduced epidermal hyperplasia associated with repeated allergen exposure (Figure 3-9G). To better characterize cutaneous T cell infiltrates, skin sections were stained for CD3, CD8, or FoxP3 and evaluated by immunofluorescence (Figure 3-11). Quantification of cells in imaged fields revealed considerable CD3⁺ T-cell infiltrates in skin from sensitized controls after DNFB challenge, the majority of which were CD8⁺ effector T cells (Figure 3-9H). In contrast, skin from TRI MP treated mice contained significantly fewer total T cells, including fewer total FoxP3⁺ Tregs;

however, the ratio of FoxP3⁺ / CD8⁺ T cells was roughly twofold greater than in sensitized and naïve controls (Figure 3-9H).

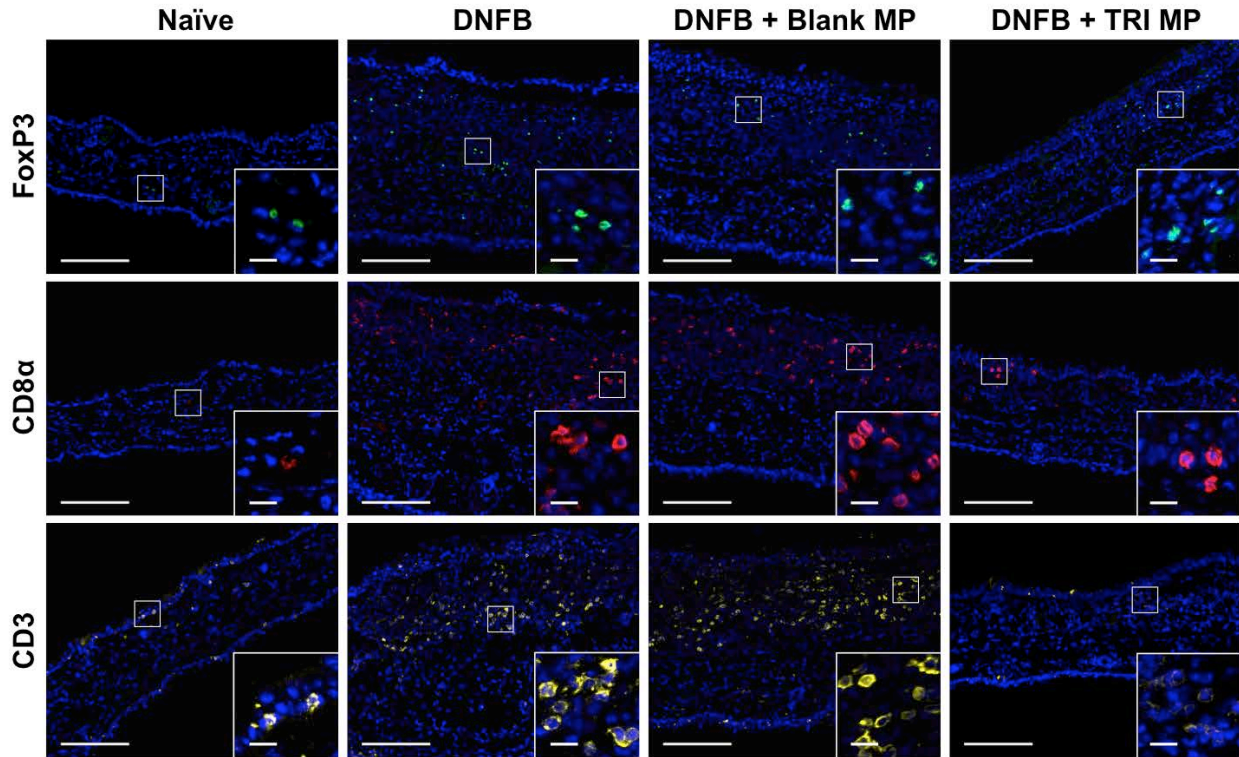


Figure 3-11. Representative immunofluorescence images of ear sections used for T-cell counts in Figure 3-9. Sections of naïve ears or ears from four days post-challenge were stained for FoxP3 (Tregs), CD8 α (cytotoxic T cells), or CD3 (total T cells), and counterstained with DAPI. False-colored immunofluorescence images were taken using a 20X objective. Large scale bars are 150 μ m. Scale bars in magnified insets are 15 μ m.

To determine whether treatment with TRI MP suppressed cutaneous production of inflammatory cytokines in response to DNFB challenge, skin tissue was harvested 48 hours post-challenge and mRNA extracted for qRT-PCR analysis. Specifically, we examined expression of IL-1 β and TNF, which are predominantly produced by keratinocytes and neutrophils [45], as well as IFN- γ , which is produced by Th1 and Tc1 cells, in response to allergen challenge [156].

As expected, expression of IL-1 β , TNF, and IFN- γ was considerably enhanced in DNFB challenged skin from DNFB sensitized controls, relative to naïve tissue (Figure 3-9I). TRI MP treatment significantly suppressed expression of these three pro-inflammatory cytokines, though expression levels were still greater than in naïve tissue (Figure 3-9I).

Finally, to confirm that suppression of hypersensitivity responses was mediated by expanded Treg populations, we used a GITR agonist to inhibit the suppressive function of Tregs [157]. Anti-GITR (DTA-1, 0.5 mg/mouse) was injected intraperitoneally 3 days before DNFB challenge of TRI MP treated mice (Figure 3-9A). These mice developed a robust DTH response to DNFB challenge, comparable to sensitized controls without TRI MP, as indicated by ear swelling (Figure 3-9B) and histological features of skin tissue 4 days post-challenge (Figure 3-9D,G). Together, these data suggest that blocking Treg function abrogates the suppressive effects of Treg-induction therapy with TRI MPs. Interestingly, treatment of mice with a Treg-depleting antibody (anti-CD25, PC-61) after DNFB sensitization only modestly abrogated the suppressive effects of TRI MPs (Figure 3-12). TRI MP treatment, with or without anti-CD25, significantly inhibited ear-swelling responses to DNFB challenge; however, ear swelling was somewhat greater 1-2 days post-challenge for mice treated with anti-CD25 (Figure 3-12B). Four days post-challenge, ear DLN from mice treated with TRI MP and anti-CD25 contained fewer FoxP3⁺ Tregs (Figure 3-12C) than those from mice treated with TRI MP alone. These results indicate that suppression of DTH responses by TRI MPs is not completely reversed by anti-CD25, possibly due to incomplete depletion of allergen-specific FoxP3⁺ Tregs, many of which are likely CD25^{low} (Figure 3-3D). Additionally, depletion of CD25⁺ effector T cells could inhibit the DTH response, offsetting the effects of depleting CD25⁺ Tregs [158].

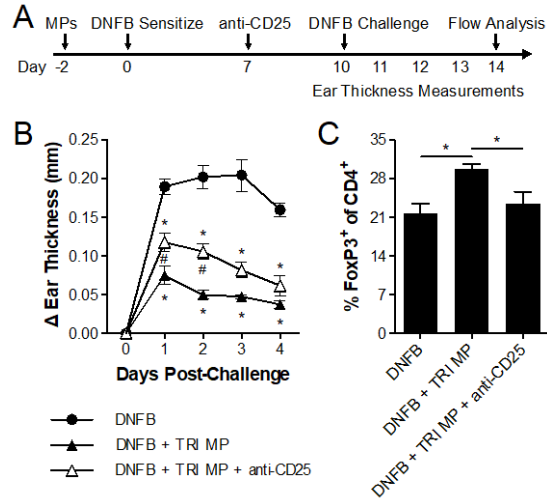


Figure 3-12. Depletion of CD25⁺ Tregs with anti-CD25 (PC-61) modestly impairs TRI MP-mediated suppression of DTH. (A) Experimental timeline. Anti-CD25 (PC-61, 0.5 mg i.p.) was used to deplete CD25⁺ Tregs. (B) Measurement of DTH response to DNFB challenge of ears. Increases in ear thickness (swelling) are relative to baseline (pre-challenge) measurements. (C) FoxP3⁺ Treg frequency in ear DLN at 4 days post-challenge, as determined by flow cytometry. Significant differences (relative to DNFB in B) are indicated by * $p < 0.001$. Significant differences relative to DNFB + TRI MP are indicated by # $p < 0.05$ (N = 4-5 mice per group).

3.2.6 Treg-inducing factors must be delivered locally (near the sensitization site), but generate systemic and specific tolerance to contact allergens.

To determine whether local treatment (at the same site as hapten challenge) was necessary, we injected TRI MPs at the abdomen, a distal site that doesn't drain to the cervical LN, and examined T-cell populations in ear DLN four days after sensitizing ears with DNFB. Interestingly, treatment at a distal site had no effect on Th1 and Tc1 populations in ear DLN, and a significantly diminished effect on Treg frequencies (Figure 3-6B). This led to Treg / Teff ratios similar to those seen in DNFB sensitized mice without treatment, and more than two-fold less than Treg / Teff ratios in DLN of mice treated with TRI MP near the sensitization site (Figure

3-13A). Since we observed significantly greater Treg / Teff ratios in non-draining inguinal LN (NDLN) of mice treated with TRI MP near the sensitization site, compared to sensitized mice (Figure 3-13A), we next wanted to see whether local treatment could generate systemic hyporesponsiveness to subsequent allergen exposure. Accordingly, we injected Blank MP or TRI MP at the abdomens of mice prior to sensitizing abdomens with DNFB, and then challenging ears (Figure 3-13B). Notably, TRI MP treatment at the sensitization site effectively suppressed the DTH response to challenge at a distal site (ears), as evidenced by a significant reduction in ear swelling (Figure 3-13C).

Finally, to demonstrate allergen-specificity of TRI MP-mediated DTH suppression, mice were treated with Blank MP or TRI MP near the site of sensitization to one allergen (OXA), and then sensitized to a second allergen (DNFB) at a different site and time (see timeline in Figure 3-13D). As with prior hapten-mediated ACD experiments (Figure 3-9 and Figure 3-10), ears were challenged 12 days after treatment with MPs. Ear-swelling responses to DNFB challenge were comparable for both TRI MP- and Blank MP-treated mice (Figure 3-13E). In contrast, TRI MP-treatment near the site of DNFB or OXA sensitization suppressed DTH responses to subsequent challenge with the same allergen (Figure 3-9B and Figure 3-10). Collectively, these results suggest that TRI MP treatment suppresses DTH responses in an allergen-specific manner, rather than by acting as a non-specific anti-inflammatory or immunosuppressant.

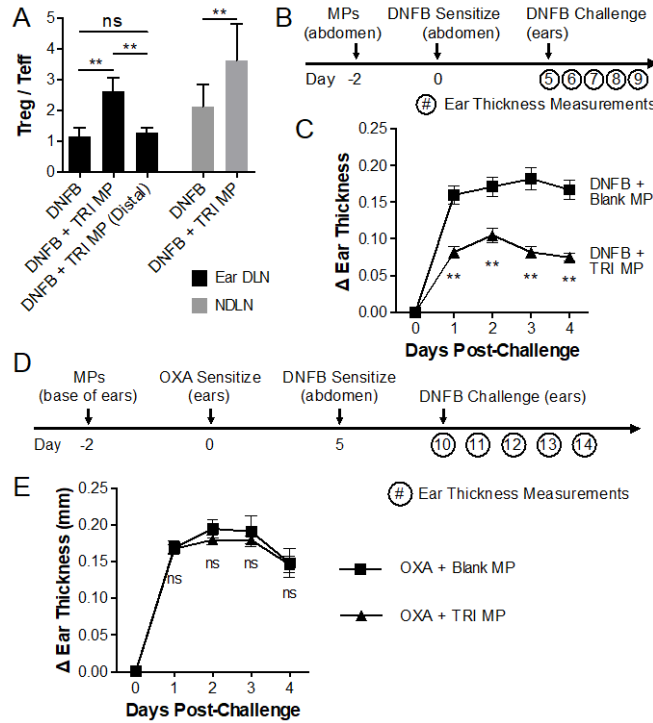


Figure 3-13. TRI MP injected near sites of skin sensitization can suppress DTH responses to challenge at distal sites. (A) Four days after sensitization of ears with DNFB, ear-draining cervical LN (DLN, black) or non-draining inguinal LN (NDLN, gray) were isolated and T-cell populations analyzed by flow cytometry ($N \geq 7$ for DLN, $N \geq 20$ for NDLN). TRI MP were injected either at the base of the ears or at the abdomen, a site “distal” to sensitization. Treg / Teff represents the ratio of $CD4^+ FoxP3^+$ Treg to $CD4^+ T-bet^+$ Th1 and $CD8^+ T-bet^+$ Tc1 effector T cells (Teff). DNFB and DNFB + TRI MP DLN data are also presented in Figure 3-3B. (B) Experimental timeline for allergen challenge at a distal site to sensitization and treatment. (C) Increases in ear thickness (ear swelling) after DNFB challenge, relative to naïve (pre-challenge) thickness ($N=10$). (D) Experimental timeline to demonstrate allergen-specific DTH suppression. (E) Ear swelling after DNFB challenge ($N=7-8$) of mice sensitized to OXA and DNFB at different sites, according to the timeline in (D). Mice were treated with Blank MP or TRI MP near the site of OXA sensitization only. Significant differences are indicated by $*p < 0.05$ or $**p < 0.001$.

3.2.7 TRI MP travel to skin DLN after injection, but therapeutic efficacy does not depend on lymphotropic delivery.

Given the requirement for local delivery of TRI factors, we sought to determine the importance of using small lymphotropic MPs that would travel to the skin DLN after injection. Previous studies have demonstrated that subcutaneously injected nanoparticles (NPs), or small MPs, can travel passively through lymphatics to DLN [71, 159-162]. For example, small NPs (50-60 nm) coated with antigen, complement proteins, and/or tolerogenic ligands have been used as lymphotropic adjuvants or modulators of immune responses [71, 159, 160]. Larger chitosan/heparin particles (200-1000 nm) also arrived in DLN within 45 minutes of injection, which is faster than tissue-resident phagocytes could take up and carry them [161]. Another study found that larger NPs (500-2000 nm) were mostly associated with DCs from the injection site, while smaller (20-200 nm) NPs could associate with lymph node resident cells [162].

Since TRI MPs are polydisperse in size, with diameters of approximately $1.7 \pm 0.9 \mu\text{m}$, we expected some to passively travel to skin DLN after injection, and some to be carried by phagocytic cells. To test this hypothesis, fluorescently labeled MPs were injected at the bases of ears of mice, and DLN were isolated 90 minutes or 48 hours later, cryosectioned, and imaged. By 48 hours, MPs were observed in paracortical regions of DLN, often associated with CD11c^+ cells (Figure 3-14), consistent with active transport by DCs at the injection site. Some presumably smaller MPs also were observed in the subcapsular sinus of DLN within 90 minutes of injection (Figure 3-15A), consistent with passive trafficking through the lymphatics. Notably, the vast majority of injected MPs remained at the injection site, even after several days.

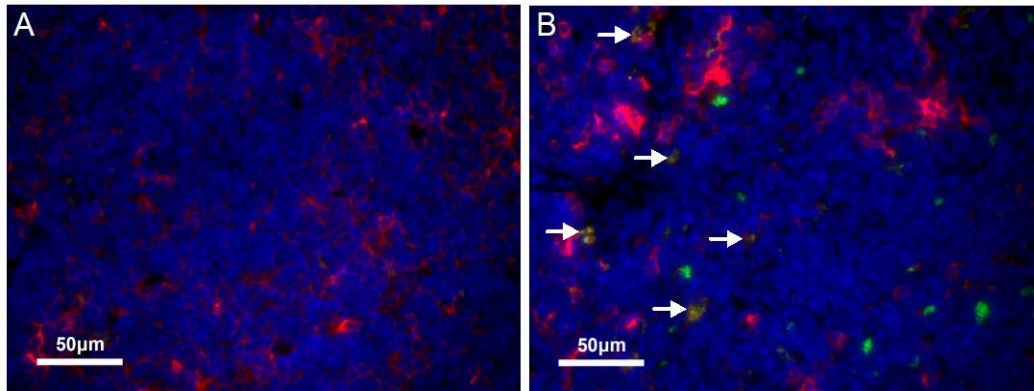


Figure 3-14. Some TRI MPs arrive in the local skin DLN after injection. Representative immunofluorescence images of paracortical regions of lymph nodes, with staining for nuclei (DAPI, blue), dendritic cells (CD11c, red), and MPs (FITC-labeled, green). (A) Naïve cervical lymph node. (B) Skin DLN 48 hours after local subcutaneous injection of FITC-labeled MPs. Arrows indicate co-localization of FITC MPs and CD11c⁺ dendritic cells.

To assess whether release of TRI factors from MPs within the DLN is necessary for efficient Treg-induction and therapeutic efficacy, treatment with the lymphotropic TRI MPs was compared to that with TRI MPs sequestered at the site of injection. The latter was accomplished by suspending MPs in a 10% pNIPAM solution instead of PBS. As a biologically inert thermoresponsive hydrogel, pNIPAM transitions from an injectable liquid at room temperature to a particle-retaining solid gel upon injection (lower critical solution temperature = 32°C [148]). Unlike TRITC-labeled MPs injected in PBS, those injected in pNIPAM did not appear in DLN at 90 minutes (Figure 3-15A-B) or at 48 hours (not shown), confirming that pNIPAM sequestered MPs at the injection site. Importantly, prior work from our lab also indicates that release of small molecule drugs from MPs is not affected by suspending MPs in pNIPAM hydrogel [163]. Compared to prophylactic treatment with TRI MPs injected in PBS, treatment with TRI MPs sequestered in pNIPAM was equally effective at enhancing Treg populations, decreasing Th1 and Tc1 effector T cell populations, and inhibiting DTH responses to DNFB challenge (Figure

3-15C-D). Collectively, these data suggest that lymphotropic MPs are not essential for therapeutic efficacy. Therefore, local injection of TRI MPs near allergen contact likely provides elevated concentrations of TRI factors in skin DLN due to sustained release at the injection site, which drains to that lymph node.

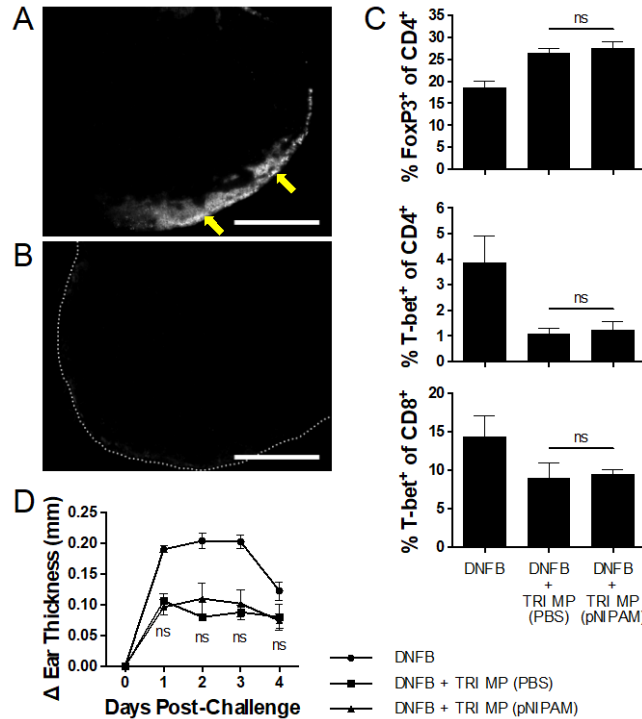


Figure 3-15. TRI MPs do not need to travel to DLN for therapeutic efficacy. (A-B) Representative fluorescence images of TRITC-labeled MPs in the DLN of mice 90 minutes after injection in PBS (A), or 10% pNIPAM (B). Arrows indicate regions of the subcapsular sinus with large quantities of MPs. For clarity, the DLN in (B) is outlined with a dotted line. Scale bars are 500 μ m. (C) Relative frequencies of Tregs (CD4⁺ FoxP3⁺), Th1 (CD4⁺ T-bet⁺), and Tc1 (CD8⁺ T-bet⁺) populations in DLN of mice 4 days after sensitization of ears with DNFB. MPs were injected at the base of ears two days prior to sensitization. (D) Increases in ear thickness (ear swelling) after DNFB challenge, relative to naïve (pre-challenge) thickness. Ear swelling for mice treated with lymphotropic TRI MP (in PBS), or TRI MP sequestered at the injection site (in pNIPAM), are not significantly different ($p > 0.05$, N=5 mice per group).

3.2.8 In previously sensitized mice, TRI MPs administered at the time of allergen challenge suppress subsequent DTH responses.

To determine whether TRI MPs could generate allergen tolerance in previously sensitized individuals, mice were exposed to DNFB twice at the abdomen prior to administration of TRI MP and challenge of left ears with DNFB. Mice were later re-challenged at the opposite ears according to the experimental timeline in Figure 3-16A. As with prophylactic treatment at the time of sensitization, TRI MP treatment of pre-sensitized mice at the time of allergen challenge significantly inhibited DTH responses, as indicated by a significant reduction in ear swelling relative to untreated mice (Figure 3-16B). Notably, TRI MP-induced tolerance persisted, resulting in suppressed DTH responses to a subsequent re-challenge (Figure 3-16C). TRI MP treatment remarkably improved ear skin histology post-challenge (Figure 3-16D) and re-challenge (not shown). As with prophylactic treatment, treatment at the time of allergen challenge reduced acanthosis, hyperkeratosis, spongiosis, and cellular infiltrates (Figure 3-16E). Skin DLN from TRI MP treated mice also contained enhanced Treg populations and decreased Th1 and Tc1 populations, relative to untreated mice, contributing to an increase in Treg / Teff (FoxP3⁺ / T-bet⁺) ratios that is consistent with a more tolerogenic immune profile (Figure 3-16F). Finally, TRI MP treatment significantly reduced the influx of T-cells into the skin after allergen challenge and re-challenge, as indicated by reductions in total CD3⁺ T cells in skin sections (Figure 3-16F,G).

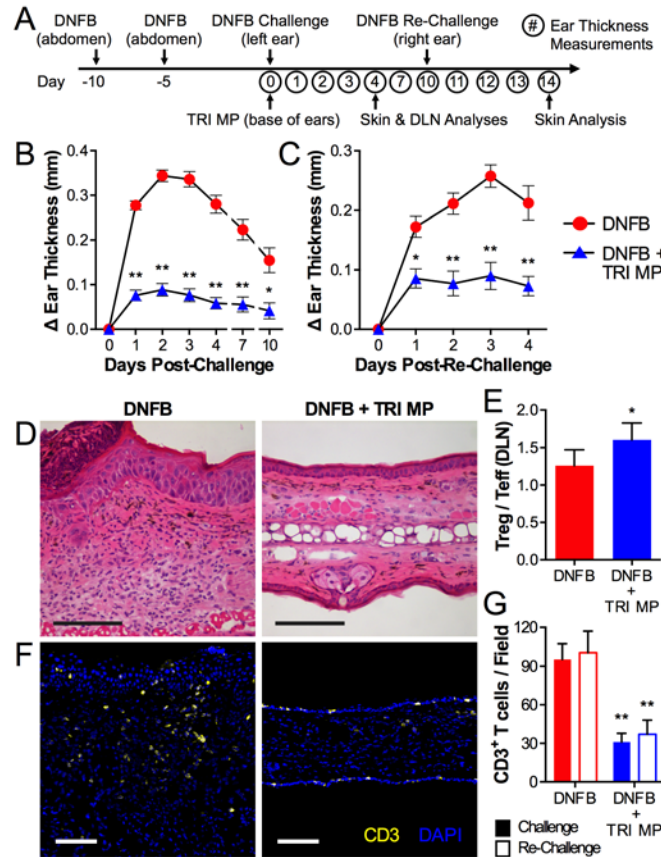


Figure 3-16. Treatment of previously sensitized mice with TRI MP at the time of allergen challenge reverses ongoing ACD and suppresses DTH responses to subsequent exposures. (A) Experimental timeline. (B-C) Increases in ear thickness (swelling) after (B) DNFB challenge and treatment (N=15) or (C) re-challenge (N=8), relative to naïve ear thickness. (D) Representative ear skin histology (H&E) from 4 days post-challenge. DNFB was applied to the dorsal side of ears (top of images). Scale bars are 100 μ m. (E) Ratio of FoxP3⁺ Treg to T-bet⁺ Th1 and Tc1 effector T cells in DLN 4 days post-challenge. (F) Representative immunofluorescence images of ear skin from 4 days post-challenge. (G) Quantification of T-cell infiltrates in skin 4 days after challenge or re-challenge, based on immunofluorescence (N=7-8). Significant differences are indicated by *p < 0.05 or **p < 0.001, relative to DNFB alone.

3.2.9 TRI MPs induce protein-specific Tregs and suppress protein-mediated ACD.

While ACD typically involves polyclonal T-cell responses to hapten-autologous protein complexes, DTH responses to foreign protein antigens can develop when sensitizing exposure occurs through skin with barrier defects (e.g. from pre-existing dermatitis, physical damage, or chemical damage by detergents). To investigate whether TRI MP could generate protein antigen-specific Tregs and suppress protein DTH responses, we used dissolvable microneedle arrays (MNAs) to deliver ovalbumin (OVA, model antigen) through the stratum corneum, into the epidermis and dermis [98]. In this application, MNAs serve as an alternative to tape-stripping and topical application of protein or intradermal injections of proteins, as others have reported for protein sensitization [81]. Adoptive transfer of CD45.2⁺ OVA-specific T cells (from OT-I and OT-II T-cell receptor transgenic mice) to congenic CD45.1 B6 mice enabled identification of OVA-specific T-cell responses to sensitization with OVA MNA and treatment with TRI MP (Figure 3-17A). OVA-sensitized mice (with Blank MP) generated strong DTH responses when challenged with OVA MNA, as indicated by ear swelling that peaked 48 hours post-challenge (Figure 3-17B). While TRI MPs alone were not able to suppress the ear swelling response (data not shown), likely due to the artificially high frequency of adoptively transferred OVA-specific T cells, treatment with TRI MP plus extra soluble factors (IL-2, TGF- β 1, and rapamycin at the same time as TRI MP administration) significantly suppressed the OVA DTH response (Figure 3-17B). Immunofluorescence stained ear tissue from 4 days post-challenge revealed a significant reduction in cutaneous CD3⁺ T-cell infiltrates (Figure 3-17C,D) with treatment, and a significantly greater proportion of FoxP3⁺ Tregs (Figure 3-17D). Finally, analysis of T-cell populations in ear skin DLN at 4 days post-sensitization revealed that Treg-inducing treatment significantly reduced OVA-specific T-cell expansion, as indicated by fewer CD45.2⁺ cells

(Figure 3-17E). Notably, increased frequencies of OVA-specific FoxP3⁺ Tregs were accompanied by significantly lower frequencies of OVA-specific T-bet⁺ Th1 and Tc1 effector T-cell populations (Figure 3-17E). Interestingly, we observed a substantial increase in a population of OVA-specific CD4⁺ CD25⁺ FoxP3⁻ T-bet⁻ T cells with potential suppressive capacity in an *in vitro* suppressive assay (Figure 3-17E and Figure 3-18). As TRI MP treatment alone was unable to suppress the OVA DTH response, it was also unable to enhance Treg populations or reduce Th1 and Tc1 populations as well (Figure 3-17E). Notably, soluble factors alone had no significant effects on OVA-specific Treg, Th1, or Tc1 populations (Figure 3-17E), suggesting sustained delivery of the Treg-inducing factors is important. Collectively, these data demonstrate that TRI MP (along with extra soluble factors as a “burst” at the time of administration) can induce protein antigen-specific Tregs *in vivo* and suppress protein DTH responses.

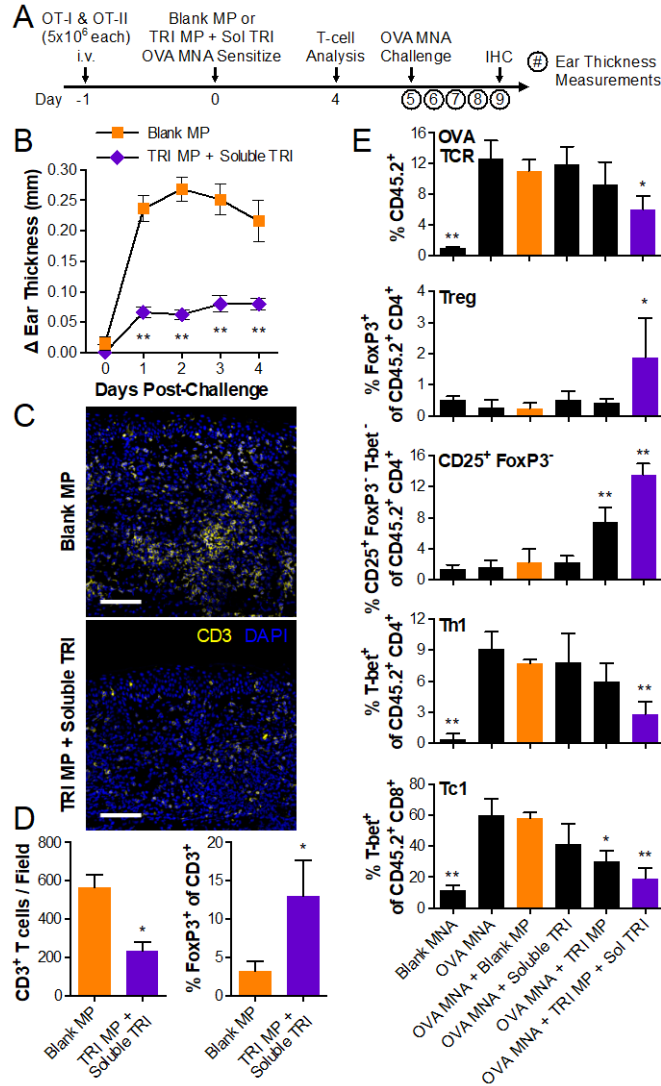


Figure 3-17. Treatment with TRI MP prior to OVA sensitization suppresses a protein-specific DTH response.

(A) Experimental timeline. OT-I & OT-II cells (CD45.2⁺) were transferred to congenic CD45.1⁺ B6 recipient mice. (B) Ear swelling after OVA challenge, represented as the difference in thickness between OVA MNA treated ears and contralateral Blank MNA treated ears (N=8). (C) Representative ear skin sections from 4 days post-challenge, stained for T cells (CD3, yellow) and counterstained with DAPI. Scale bars are 100 μ m. (D) Quantification of cutaneous T cells per imaged field (as in C) and % Treg, based on similar IHC images with FoxP3 staining (N=5). (E) Frequencies of various OVA-specific (CD45.2⁺) T-cell subsets in skin DLN at 4 days post-sensitization (N \geq 5). Significant differences, relative to OVA MNA + Blank MP, are indicated by *p<0.05 or **p<0.001.

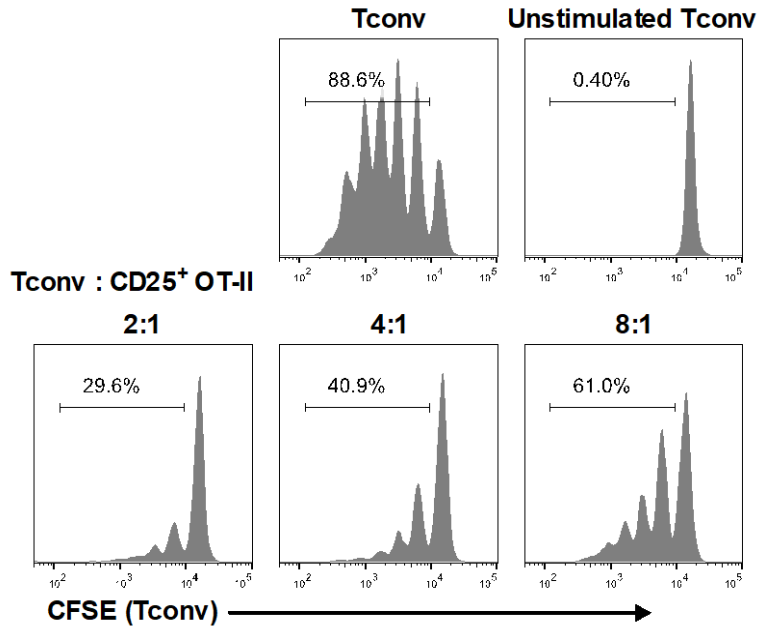


Figure 3-18. TRI MP-induced CD25⁺ OT-II T cells suppress proliferation of naïve CD4⁺ CD25⁻ conventional T cells (Tconv). Live CD45.2⁺ CD4⁺ CD25⁺ cells (CD25⁺ OT-II) were FACS sorted from DLN of CD45.1 B6 mice five days after adoptive transfer of 5x10⁶ CD45.2⁺ OT-II cells, and four days after OVA sensitization and TRI MP treatment. CFSE-labeled CD45.1⁺ Tconv (5x10⁴ / well) were cultured with anti-CD3/anti-CD28 beads (5x10⁴ / well) and CD25⁺ OT-II cells at the indicated ratios. Unstimulated Tconv were cultured without anti-CD3/anti-CD28 beads. Based on flow cytometry analysis (Fig. 6E), the CD25⁺ OT-II population contains less than 12.5% FoxP3⁺ Tregs; therefore, a Tconv : CD25⁺ OT-II ratio of 8:1 corresponds to a Tconv : FoxP3⁺ OT-II ratio of at least 64:1. Representative CFSE-dilution histograms depict proliferation of Tconv, and gates indicate percent of cells proliferating after 72 hours. Data are representative of two co-cultures, and CD25⁺ OT-II T cells were pooled from five mice.

3.3 DISCUSSION

As an alternative to the current symptomatic treatments for ACD, which use non-specific anti-inflammatories (e.g. corticosteroids; see Chapter 1.1.2), our first therapeutic approach to promote allergen tolerance involved using the TRI MP delivery system to condition the local skin DLN microenvironment and expand Treg populations *in vivo*. The overall therapeutic goal of expanding Treg populations (described in Chapter 1.2) stems from their ability to suppress aberrant immune responses in a variety of inflammatory and autoimmune diseases [14]. Accordingly, in the present study, we demonstrated that sustained local release of TGF- β 1, rapamycin, and IL-2 from TRI MPs injected near the site of cutaneous sensitization or challenge expanded allergen-specific Treg populations and suppressed pro-inflammatory Th1 and Tc1 effector T-cell populations in skin DLN (Figure 3-3 and Figure 3-16E). Although an injection of un-encapsulated TRI factors 0 to 3 days after sensitization suppressed effector T cells, expansion of Treg populations required sustained release from TRI MPs (Figure 3-6A). This could be due to the fact that rapamycin, which can suppress effector T-cell proliferation, has a relatively long half-life of at least 6 hours in mice [164]. In contrast, IL-2 and TGF- β 1, which are essential for Treg differentiation and proliferation [151], have very short *in vivo* half-lives of a few minutes [68, 165]. TRI MPs extend the presence of these immunomodulatory cytokines, presumably providing a tolerogenic microenvironment in which antigen presentation by skin-emigrating DCs occurs during the sensitization phase. Importantly, MP formulations directed toward conditioning the local antigen presentation microenvironment significantly reduce therapeutic doses of TRI factors. For example, TRI MP treatment translates to less than 100 ng/kg/day of cytokines and 0.15 mg/kg/day of rapamycin, doses which are orders of magnitude less than those typically used for systemic immunomodulation [166, 167]. These dose-sparing effects associated

with controlled release formulations are important because of adverse effects associated with high-dose cytokine and immunosuppressant therapies [64, 68]. Notably, while TRI MP do not appear to release sufficient amounts of factors to affect T-cell differentiation at distal sites (Figure 3-13A), local effects on Treg and effector T-cell populations can generate systemic tolerance and suppress DTH responses to subsequent allergen exposure at distal sites (Figure 3-13B), presumably due to circulation of locally expanded Tregs and fewer circulating effector T cells.

In addition to increasing the ratio of anti-inflammatory, tissue-protective Tregs to pro-inflammatory, tissue destructive effector T cells, TRI MP treatment during sensitization suppressed DTH responses to subsequent allergen exposures (Figure 3-9, Figure 3-5, Figure 3-17). Hyporesponsiveness persisted through at least two allergen challenges 10 and 20 days after sensitization (Figure 3-9), and TRI MP reduced ear swelling to levels seen in un-sensitized mice when first exposed to DNFB (data not shown). In other words, ear swelling in TRI MP treated mice was comparable to that caused by the innate immune response to a hapten without T-cell involvement [45]. Furthermore, TRI MPs appeared to suppress DTH responses in an allergen-specific manner, with minimal non-specific or off-target immunosuppression. While TRI MPs may potentially expand some non-allergen-specific Tregs, the increased populations of OXA-specific Tregs and/or non-specific Tregs (Figure 3-5) failed to inhibit DTH responses to challenge with a second allergen (DNFB), for which sensitization occurred at a distal site and time, relative to TRI MP treatment (Figure 3-13E). This allergen-specific suppression of ACD distinguishes TRI MP-treatment from traditional therapies involving anti-inflammatories (e.g. corticosteroids) applied topically after allergen challenge to reduce inflammation non-specifically, regardless of the allergen. Finally, TRI MPs were also able to reverse established

allergen-specific immune responses in previously sensitized mice and promote allergen tolerance, as evidenced by inhibited DTH responses to allergen challenge and re-challenge (Figure 3-16).

Suppression of DTH responses appear to be mediated by the expanded Treg populations, as impairing Treg suppressive function via anti-GITR administration [157] reversed the beneficial effects of treatment with Treg-inducing MPs (Figure 3-9B). Previously, circulating Tregs were shown to suppress DTH responses by blocking influx of effector T cells into inflamed tissue. This process is mediated by contact-independent mechanisms, including production of cytokines and adenosine (by CD39), which inhibit effector T-cell adherence to vascular endothelial cells and subsequent extravasation [21, 49]. Immunohistochemical analysis of skin from TRI MP treated mice revealed a significant reduction in total T-cell infiltrates (Figure 3-9H, Figure 3-16F-G), and especially CD8⁺ effector T cells (Figure 3-9H). Interestingly, although there were fewer total FoxP3⁺ Tregs in skin tissue after TRI MP treatment, there was at least a two-fold increase in the ratio of FoxP3⁺ to CD8⁺ T cells (Figure 3-9H). We observed a similar trend in the protein-mediated OVA DTH model, where total T-cell infiltrates were significantly reduced in TRI MP + Soluble TRI treated skin, and the frequency of FoxP3⁺ Tregs was enhanced (Figure 3-17C,D). In that model, we also observed increases in a population of CD25⁺ FoxP3⁻ OT-II cells, which, given their apparent suppressive function (Figure 3-18) and lack of T-bet expression (Figure 3-17), may be an unstable population or a type of unconventional FoxP3⁻ Treg reported previously in the setting of allergic disease [168, 169]. Future studies will be needed to delineate the contributions of skin-resident and circulating Tregs toward suppressing the DTH responses, and to identify allergen-specific Tregs with resident-memory or central memory phenotypes at extended time-points. Additionally, future

studies will be needed to determine the maximum duration of tolerance induced by TRI MP under various conditions, including repeated allergen exposure or challenge more than three weeks after treatment. In the event that repeated allergen exposure eventually breaks tolerance induced by TRI MPs, a booster treatment and/or greater initial dose of TRI factors may be necessary. These longer-term studies will require the IL-2 and TGF- β 1 release assays to be extended beyond three weeks, and if bioactive cytokines are detected at later time points, formulations may be modified to restrict release to one week. This could involve increasing the overall PEG:PLGA ratio or blending the PEG-PLGA co-polymer with a lower molecular weight PLGA [170].

In addition to demonstrating efficacy of Treg-inducing MPs in models of hapten-mediated ACD, which involve polyclonal allergen-specific T-cell responses, we were also able to induce monoclonal protein-specific Tregs in a well-defined TCR transgenic adoptive transfer model. The fact that TRI MP alone did not expand OVA-specific FoxP3⁺ Tregs or suppress DTH responses in this model emphasizes that different amounts of Treg-inducing factors may be needed depending on the nature of the acute immune response to be modulated. In this particular case, adoptive transfer of a pool of clonal OVA-specific T cells from OT-II Rag2^{-/-} mice significantly alters both the frequency and range of T-cell receptor binding affinities of available T-cell precursors. Consistent with this notion, difficulty in inducing OVA-specific Tregs also may be related to the dose of antigen delivered (up to 100 μ g OVA per MNA). Dose-dependent responses to antigen have been reported, with maximal Treg proliferation observed at low antigen doses, and Th1 proliferation favored at high antigen doses *in vitro* [171]. Accordingly, protein-specific Treg induction *in vivo* may be further enhanced by optimizing the dose and concentration gradient of protein antigens delivered with MNAs. For previously sensitized

individuals, application of MHC-II-restricted peptides (e.g. OVA₃₂₃₋₃₃₉, a CD4⁺ T cell epitope) instead of whole proteins, at the time of TRI MP treatment could prevent further expansion of class I restricted peptide-specific CD8⁺ effector T cells, while still allowing TRI MPs to induce and expand class II restricted peptide-specific Treg populations [81]. Ultimately, such considerations would be relevant to both inducing tolerance to protein allergens, as well as treating autoimmune diseases by loading MNAs with auto-antigenic peptides or proteins.

The current study focused on two distinct strategies for tolerance induction. The first involved administration of TRI MPs at the time of allergen sensitization, a prophylactic approach that would be clinically relevant for common and potent contact allergens, such as urushiol in poison ivy, which sensitizes an estimated 85% of the population. Alternatively, for less common and/or weakly sensitizing contact allergens, limiting treatment to patients with established ACD is more feasible. In this case, TRI MP treatment delivered in the context of a patch test defined allergen would need to expand Treg populations sufficiently to subdue the primed memory T-cell response. This scenario may be more difficult than inducing tolerance with treatment at the time of sensitization, as memory T cells can be more resistant to Treg-mediated suppression than naïve T cells under some conditions [172]. Encouragingly, in the hapten-mediated ACD model, we found that treatment of previously sensitized mice with the same dose of TRI MPs at the time of allergen challenge was able to suppress the ensuing DTH response and prevent a subsequent DTH response to a re-challenge (Figure 3-16). Optimizing the dosing and/or ratios of TRI factors for prophylactic and curative therapies may enhance therapeutic efficacy even more. Further investigation will be necessary to determine whether TRI MPs can permanently reverse the allergen-specific memory T-cell response in previously sensitized subjects and induce persistent tolerance to protect against chronic, repeated allergen exposure.

Finally, unlike other experimental approaches to Treg expansion, treatment with TRI MPs enables expansion of allergen-specific Tregs, regardless of whether the antigens are specific known proteins (e.g. OVA), or a broad array of unknown haptened epidermal proteins. This is especially important for treatment of hapten-mediated ACD, since a single defined allergenic protein or peptide is unlikely to be available for therapy, and immunogenicity of the extensive, heterogeneous repertoire of hapten-protein conjugates differs among individuals. This approach may also be suitable for suppressing allograft rejection and graft vs. host disease, which involve T-cell responses against multiple unknown graft-associated or self-antigens. Ultimately, sustained local delivery of Treg-inducing factors from TRI MP may also be used to generate tolerance and halt the destructive inflammation responsible for a variety of other autoimmune diseases. In these scenarios, the patient's tissue or allograft would serve as a source of unidentified antigens, and a Treg-inducing microenvironment for antigen presentation would be provided by TRI MP.

4.0 CO-DELIVERY OF ALLERGEN AND VITAMIN D3 ANALOG WITH MICRONEEDLE ARRAYS ENGINEERS THE SKIN MICROENVIRONMENT TO PROMOTE ALLERGEN TOLERANCE

4.1 INTRODUCTION

The cutaneous microenvironment, through which exposure to potential allergens occurs, dictates the nature of immune responses to proteins and chemical haptens. Specifically, allergen sensitization is enhanced by pro-inflammatory microenvironments, while antigen exposure in the absence of pro-inflammatory “danger” signals, or combined with pro-tolerogenic signals, may promote antigen-specific hyporesponsiveness, or tolerance. Pro-inflammatory cutaneous microenvironment may exist prior to allergen exposure—as in individuals with atopic dermatitis [173]—or may result from innate immune responses to allergen exposure. Some allergens evoke innate inflammatory responses directly by signaling through pattern recognition receptors (e.g. TLR4 activation by nickel and cobalt [174, 175], or dust mite allergens Derp2 and Derf2 [176]). Alternatively, many contact allergens induce reactive oxygen species (ROS) and release of ATP and other damage-associated molecular patterns (DAMPs), such as low-molecular-weight hyaluronic acid, which signal through P2X7R and TLR2/4, respectively [177-179]. Simultaneous exposure to a potential allergen and contact irritant (e.g. sodium lauryl sulfate

[180]), multiple allergens [181-183], or allergen and adjuvant (e.g. TLR4 ligand lipopolysaccharide [184, 185]) may also enhance sensitization.

In contrast, exposure to potential allergens in the absence of pro-inflammatory “danger” signals, or with pro-tolerogenic context can lead to failed sensitization or even allergen tolerance. For example, structural analogs of haptens that fail to activate the inflammasome and induce pro-inflammatory cytokines can induce tolerance to related allergens (e.g. dinitrothiocyanobenzene (DNTB), an analog of the strong sensitizers dinitrofluorobenzene (DNFB), dinitrochlorobenzene (DNCB), and trinitrochlorobenzene (TNCB) [77]). Repeated cutaneous exposure to haptens at non-irritant, sub-sensitizing doses [78-80], or oral administration of allergens [186-193], also may promote tolerance rather than sensitization. Unfortunately, non-immunogenic structural analogs are not available for most allergens, including more than 4350 known chemical haptens [2], and sub-threshold doses vary greatly among allergens and among individuals [194]. Furthermore, oral tolerance induction is typically less effective and persistent after sensitization [195, 196], and may be associated with local and gastrointestinal side effects [197].

While the aforementioned approaches to tolerance induction involve modifying allergen chemical structure, dose, and/or site of introduction, the skin microenvironment also may be altered to provide pro-tolerogenic context for cutaneous introduction of unmodified allergens. For example, ultraviolet B (UVB) irradiation generates several immunosuppressive factors in the skin, including DNA photoproducts, oxidized membrane lipids and proteins, *cis*-urocanic acid, and 1,25-dihydroxyvitamin D3 [83]. These factors, as well as DNA damage, promote migration of Langerhans cells to skin draining lymph nodes (DLN) and sub-optimal presentation of antigen to T cells [198, 199]. Notably, application of proteins or haptens to UVB-irradiated skin results

in impaired priming of effector T-cell responses and enhanced induction of antigen-specific Tregs, which inhibit subsequent delayed-type hypersensitivity (DTH) responses [81-84].

Since UVB-mediated tolerance induction is mediated—at least in part—by cutaneous synthesis of 1,25-dihydroxyvitamin D3 [83, 84], the immunosuppressive active form of vitamin D3 [200-202], topical application of 1,25-dihydroxyvitamin D3, or synthetic analogs (e.g. MC903), has been investigated as an alternative method to modulate the skin microenvironment and promote antigen-specific immune tolerance. As with UVB-irradiation, topical application of 1,25-dihydroxyvitamin D3 or MC903 promoted allergen-specific Treg-induction and inhibited effector T-cell priming, leading to allergen tolerance upon subsequent application of haptens or proteins to treated skin in murine models [84-86]. While this approach eliminates the acute burns, DNA damage, and increased risk of skin cancer associated with UVB-irradiation, the reported tolerance induction protocols are extensive and “messy.” Typically, epicutaneous allergen application follows treatment with 1,25-dihydroxyvitamin D3, or MC903, for 3-4 days, and optimal introduction of protein allergens requires barrier layer disruption (e.g. tape-stripping) and occlusive dressings [84, 86]. Each of these components of the treatment regimen introduces potential sources of error, including inconsistent regions of application (e.g. allergen applied outside the pre-treated area could promote sensitization), variable per area dosing, and excessive or sub-optimal barrier disruption.

To address some of these limitations, we used dissolvable microneedle arrays (MNAs) to simultaneously deliver allergen and MC903 into the skin, thereby engineering the skin microenvironment to promote allergen-specific tolerance. Dissolvable MNAs are convenient off-the-shelf therapeutics that can efficiently deliver proteins and/or drugs into the epidermal and dermal layers of the skin, and enable reproducible treatment (i.e. consistent application area and

dose per area). In this chapter, we describe allergen tolerance induction with Allergen + MC903 MNA in murine models of ACD, and report effects of MC903 MNA on murine and human skin microenvironments and skin migratory cells.

4.2 METHODS

4.2.1 Mice

Female C57BL/6 and congenic CD45.1 B6 (B6.SJL-*Ptprc^a* *Pepc^b*/BoyJ) mice were purchased from The Jackson Laboratory (Bar Harbor, ME) and used at 8-12 weeks of age. OVA TCR-transgenic B6 Rag1^{-/-} OT-I (B6.129S7-Rag1^{tm1Mom} Tg(TcraTcrb)1100Mjb) and B6 Rag2^{-/-} OT-II (B6.129S6-Rag2^{tm1Fwa} Tg(TcraTcrb)425Cbn) mice were purchased from Taconic (Rensselaer, NY). All mice were maintained under specific pathogen-free conditions at the University of Pittsburgh, and experiments were conducted in with the approval of the Institutional Animal Care and Use Committee and in accordance with NIH guidelines.

4.2.2 Microneedle Array Fabrication

Dissolvable microneedle arrays (MNAs) were fabricated using a previously reported spin-casting technique [98, 203]. Mastermolds were manufactured from a rigid polymer, poly(methyl methacrylate), via the micromilling technique described in [98], and used to create poly(dimethylsiloxane) (PDMS; Sylgard® 184; Dow Corning, Auburn, MI) production molds [98]. The PDMS molds were then used to spin-cast MNAs with the geometry and dimensions

depicted in Figure 4-1. MNAs were tip-loaded with 100 μg ovalbumin containing endotoxin (OVA_{AETX}; grade V ovalbumin; Sigma Aldrich, St. Louis, MO), 100 μg EndoGrade® ovalbumin (OVA; endotoxin <0.1 EU/mg; Hyglos GmbH, Germany), 100 μg Alexa Fluor 647-labeled OVA (Thermo Fisher Scientific, Waltham, MA), 20 μg OVA₃₂₃₋₃₃₉ peptide (OVAp; Anaspec, Fremont, CA), 1-5 μg calcipotriol (MC903; Cayman Chemical, Ann Arbor, MI), and/or 100 μg 2,4-dinitrochlorobenzene (DNCB; Sigma Aldrich). Unloaded Blank MNAs were fabricated for controls. For OVA MNA formulations, protein or peptide was added to a 2% (w/v) solution of low-viscosity sodium carboxymethyl cellulose (CMC, Mw 90 kDa; Aldrich) in sterile-filtered cell-culture grade water (Sigma). For MC903 and/or DNCB MNA formulations, the poorly water-soluble chemicals were first dissolved in N,N-dimethylformamide (DMF, Sigma Aldrich), and then added to the 2% CMC solution at a 1:1 ratio. Given the total microneedle volume of 2.3 μL per MNA, OVA and MC903 concentrations dictate total loading. For example, 4.4 $\mu\text{g}/\mu\text{L}$ MC903 in DMF plus 87 $\mu\text{g}/\mu\text{L}$ OVA in 2% CMC yielded MNA with 5 μg MC903 and 100 μg OVA. For tip-loading, 15 μL of the solution of bioactive agent(s) was dispensed onto each MNA production mold, followed by centrifugation in covered rotors for 1 min at 3500 rpm. Excess solution was removed, leaving ~ 2.3 μL per MNA in the obelisk-shaped cavities, and the molds were centrifuged uncovered for 30 min at 3500 rpm, with 20 L/min filtered airflow, leaving dry bioactive agent(s) in the tips of the microneedles. After tip-loading, molds were loaded with 80 mg of 25 wt% hydrogel consisting of 3:2 CMC:trehalose (D-(+)-trehalose dihydrate; Sigma) to fill the remainder of the microneedle cavities and form the MNA backing. Molds were centrifuged in covered rotors for 15 min at 4500 rpm, followed by covered incubation for 15 min. Rotor bucket covers were then removed, and molds centrifuged for 4 hours and 3500 rpm, with 20 L/min filtered airflow, leaving dry MNAs. All spin-casting steps

were carried out at room temperature ($\sim 22\text{ }^{\circ}\text{C}$) in a Sorvall Legend XTR centrifuge (TX-750 rotor, rectangular buckets; Thermo Scientific).

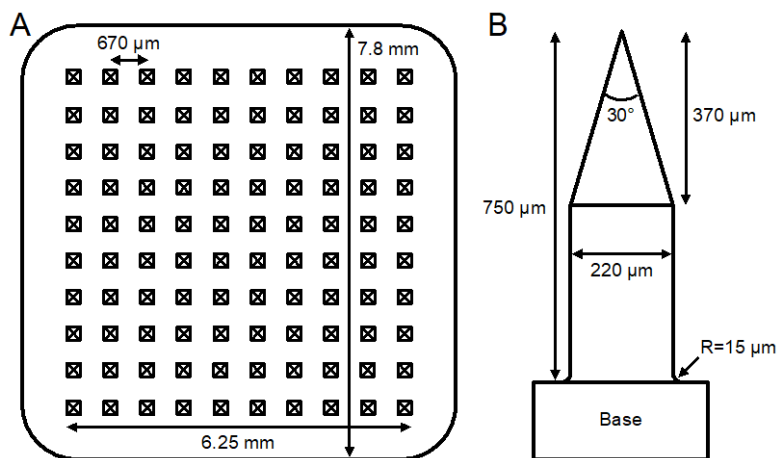


Figure 4-1. Microneedle Array (MNA) geometry and dimensions. (A) Schematic top-view of an MNA, which consists of an evenly distributed 10x10 matrix of microneedles. (B) Dimensions of a single obelisk-shaped microneedle, with square cross-section, apex angle of 30° , and fillet radius of $15\text{ }\mu\text{m}$. The total volume of a single microneedle is $0.023\text{ }\mu\text{L}$.

4.2.3 MNA Characterization

MNA geometry was evaluated by optical microscopy using a dissecting microscope (ZEISS Stemi 2000-C with an Olympus OM-D E-M5II camera). MNAs were viewed at an angle of 45° with respect to the objective lens. To obtain images with extended depth of field, several images captured at different focal planes were focus-stacked using the *Photomerge* and *Auto Blend Layers* functions in Adobe Photoshop CS6 (Adobe Systems, San Jose, CA). Endotoxin content in MNAs was measured by chromogenic LAL assay. Each MNA was dissolved in 1 mL reagent H_2O and further diluted 1:10 for Blank and OVA MNAs, or 1:125 for OVA_{ETX} MNAs. Endotoxin concentrations in diluted samples were then measured with a chromogenic LAL endotoxin assay kit (ToxinSensor; GenScript, Piscataway, NJ).

4.2.4 Murine Models of OVA Delayed Type Hypersensitivity (DTH)

Mice were sensitized to ovalbumin by transdermal application of an OVA_{ETX} MNA to the left side of shaved abdomens. To elicit a DTH response, mice were challenged 5 days post-sensitization (unless otherwise indicated) by applying an OVA_{ETX} MNA to the right ear. For some experiments, OVA MNAs were used for sensitization and/or challenge. A Blank MNA was applied to the left ear to control for any swelling caused by MNA application itself. Ear thickness was measured using an engineer's spring-loaded micrometer (Mitutoyo, Aurora, IL) prior to the OVA_{ETX} challenge and on days 1-4 post-challenge, and data are presented as differences between OVA_{ETX} MNA-treated and Blank MNA-treated ears. Prophylactic tolerization to OVA involved application of the indicated MNA (e.g. OVA + 5 µg MC903) to the right side of the shaved abdomen 9, 6, and 3 days prior to sensitization with OVA_{ETX} MNA. For tolerization of previously sensitized mice, mice were sensitized twice with an OVA_{ETX} MNA (days 0 and 5), followed by tolerization with OVA + MC903 MNA (days 10, 13, and 16), and challenge with OVA_{ETX} MNA (day 19). To investigate OVA-specific T-cell responses to OVA±MC903 MNA formulations, OVA-specific CD8⁺ and CD4⁺ T cells were isolated from spleens of OT-I and OT-II mice (CD45.2⁺) and adoptively transferred to congenic CD45.1 B6 mice by tail vein injection (5x10⁶ OT-I and 5x10⁶ OT-II cells per mouse) one day prior to MNA application.

4.2.5 Evaluation of Skin Histology by H&E Staining

Ears from mice were excised, flash frozen in OCT compound, and cryosectioned. Skin sections (7 µm thick) were stained with hematoxylin and eosin (H&E). Human skin explants were fixed

in 10% neutral buffered formalin for several days, dehydrated in 100% ethanol, cleared with xylene, and embedded in paraffin. Paraffin blocks were sectioned (5 μ m thick) and stained with H&E. Stained tissue sections were imaged using a Nikon Eclipse E400 microscope with ProgRes C5 camera and ProgRes CapturePro v2.9 software (Jenoptik AG, Jena, Germany).

4.2.6 Evaluation of Cellular Immune Responses by Flow Cytometry

Ear-draining cervical lymph nodes and spleens were harvested, passed through 70 μ m nylon cell strainer to create single cell suspensions. Splenocyte suspensions were depleted of erythrocytes by hypotonic lysis with 0.83% (w/v) ammonium chloride buffer. Ears were split along the central cartilage plate, and the dorsal sides chopped into small fragments and incubated in serum-free IMDM (Gibco, Life Technologies, Carlsbad, CA), supplemented with 1 mg/mL DNase I (grade II, Roche, Sigma Aldrich) and 1 mg/mL Collagenase D (Roche, Sigma Aldrich) at 37 °C for 1 hour. After passing twice through 70 μ m cell strainers, cells were collected and washed with cold PBS before staining. Cells were stained with fluorescently labeled antibodies purchased from BD Biosciences (San Jose, CA), eBioscience (San Diego, CA), or BioLegend (San Diego, CA). To identify Treg, Th1, Th2, and Tc1 populations, cells were blocked with anti-CD16/32 (2.4G2; BD) and stained for CD4 (RM4-5; eBio), CD8b (H35-17.2; eBio), and CD25 (PC61; BD). Transcription factor staining for FoxP3 (FJK-16s; eBio), T-bet (O4-46; BD), and GATA3 (L50-823; BD) was performed using the FoxP3 / Transcription Factor Staining Buffer Set (eBio). Skin-resident leukocytes and adoptively transferred OVA-specific T cells were identified by staining for CD45.2 (104; BD). Skin cell suspensions were also stained with a fixable viability dye (eBio) and antibodies for I-A^b (AF6-120.1; BD), CD11c (HL3; BD), CD11b (M1/70; BD), Ly6G (1A8; BD), F4/80 (BM8; BioLegend), and CD169 (3D6.112; BioLegend)

for some experiments. Data were acquired with 5-laser BD LSR-II or BD LSRFortessa flow cytometers, and analyzed using FlowJo (Tree Star, Ashland, OR). Population gates were set based on isotype, single-stain, and fluorescence minus one controls.

4.2.7 Evaluation of Humoral Immune Responses by ELISA

Blood was collected from anesthetized mice at the time of sacrifice (typically 4 days post-challenge) by cardiac puncture, and transferred to serum separator BD Microtainer® serum separator tube. After centrifugation (15 min at 16,000 xg), supernatant serum was collected and frozen for subsequent assessment. OVA-specific IgG1 and IgG2c levels in serum were determined by indirect ELISAs. High-binding 96-well plates (Costar EIA/RIA; Corning Inc., Corning, NY) were incubated overnight at 4 °C with Grade V OVA (100 µg/mL in 0.5 M carbonate-bicarbonate buffer, pH 9.6; Sigma). Plates were washed (3x) with 0.05% Tween20 in PBS, and blocked with 1% goat serum in PBS for 1 hour at 37 °C. Serum samples and standards (anti-OVA IgG1 from Cayman Chemical, Ann Arbor, MI; anti-OVA IgG2c from Chondrex, Redmond, WA) were diluted with 1% goat serum, added to plates, and incubated 2 hours at 37 °C. After washing (3x), plates were incubated for 1 hour at 37 °C with biotinylated secondary antibodies (goat anti-mouse IgG1 or IgG2c, 1:20,000 in 1% goat serum; Jackson ImmunoResearch, West Grove, PA). Plates were then washed (3x) and incubated for 30 min with streptavidin-HRP (1:1000 in 1% goat serum; BD Pharmingen). Plates were washed (3x) again and incubated at room temperature with 4,4',5,5'-tetramethylbenzidine (TMB) peroxidase substrate (Sigma) for 2-3 minutes, and the reaction quenched with 1.0 M H₂SO₄. OVA-specific IgE was quantified via sandwich ELISA using rat anti-mouse IgE capture antibody (R35-72, 4 µg/mL in PBS; BD Biosciences) and biotinylated-OVA (4 µg/mL in PBS + 1% BSA; Nanocs,

New York, NY) for detection. Serum samples and standards (anti-OVA IgE, Cayman Chemical) were diluted in 1% BSA in PBS. For all ELISAs, absorbance at 450 nm (OD₄₅₀) was read with a SpectraMax 340PC plate reader (Molecular Devices, Sunnyvale, CA), and serum concentrations calculated using standard curves known dilutions.

4.2.8 Murine Skin Microenvironment Evaluation After Treatment with Topical MC903 or MNAs Containing MC903 and/or DNCB

Ears of mice were treated epicutaneously with 5 µg MC903 dissolved in ethanol or intradermally with MNAs containing 5 µg MC903. Ethanol and Blank MNAs served as vehicle controls. Some mice were treated with MNAs containing MC903 and/or DNCB. After 6, 24, or 48 hours, ears tissue was homogenized at 4 °C in TRI-reagent (Molecular Research Center, Cincinnati, OH) using a Bullet Blender Storm 24 with stainless steel beads in Navy RINO tubes (Next Advance, Averill Park, NY). Total RNA was extracted according to the TRI-reagent manufacturer's protocol, and quantified using a DeNovix DS-11 spectrophotometer (Wilmington, DE). For each reverse transcriptase assay, 2 µg RNA was converted to cDNA using a QuantiTect Reverse Transcription Kit (Qiagen, Valencia, CA). Quantitative real-time PCR was then performed using VeriQuest Probe qPCR Mastermix (Affymetrix, Santa Clara, CA), according to the manufacturer's instructions, with 5' nuclease PrimeTime qPCR assays (Applied Biosystems, Thermo Scientific) specific for IL-10 (Mm01288386_m1), IL-18 (Mm00434226_m1), TSLP (Mm01157588_m1), IL-1B (Mm00434228_m1), TNF (Mm00443258_m1), NLRP3 (Mm00840904_m1), and β-glucuronidase (GUSB, endogenous control, Mm01197698_m1). Duplex reactions (FAM-labeled target gene primer and VIC-labeled GUSB primer) were run and analyzed on a StepOnePlus Real-Time PCR System

(Applied Biosystems, Carlsbad, CA). Relative fold changes in expression were calculated and normalized based on the $2^{-\Delta\Delta Ct}$ method, with naïve ear skin as the untreated control.

4.2.9 Human Skin Explant Cultures with MC903 MNA

Normal skin from healthy donors undergoing breast reduction surgery was acquired through the Magee-Women's Hospital Tissue Bank with institutional review board approval, and used according to University of Pittsburgh Medical Center guidelines. Tissue was rinsed in 70% ethanol and PBS, and skin explants (~ 1 mm thick) harvested with a Silver's miniature skin graft knife (Padgett, Integra Miltex, Plainsboro, NJ). Explants were cut into 2x2 cm squares, washed with 70% ethanol and twice with PBS, and placed epidermis up on wetted sterile filter paper on a silicone backing. Explants were covered with thin plastic wrap, and MNAs (4 per explant) were applied through the plastic wrap into the skin. Plastic wrap prevents MNA tips from starting to dissolve before penetrating the damp skin tissue. MNAs were removed after 5 minutes, and two explants with the same MNA treatment were placed epidermis up on steel mesh (1 mm pores) in 100 mm petri dishes (Falcon, Corning) with AIM-V serum-free media (Gibco, Life Technologies) supplemented with antibiotic antimycotic solution (Sigma Aldrich). This arrangement maintains an air-epidermal interface, while the dermis is in contact with media. After culture for 48 hours at 37 °C in 5% CO₂, explants were removed, cut into thin strips, and flash frozen for subsequent RNA isolation. Non-adherent cells that migrated out of explants into the media were collected for analysis by flow cytometry and counted with a hemocytometer.

4.2.10 Human Skin Microenvironment Evaluation by qRT-PCR Array

Skin was homogenized at 4 °C in TRI-reagent (Molecular Research Center, Cincinnati, OH) using a Bullet Blender Storm 24 with stainless steel beads in Navy RINO tubes (Next Advance, Averill Park, NY). Total RNA was extracted according to the TRI-reagent manufacturer's protocol, and quantified using a DeNovix DS-11 spectrophotometer (Wilmington, DE). RNA quality was assessed with the Agilent TapeStation 4200 at the University of Pittsburgh HSCRF Genomics Research Core (Agilent Technologies, Santa Clara, CA). For each reverse transcription assay, 1 µg RNA was converted to cDNA using an RT² First Strand Kit (Qiagen, Germantown, MD). Quantitative real-time PCR was then performed using a Human Inflammatory Response & Autoimmunity RT² Profiler PCR Array (Qiagen), RT² SYBR Green ROX qPCR Mastermix (Qiagen), and StepOnePlus Real-Time PCR System (Applied Biosystems, Foster City, CA). Thresholds were set consistently for all plates. Threshold cycles (C_T) for target genes (i) and three reference genes ($ActB$, $GAPDH$, and $HPRT1$) were used to calculate fold change (FC) in gene expression, relative to untreated (naïve) skin, for each patient tissue sample (j), according to:

$$FC_{i,j} = \frac{2^{-\Delta C_{T,i,j,treated}}}{2^{-\Delta C_{T,i,j,naive}}} = 2^{-\Delta \Delta C_{T,i,j}} \quad (1)$$

where

$$\Delta C_{T,i,j} = C_{T,i,j} - \frac{1}{3} (C_{T,ActB,j} + C_{T,GAPDH,j} + C_{T,HPRT1,j}) \quad (2)$$

4.2.11 Human Skin Migratory Cell Phenotype Analysis by Flow Cytometry

Migratory cells were blocked with Human BD Fc Block™ (BD Biosciences) for 20 min at 4 °C, and then stained with fluorescently labeled antibodies for CD11c (3.9, BD), HLA-DR (L243, BioLegend, San Diego, CA), CD1a (HI149, BD), CD14 (M5E2, BD), CD207 (10E2, BioLegend), and CD163 (GHI/61, BD). Cells were then analyzed by flow cytometry (BD LSRFortessa, FlowJo software). Population gates were set based on isotype, single-stain, and fluorescence minus one controls.

4.2.12 Statistical Analyses

Statistical analyses were performed with GraphPad Prism v6 (San Diego, CA). Data from experiments with multiple treatment groups were analyzed by one-way ANOVA, followed by Tukey's or Sidak's post-hoc testing. For experiments with only two groups, two-tailed independent t-tests (with Welch's correction as needed) were used. Data that were not normally distributed were compared using non-parametric tests (Mann-Whitney test, or Kruskal-Wallis test followed by Dunn's multiple comparisons). Ear thickness measurements from multiple time points were analyzed by two-way mixed ANOVA, followed by post-hoc testing of treatment effect with a Sidak or Tukey correction. Data represent mean \pm SD, except for ear thickness measurements, which are mean \pm SEM.

4.3 RESULTS

4.3.1 Characterization of dissolvable tip-loaded MNAs

The geometry of dissolvable MNAs was characterized by optical microscopy (Figure 4-2A-D). Each MNA consists of a 10x10 array of obelisk-shaped microneedles with sharp edges and tips and fillets at the base (Figure 4-2A-B), and detailed dimensions are provided in Figure 4-1. All MNAs were tip-loaded with OVA and/or MC903, and use of Alexa Fluor 647-labeled OVA allowed protein in the microneedle to be visualized (Figure 4-2C). The dark blue microneedle tip indicates the region containing most of the OVA, while the pale blue color toward the base of the pyramidal tip and top of the stem is consistent with less concentrated OVA (Figure 4-2C). MNAs were also examined before and after application to murine abdominal skin or human skin explants to confirm that the tip-loaded cargo had been deposited. (Figure 4-2D-F). Though a larger portion of microneedle stems remain after application to murine skin (Figure 4-2E), compared to human skin (Figure 4-2F), it appears that the tips, which contain most of the therapeutic payload (depicted in Figure 4-2C), have dissolved in both cases.

In addition to geometry, endotoxin levels in various MNA formulations were measured since endotoxin is known to promote innate immune responses that can enhance sensitization and drive Th1-mediated hypersensitivity [204-206]. Total endotoxin content of Blank MNAs, or MNAs containing 100 μg of grade V OVA with endotoxin (OVA_{ETX}) or EndoGrade OVA (OVA), were quantified by chromogenic LAL assay. Average endotoxin levels for Blank and OVA MNAs were less than 1 EU / MNA (Figure 4-3G). As expected, OVA_{ETX} MNA contained substantially more endotoxin (65 ± 6 EU, Figure 4-3G). These results suggest that minimal endotoxin is present in the bulk components of the MNAs (CMC and trehalose), or introduced by

the fabrication process, and the majority of endotoxin in OVA_{ETX} MNAs comes from the grade V OVA.

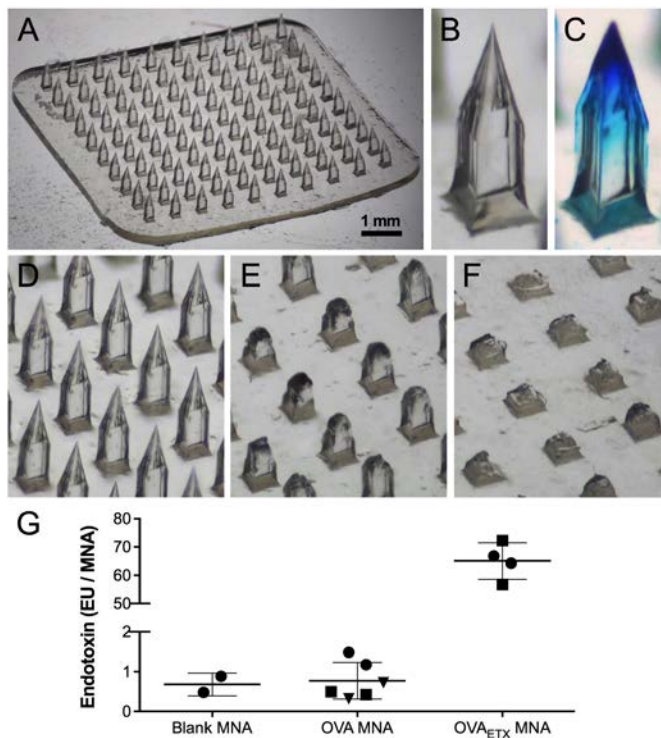


Figure 4-2. MNA characterization. (A) Optical microscopy image of a whole MNA, taken at low magnification with a dissecting microscope. (B) High magnification image of a single microneedle from the MNA. (C) Single microneedle from an MNA that was tip-loaded with 100 µg Alexa Fluor 647-labeled OVA (blue). (D-E) MNAs before application (D) and after application to mouse abdominal skin (E), or a human skin explant (F). (G) Total endotoxin content in MNAs, as determined by chromogenic LAL assay. Bars are mean ± SD. Each dot represents a single MNA, and different shapes within a given formulation indicate MNAs from distinct batches.

4.3.2 Delayed-type hypersensitivity (DTH) responses to different OVA MNA formulations

To characterize baseline responses to OVA sensitization and challenge with different OVA MNA formulations, ear thickness was measured before and after application of different MNAs

to ears of naïve or previously sensitized mice. Application of Blank MNAs causes some ear swelling, which peaks within 24 hours and then decreases (Figure 4-3A). To control for this antigen-independent tissue trauma response, measurements of DTH responses are presented as differences in thickness of ears treated with OVA MNA and contralateral ears treated with Blank MNA. In naïve, unsensitized mice, OVA_{ETX} MNAs cause modest but significant increases in ear thickness at 1-2 days post-application, relative to Blank MNA (Figure 4-3B). This may be due to an enhanced innate immune response to endotoxin in these MNAs, as OVA MNAs do not cause enhanced swelling beyond that attributed to Blank MNAs (Figure 4-3B). Notably, mice sensitized with OVA_{ETX} MNA develop strong DTH responses to subsequent challenge with OVA_{ETX} MNA or OVA MNA, which peak around 2 days and last for at least 4 days (Figure 4-3C). Interestingly, mice sensitized with OVA MNA do not develop a strong ear-swelling response to challenge with OVA MNA, but do exhibit strong DTH responses to OVA_{ETX} MNA challenge (Figure 4-3C). This suggests OVA MNA sensitize mice, but not to the same extent that OVA_{ETX} MNA do. Based on these preliminary findings, subsequent tolerance induction and DTH suppression experiments involved mice that were sensitized and challenged with OVA_{ETX} MNA, the combination that yields the strongest DTH responses.

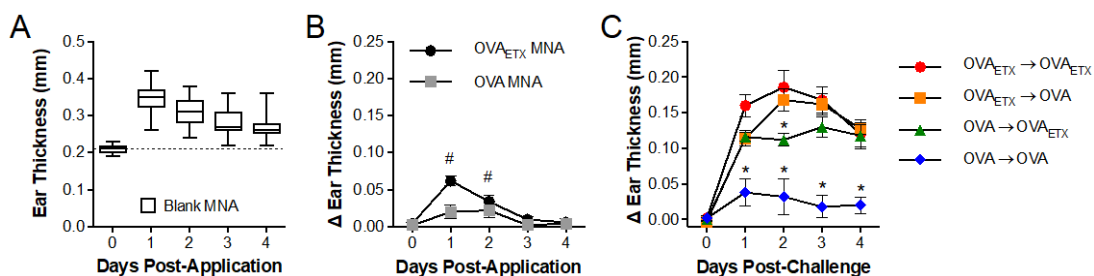


Figure 4-3. Ear swelling responses to Blank, OVA, or OVA_{ETX} MNA in unsensitized and sensitized mice. (A) Ear swelling response to Blank MNA application, presented as absolute ear thickness (N = 70). (B) Ear swelling response to OVA_{ETX} or OVA MNA in unsensitized mice (N = 5). Data represent differences in thickness between OVA MNA treated ears and contralateral Blank MNA treated ears. Significantly ear swelling caused by OVA

MNAs, relative to Blank MNAs, is indicated by # $p < 0.05$ (one-sample t-tests). (C) Ear swelling response to OVA challenge in previously sensitized mice ($N = 5$). Mice were sensitized at the abdomen and challenged five days later at the right ear with the indicated OVA MNAs. Significant differences relative to OVA_{ETX} sensitized and challenged mice are indicated by * $p < 0.05$ (two-way mixed ANOVA followed by Dunnett's multiple comparisons).

To characterize cutaneous cellular infiltrates associated with the DTH response to OVA-challenge, mice were sensitized with OVA_{ETX} MNA at the abdomen and then challenged with OVA_{ETX} MNA or Blank MNA at the ears 5 days later. As expected, ear skin histology from 48 and 96 hours post-challenge revealed substantial cellular infiltrates and edema in OVA-challenged ears, compared to ears treated with Blank MNA (Figure 4-4A). Consistent with ear thickness measurements (Figure 4-3C), OVA-challenged ears exhibited greater edema and overall thickness 48 hours post-challenge, compared to 96 hours post-challenge (Figure 4-4A). In order to characterize the composition of leukocytes infiltrating the skin, ear tissue from 48 or 96 hours post-challenge was also enzymatically digested and the resulting cell suspensions analyzed by flow cytometry. OVA-challenged ears contained 2-3 times more leukocytes (live CD45⁺ cells) than ears treated with Blank MNAs at both time points, and there were slightly, though not significantly, fewer total infiltrating cells 96 hours post-challenge (Figure 4-4B). Ly6G⁺ neutrophils (also CD11b⁺ I-A^{b-}) comprised approximately 40 percent of total leukocytes in both OVA_{ETX} and Blank MNA-treated skin 48 hours post-challenge, but only 18 percent or 6 percent of total leukocytes in OVA_{ETX} and Blank MNA-treated skin at 96 hours (Figure 4-4B). F4/80⁺ cells, which include monocytes, macrophages, and eosinophils, comprised approximately 35-40 percent of total leukocytes at 48 and 96 hours post-challenge with both types of MNAs (Figure 4-4B). Compared to Blank MNAs, OVA_{ETX} MNAs induced greater infiltration of

monocytes and/or eosinophils (F4/80⁺ I-A^b CD169⁻) and inflammatory macrophages (F4/80⁺ I-A^b CD169⁺) 96 hours post-challenge, while tissue-resident dermal CD169⁺ macrophages (F4/80⁺ I-A^b CD169⁺ [207]) were found at similar levels in both OVA_{ETX} and Blank MNA-treated skin (Figure 4-4C). Finally, CD4⁺ and CD8⁺ T cells comprised a small percentage of total leukocytes, but T cells in the skin increased significantly over time in OVA-challenged, but not Blank MNA-treated, skin. There were also more CD4⁺ T cells than CD8⁺ T cells at both time points (Figure 4-4B).

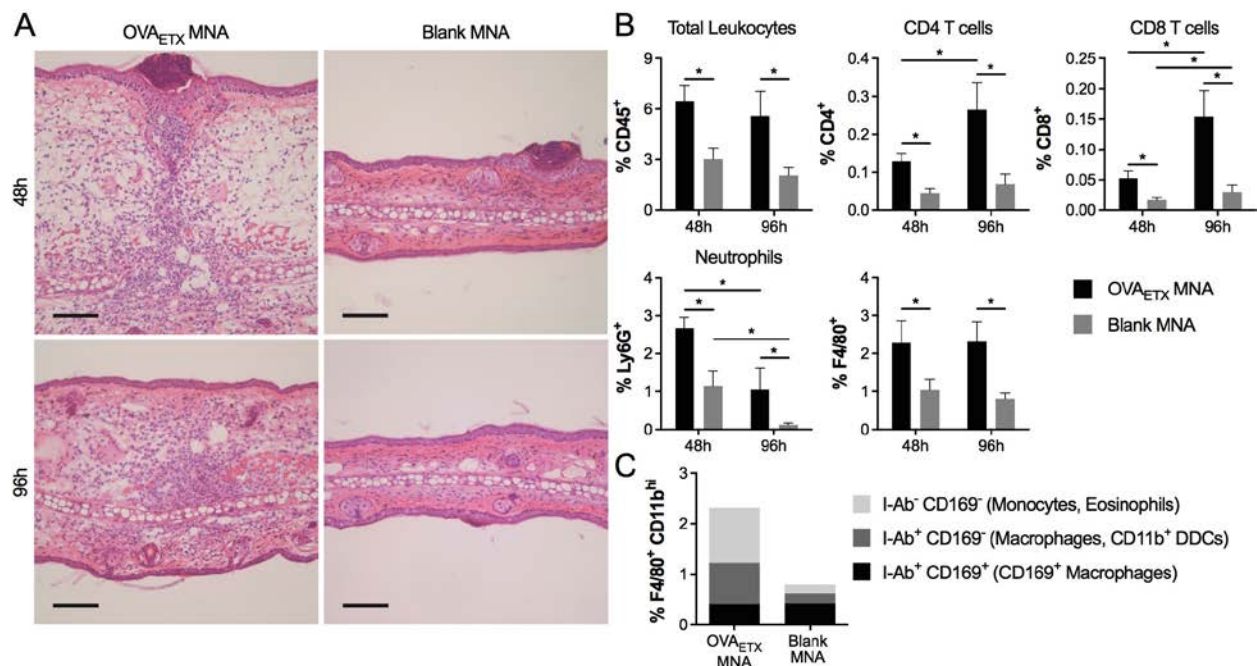


Figure 4-4. Characterization of infiltrating leukocyte populations in skin following OVA challenge in sensitized, intolerant mice. (A) Representative ear skin histology (H & E) from 48 or 96 hours post-challenge. Mice were sensitized at the abdomen 5 days prior to challenge with OVA_{ETX} MNA or Blank MNA. Scale bars are 100 μ m. (B) Leukocytes in ear skin tissue were quantified by flow cytometry 48 or 96 hours post-challenge with OVA_{ETX} MNA (black) or Blank MNA (grey). Data represent percent of total skin cells, and all cells in the indicated populations were live, as determined by viability staining (mean \pm SD, N = 5 ears). (C) Ears from 96 hours post-challenge, analyzed individually in (B), were pooled and stained for additional markers: CD11b, MHC-II (I-A^b), and

CD169. All F4/80⁺ cells were CD11b^{hi} and were divided into three populations based on expression of I-A^b and CD169.

4.3.3 Local and systemic T-cell responses to different OVA MNA formulations

In addition to characterizing DTH responses to sensitization and challenge, we evaluated local and systemic T-cell responses to different OVA MNA formulations. One day after adoptive transfer of OT-I and OT-II cells to expand the initial pool of OVA-specific T cells, different MNA formulations were applied to ears of mice. T-cell responses were measured four days later by flow cytometry on lymphocytes from local skin draining lymph nodes (DLN) and splenocytes. OVA_{ETX} MNAs substantially expanded CD4⁺ T-bet⁺ Th1 and CD8⁺ T-bet⁺ Tc1 populations both locally (in DLN) and systemically (in spleen), relative to treatment with Blank MNA (Figure 4-5). OVA MNA and OVA_{ETX} MNA enhanced Th1 populations locally and systemically to a similar extent, but OVA MNA only expanded Tc1 populations half as much as OVA_{ETX} MNA did (Figure 4-5). Notably, OVA + MC903 MNAs did not significantly expand Th1 or Tc1 populations locally or systemically, compared to Blank MNAs (Figure 4-5). Mice treated with OVA ± MC903 MNAs, but not OVA_{ETX} MNAs, had greater frequencies of CD4⁺ FoxP3⁺ Tregs in local DLN, but not systemically; however, mice treated with each of OVA-containing MNA formulations had reduced Treg frequencies among splenocytes, relative to Blank MNA-treated mice (Figure 4-5). Finally, mice treated with class II MHC-restricted OVA₃₂₃₋₃₃₉ peptide ± MC903 MNAs exhibited no increase in Tc1 populations, relative to Blank MNA, and fewer Th1 than OVA_{ETX} or OVA MNAs (data not shown).

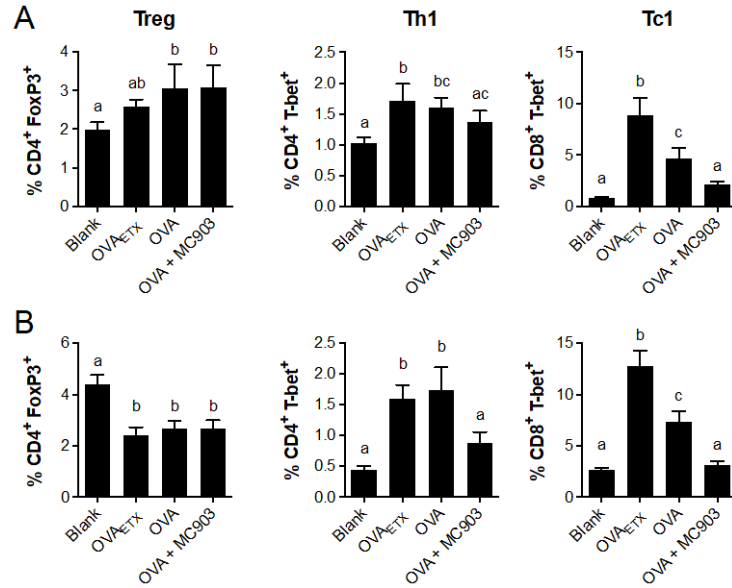


Figure 4-5. Local and systemic T-cell responses to MNAs in unsensitized mice. To enhance the pool of naïve OVA-specific T cells, OT-I and OT-II T cells (5×10^6 of each) were adoptively transferred to wild-type mice one day prior to application of the indicated MNAs to each ear. Ear skin DLN and spleens were isolated four days later, and T-cell subsets analyzed by flow cytometry. (A) Frequencies of Treg, Th1, and Tc1 cells in DLN. (B) Frequencies of Treg, Th1, and Tc1 in spleen. Data represent mean \pm SD ($N = 4-5$), and significant differences ($p < 0.05$) are indicated by different letters (ANOVA followed by Tukey's multiple comparisons).

4.3.4 Prophylactic tolerization with OVA + MC903 MNAs inhibits subsequent OVA sensitization

To determine whether OVA + MC903 MNAs could generate tolerance to OVA and prevent subsequent sensitization, mice were treated (tolerized) with MNAs containing OVA and/or MC903 prior to sensitization and challenge with OVA_{ETX} MNAs (see experimental timeline in Figure 4-6A). Tolerization with OVA + MC903 MNAs inhibited DTH responses to OVA challenge, relative to untolerized mice, with significantly reduced ear swelling from 1-4 days post-challenge (Figure 4-6B). Interestingly, tolerization with OVA MNA did not affect early

DTH responses (1 day post-challenge), but did reduce ear swelling 2-4 days post-challenge, relative to intolerized controls, though to a lesser extent than OVA + MC903 MNA treatment (Figure 4-6B). Finally, pre-treatment with MC903 MNAs had only a modest reduction on ear swelling at 4 days post-challenge, relative to intolerized mice (Figure 4-6B).

Ear thickness measurements were corroborated by histology 4 days post-challenge, which qualitatively revealed substantially greater edema and cellular infiltrates in skin from intolerized mice, compared to OVA+MC903 tolerized mice (Figure 4-6C). Cellular infiltrates were quantified by flow cytometry analysis of enzymatically digested ear tissue 4 days post-challenge. The frequency of total infiltrating leukocytes (live CD45⁺ cells) in OVA-challenged ear skin was approximately three times less in skin tissue from OVA + MC903 treated mice, compared to intolerized mice (Figure 4-6D). Consistent with ear thickness measurements at 4 days post-challenge, infiltrating leukocytes in ear skin from OVA, but not MC903, tolerized mice were also substantially reduced, relative to intolerized mice (Figure 4-6D). Collectively, these results demonstrate that prophylactic treatment of naïve mice with OVA + MC903 MNA can prevent subsequent OVA sensitization and DTH responses.

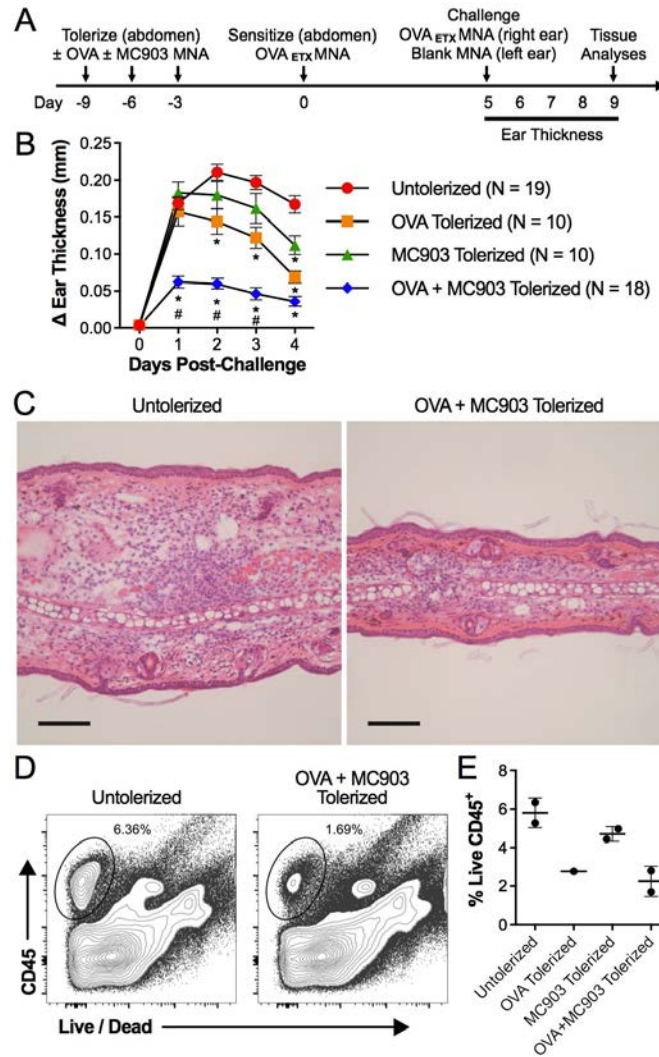


Figure 4-6. Prophylactic tolerization with OVA + MC903 MNAs prevents OVA sensitization, inhibiting DTH responses to subsequent OVA challenge. (A) Experimental timeline. Untolerized mice were not treated before sensitization. (B) Ear swelling after OVA challenge, presented as the difference in thickness between OVA_{ETX} MNA treated ears and contralateral Blank MNA treated ears (mean ± SEM). Significant differences relative to untolerized mice are indicated by * $p < 0.05$. Significant differences between OVA ± MC903 tolerized groups are indicated by # $p < 0.05$ (two-way mixed ANOVA followed by Tukey's multiple comparisons). (C) Representative ear skin histology (H & E staining) from 4 days post-challenge with OVA_{ETX} MNA. Scale bars are 100 μm. (D) Representative flow cytometry plots of total cells from ear skin harvested 4 days post-challenge with OVA_{ETX} MNA. Gates indicate total infiltrating leukocytes (live CD45⁺ cells). (E) Frequency of infiltrating leukocytes (as in D) for all treatment groups. Each dot represents OVA-challenged ears pooled from 3-5 mice.

4.3.5 Prophylactic tolerization alters cellular and humoral immune responses

To determine whether prophylactic tolerization altered overall T-cell responses, frequencies of T-cell subsets in ear skin draining lymph nodes (DLN) were measured 4 days post-challenge by flow cytometry. Compared to untolerized mice, only tolerization with OVA + MC903 MNAs significantly increased the prevalence of CD4⁺ FoxP3⁺ Tregs and reduced CD8⁺ T-bet⁺ Tc1 populations in the DLN (Figure 4-7). Treatment with OVA ± MC903 MNAs led to diminished CD4⁺ T-bet⁺ Th1 populations and enhanced CD4⁺ GATA-3⁺ Th2 populations, contributing to significantly reduced Th1:Th2 ratios (Figure 4-7). In contrast, MC903 MNAs had no detectable

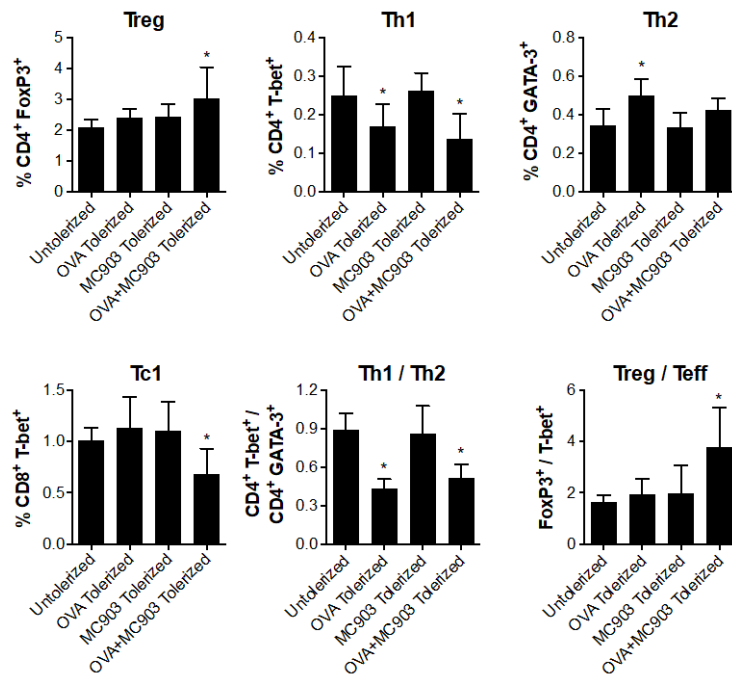


Figure 4-7. Prophylactic tolerization with OVA + MC903 MNAs shifts Th1 / Th2 and Treg / Teff ratios in DLN. T-cell subsets in ear skin DLN were identified and quantified by flow cytometry 4 days post-challenge. Frequencies of Treg, Th1, Th2, and Tc1 cells are presented as the percent of total lymphocytes (mean ± SD; N = 9-14 for Treg, Th1, and Tc1; N = 5-9 for Th2). Mice were tolerized, sensitized, and challenged with MNAs according to the experimental timeline in Figure 4-6A. Significant differences, relative to untolerized mice, are indicated by

* p < 0.05 (ANOVA followed by Dunnett's multiple comparisons).

effect on T-cell populations, relative to intolerized mice (Figure 4-7). Finally, concomitant changes in Treg, Th1, and Tc1 populations with OVA + MC903 MNA pre-treatment significantly increased the ratio of Tregs to type 1 effector T cells (Teff; Th1 and Tc1), which was not observed with other prophylactic treatments (Figure 4-7).

To evaluate the effects of prophylactic tolerization on humoral immunity, serum levels of OVA-specific Th1-associated (IgG2c) and Th2-associated (IgG1 and IgE) antibodies were measured by ELISAs. Sensitization and challenge with OVA_{ETX} MNAs induced significant production of OVA-specific IgG1 and IgG2c (intolerized, Figure 4-8). In contrast, serum from mice treated only with OVA + MC903 MNAs contained elevated levels of OVA-specific IgG1, but not IgG2c (Figure 4-8). Tolerization with OVA ± MC903 MNAs prior to sensitization and challenge also led to significantly greater OVA-specific IgG1 serum levels post-challenge; however, no change in OVA-specific IgG2c production was detected (Figure 4-8). Though pre-treatment with MC903 MNAs had no influence on OVA-specific IgG1 levels, IgG2c serum concentrations were significantly greater post-challenge than in intolerized mice (Figure 4-8). This unexpected increase in IgG2c production was also observed in mice treated with OVA_p + MC903 MNAs prior to sensitization (data not shown). Interestingly, despite increasing Th2-associated IgG1 levels, OVA ± MC903 MNA treatments did not enhance OVA-specific IgE production (Figure 4-8).

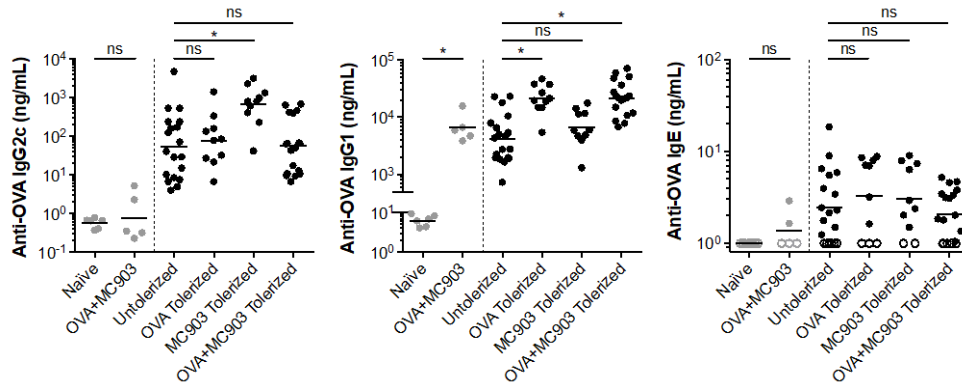


Figure 4-8. Prophylactic tolerization alters humoral immune response to OVA. Serum concentrations of OVA-specific IgG1, IgG2c, and IgE (bars are geometric means). Black circles represent mice from which serum was collected 4 days post-challenge, according to the experimental timeline in Figure 4-6A. Grey circles represent mice that were not sensitized or challenged, and serum was collected 3 days after application of the third OVA + MC903 MNA. Open circles indicate levels below the detection limit (1.5 ng/mL for IgE). Significant differences are indicated by * $p < 0.05$ (Kruskal-Wallis test followed by Dunn's multiple comparisons to untolerized mice; independent t-test with Welch's correction for naïve vs. OVA + MC903).

4.3.6 Tolerization of previously sensitized mice suppresses subsequent DTH responses and alters cellular and humoral immune responses

To determine whether allergen tolerance could be established in previously sensitized individuals, mice were sensitized with OVA_{ETX} MNAs twice prior to tolerization with OVA + MC903 MNAs (Figure 4-9A). As with prophylactic tolerization, OVA + MC903 MNA treatment after sensitization inhibited DTH responses to a subsequent OVA challenge, as indicated by a significant reduction in ear swelling, relative to untolerized mice (Figure 4-9B). Reduced ear swelling in tolerized mice was supported by histological evaluation of ear tissue, which revealed substantially fewer cellular infiltrates and less dermal edema than in ears from untolerized mice (Figure 4-9C).

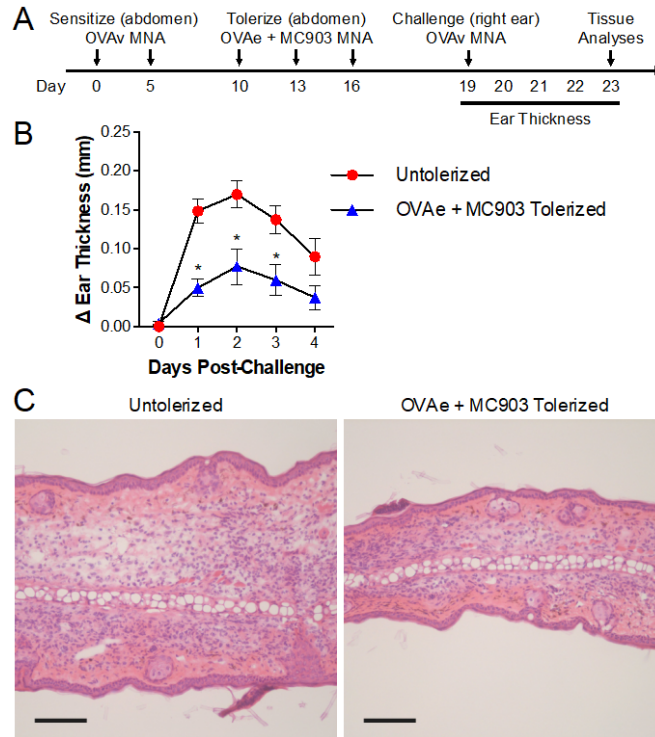


Figure 4-9. Tolerization of previously sensitized mice with OVA + MC903 MNAs suppresses subsequent DTH response. (A) Experimental timeline. Untolerized mice received no treatment between sensitization and challenge. (B) Ear swelling after OVA challenge, presented as the difference in thickness between OVA_{ETX} MNA treated ears and contralateral Blank MNA treated ears (N = 7). (C) Representative ear skin histology (H & E staining) from 4 days post-challenge. Scale bars are 100 μm. Significant differences are indicated by * p < 0.05 (two-way mixed ANOVA followed by Sidak's multiple comparisons).

As with prophylactic tolerization, OVA + MC903 MNA treatment after sensitization altered cellular and humoral immune responses. Specifically, the frequency of CD4⁺ FoxP3⁺ Tregs in skin DLN after OVA challenge was significantly enhanced by tolerization; however, no differences in Th1 or Tc1 populations were detected in DLN or spleens (Figure 4-10A). Though Th2 populations were not quantified in this experiment, OVA + MC903 tolerization did augment serum concentrations of OVA-specific Th2-type IgG1, but not IgE (Figure 4-10B). Finally, as

with prophylactic tolerization, treatment of previously sensitized mice did not affect OVA-specific Th1-type IgG2c levels (Figure 4-10B).

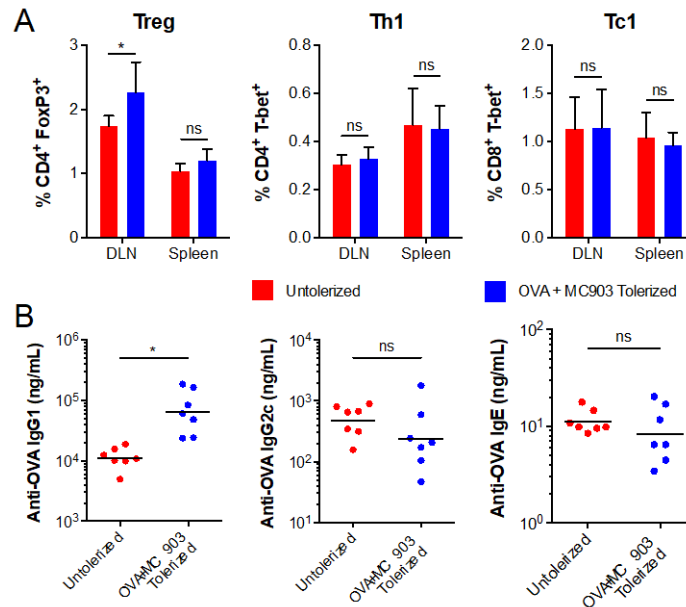


Figure 4-10. Tolerization of previously sensitized mice with OVA + MC903 MNA influences cellular and humoral immune responses. (A) Frequencies of T-cell subsets in skin DLN and spleen 4 days post-challenge, according to experimental timeline in Figure 4-9A. Data are percent of total lymphocytes or splenocytes (mean \pm SD, N = 7). (B) Serum concentrations of OVA-specific IgG1, IgG2c, and IgE 4 days post-challenge (bars are geometric means). Significant differences are indicated by * $p < 0.05$ (independent t-test with Welch's correction as needed).

4.3.7 MC903 applied topically or with MNAs alters the murine skin microenvironment

To determine the influence of MC903 MNA on the murine skin microenvironment (for comparison to human skin responses), MC903 (5 μ g) or Blank MNAs were applied to ears of naïve mice, and RNA was isolated from ear skin 24-48 hours later and analyzed by qRT-PCR. Consistent with results from human skin explants (Figure 4-13), cutaneous IL-10 expression was significantly enhanced and IL-18 expression significantly reduced by MC903 MNA (Figure

4-11A). To determine the impact of MC903 delivery route on cutaneous cytokine responses, ears of naïve mice were treated with 5 µg MC903 either applied epicutaneously in ethanol, or intradermally via MNA. Ethanol and Blank MNA served as vehicle controls. We hypothesized that topical application of MC903 would have a greater effect on cytokines produced exclusively by epidermal keratinocytes (e.g. thymic stromal lymphopoietin, TSLP). In contrast, MNAs that provide deeper delivery of MC903 to the dermal layer would have a greater effect on expression of cytokines also produced by immune cells in the dermis (e.g. IL-10) [208]. As expected, topical MC903 increased expression of TSLP significantly more than MC903 MNA did, while MC903 MNA enhanced IL-10 expression to a greater extent than topical MC903 (Figure 4-11B).

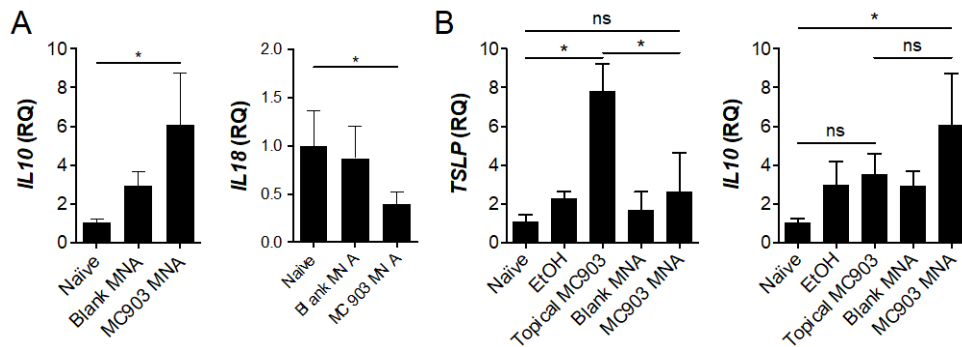


Figure 4-11. Cutaneous cytokine expression in murine skin is altered by MC903 MNA and differentially regulated by epicutaneously applied MC903. (A) MC903 (5 µg) MNA were applied to ears of naïve mice, and cytokine expression was quantified in ear tissue 24-48 hours later by qRT-PCR. (B) MC903 (5 µg) was applied to ears of mice epicutaneously (dissolved in ethanol) or intradermally via MNA. Cytokine expression was quantified in ear tissue 48 hours later by qRT-PCR. Data represent mean ± SD fold change in expression ($RQ = 2^{-\Delta\Delta Ct}$) relative to naïve tissue ($N \geq 4$ for controls; $N = 8$ for MC903 treatments). Significant differences indicated by * $p < 0.05$ (ANOVA followed by Tukey's multiple comparisons).

4.3.8 Co-delivery of allergen and MC903 via MNA inhibits allergen-induced expression of pro-inflammatory mediators in murine skin

To evaluate the capacity for MC903 to counteract pro-inflammatory innate responses to contact allergens, MNAs were loaded with a model chemical allergen (DNCB) with or without MC903. DNCB \pm MC903 MNAs were applied to ears of mice, and cutaneous expression of innate pro-inflammatory mediators measured 6 and 24 hours post-application by qRT-PCR. Co-delivery of DNCB with MC903 via MNA significantly inhibited expression of DNCB-induced pro-inflammatory cytokines IL1B and TNF, as well as the NLRP3 inflammasome (Figure 4-12). Interestingly, although IL18 expression was reduced by MC903 MNA treatment (\pm DNCB), DNCB MNA did not enhance IL18 mRNA expression as expected. Collectively, these results suggest that MC903 may block sensitization-promoting innate responses to chemical allergens.

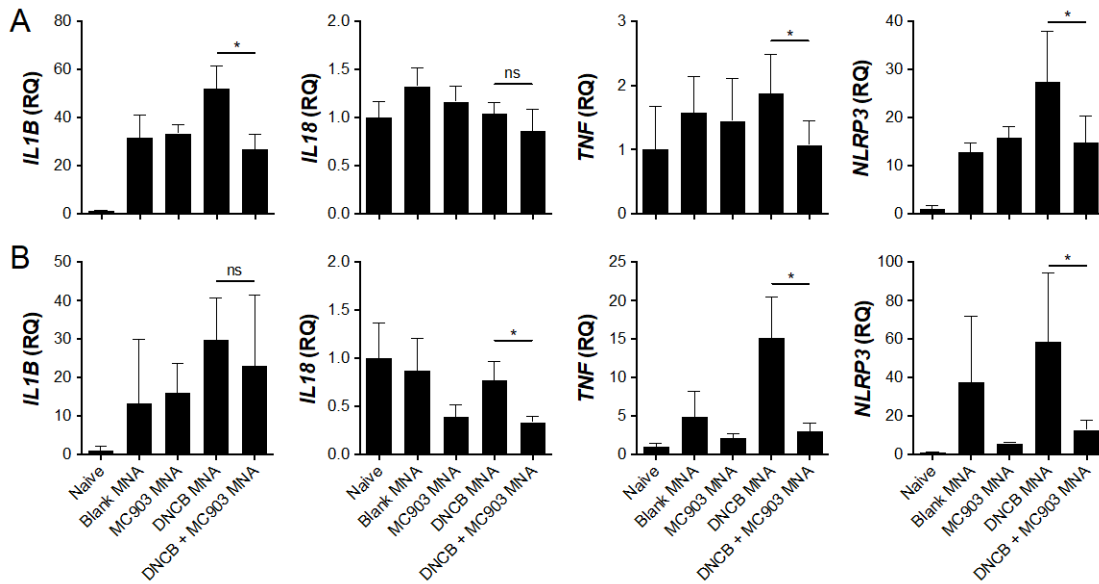


Figure 4-12. Co-delivery of allergen plus MC903 in MNAs inhibits innate response to allergen in murine skin.

The indicated MNA formulations were applied to ears of naïve C57BL/6 mice, and was RNA isolated from ear tissue (A) 6 hours or (B) 24 hours later. Cytokine expression was quantified by qRT-PCR, and data represent mean

± SD expression relative to naïve tissue ($RQ = 2^{-\Delta\Delta Ct}$) (N = 4-6 mice per group). Significant differences indicated by * $p < 0.05$ (ANOVA followed by Sidak's comparison of DNCB vs. DNCB + MC903).

4.3.9 MC903 MNA alter human skin microenvironment

To evaluate effects of MC903 MNAs on the human skin microenvironment, human skin explants were treated with MC903 MNAs (1 µg or 5 µg MC903 per MNA). Controls included untreated skin and skin treated with Blank MNAs. Explants were cultured for 48 hours, and then the skin microenvironment was assessed using qRT-PCR arrays. Blank and MC903 MNAs consistently increased cutaneous expression of several CXC chemokines (CXCL1, 2, 3, 5, 6, 8, and 10), as well as IL-6, PTGS2 (COX-2), and some CC chemokines (CCL3 and CCL5) (Figure 4-13). MNAs also consistently decreased expression of CCL13, CCL2, and CCR3, relative to untreated skin (Figure 4-13). MC903 MNAs further enhanced expression of several CXC chemokines, and further reduced expression of CCL13 (Figure 4-13). Additionally, MC903 MNAs alone consistently upregulated expression of CD14, IL-10, IL-1RN, and FOS, and downregulated CCR2, TLR7, IL-18, and IL-22 (Figure 4-13).

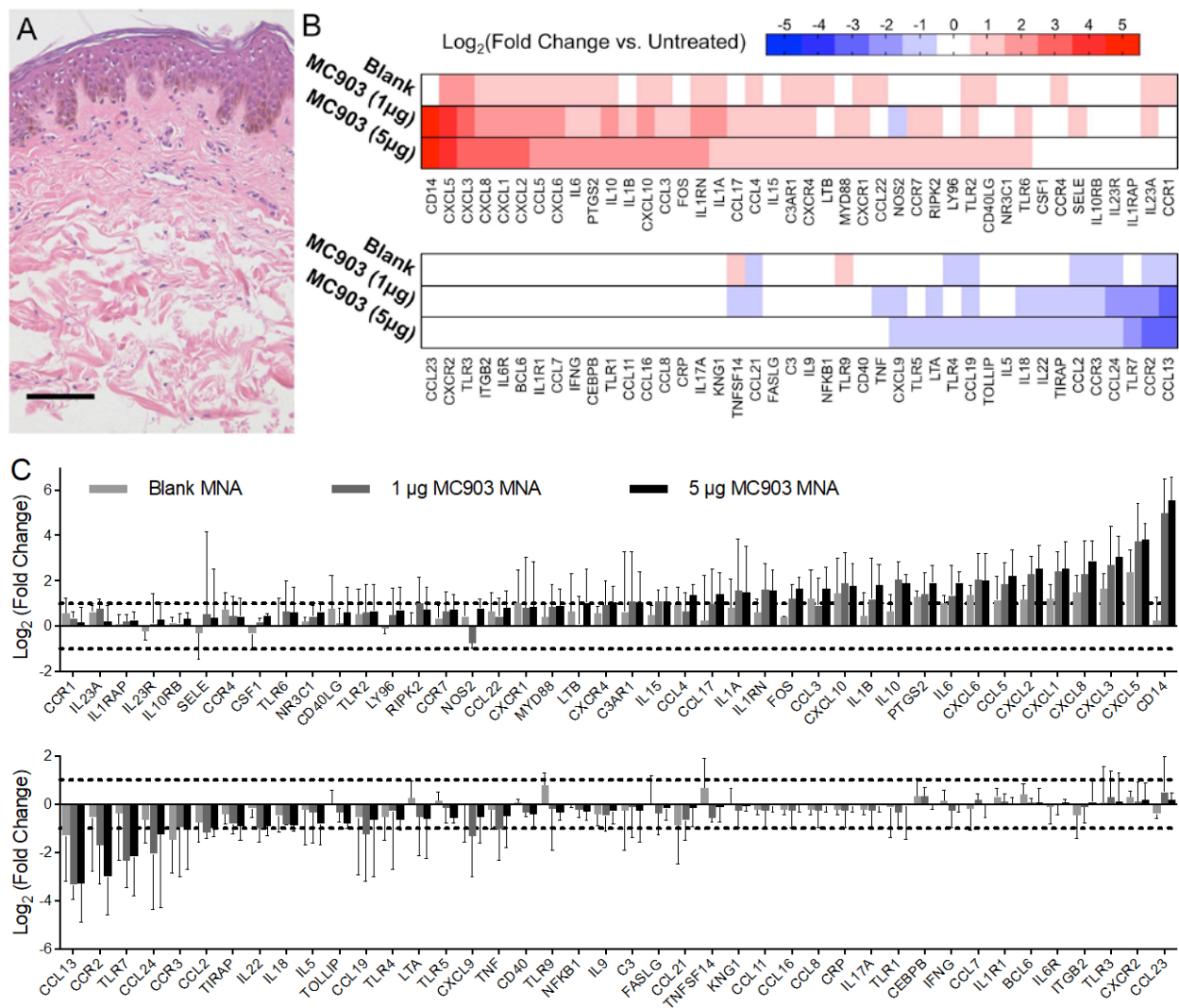


Figure 4-13. MC903 MNAs alter expression of inflammatory immune response genes in human skin explants.

After 48 hours, RNA was isolated from human skin explants and expression of 84 genes (cytokines, chemokines, cytokine/chemokine receptors, pattern recognition receptors, and downstream signaling proteins) assayed by qRT-PCR. (A) Histology (H&E) of untreated human skin explant after 48 hours (100 µm scale bar). (B) Heat map of average relative gene expression for skin explants treated with the indicated MNAs. Red indicates increased expression and blue indicates decreased expression relative to untreated skin. (C) Relative expression (as in B) showing variability among individual tissue donors. Data represent average log_2 fold changes in gene expression ($N = 3$, SD error bars) for each MNA treatment, relative to untreated skin. Dotted lines correspond to two-fold changes in mRNA expression.

4.3.10 MC903 MNAs enhance migration of CD14⁺ dermal DCs from human skin

In addition to evaluating effects of MC903 MNAs on the skin microenvironment, DCs migrating out of human skin explants in response to MNA application were analyzed by flow cytometry 48 hours post-application. Total migratory DCs in culture media were identified as SSC^{int/hi} HLA-DR⁺ CD11c^{lo/hi} (Figure 4-14A), and three subsets of skin migratory DCs were identified based on differential expression of CD1a, CD14, and CD207 (Langerin): epidermal Langerhans cells (LCs; CD1a^{hi} CD14⁻ CD207⁺), CD1a⁺ dermal DCs (CD1a^{int} CD14⁻ CD207⁻), and CD14⁺ dermal DCs (CD1a^{lo/int} CD14⁺ CD207⁻) (Figure 4-14B-C). While MNAs did not significantly affect total numbers of migrating DCs, low and high dose MC903 MNAs selectively enhanced migration of CD14⁺ DDCs, and reduced migration of CD1a⁺ DDCs (Figure 4-14B, E). Finally, approximately 25% of CD14⁺ migratory cells were CD163⁺ (Figure 4-14D), indicating the “CD14⁺ dermal DCs” are actually a heterogeneous population, including some M2 macrophage-like CD163⁺ cells [209]).

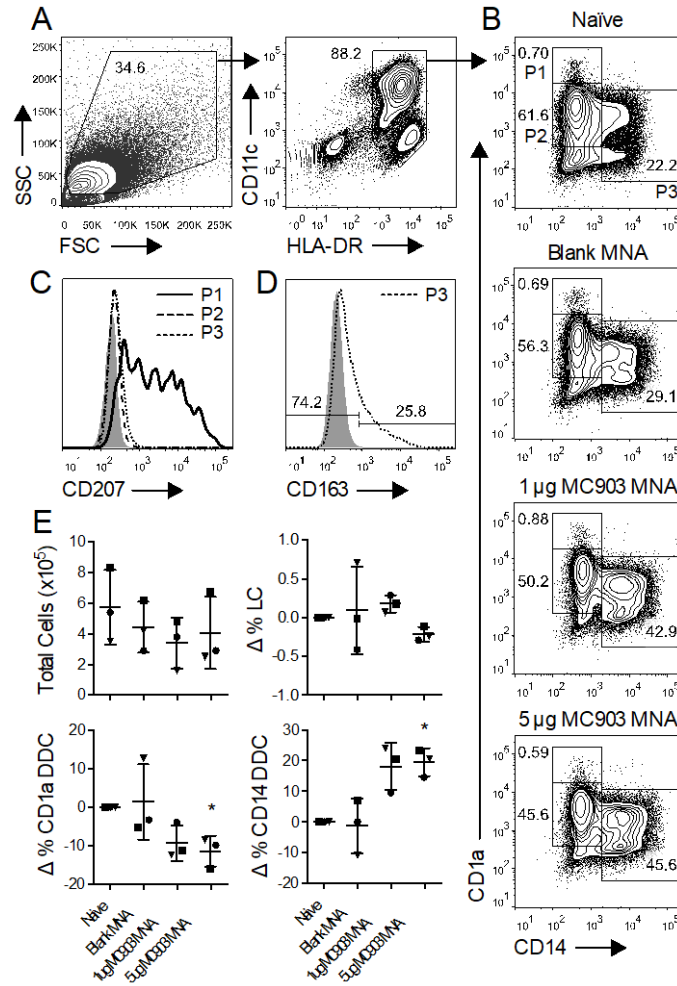


Figure 4-14. MC903 MNAs enhance migration of CD14⁺ dermal DCs (DDC) from human skin explants. (A) Flow cytometry gating strategy for skin migratory DCs (SSC^{int/high} HLA-DR⁺ CD11c^{+/-}). Cells migrating out of human skin explants were obtained from media after 48 hours of culture. **(B)** Migratory DCs were divided into three populations based on expression of CD1a and CD14: CD1a^{high} CD14⁻ Langerhans cells (LC, P1), CD1a^{int} CD14⁻ DCs (CD1a⁺ dermal DC, P2), and CD1a^{int/-} CD14⁺ DCs (CD14⁺ dermal DC, P3). **(C)** Selective expression of CD207 (Langerin) by CD1a^{high} cells (P1). **(D)** Expression of the scavenger receptor CD163, a monocyte- and macrophage-restricted marker [210, 211], by CD14⁺ cells (P3). **(E)** Total migratory cells per 8 cm² skin explant, and changes in % LC (P1), CD1a⁺ dermal DC (P2), and CD14⁺ dermal DC (P3) cells, relative to naïve untreated skin. Different symbols denote skin migratory DCs from three distinct patient samples. Significant changes in frequencies of skin migratory DC populations are indicated by * p < 0.05 (one sample t-test).

4.4 DISCUSSION

Though MNAs have been widely used for vaccination against pathogens (reviewed in [212-214]), there are very few reports of MNAs being used to treat inflammation or induce immune tolerance [203, 215], and we are unaware of any that describe co-delivery of immunoregulatory agent(s) and antigens. In the current study, dissolvable MNAs were used to induce allergen-specific tolerance by co-delivering allergen (OVA or DNCB) with vitamin D3 analog (MC903) to the skin microenvironment. In experiments with mice, treatment with OVA + MC903 MNA induced fewer Tc1 cells and suppressed expansion of Th1 populations both locally (skin DLN) and systemically (spleen), relative to treatments with OVA_{ETX} MNA or OVA MNA (Figure 4-5). This finding is consistent with a previous report that transcutaneous immunization through MC903-treated skin inhibits priming of Tc1 responses [86]. OVA_{ETX} MNA used for sensitization also yielded larger Tc1 populations than OVA MNA (Figure 4-5), likely due to adjuvant effects of endotoxin in OVA_{ETX} MNA (Figure 4-3G) [184, 185, 206]. In contrast to a previous report [86], however, OVA + MC903 MNA did not significantly increase Treg frequencies, relative to OVA_{ETX} MNA, in unsensitized mice (Figure 4-5). Future experiments will be needed to determine whether this lack of OVA-specific Treg expansion is due to intrinsic properties of TCR-transgenic OT-II Rag2^{-/-} T cells, compared to OT-II Rag2^{+/+} T cells used previously [86] or wild-type CD4⁺ T cells, subsets of which could be identified as OVA-specific by MHC-II tetramer staining. Future studies will also investigate expansion of suppressive FoxP3⁻ IL-10⁺ CD49b⁺ LAG-3⁺ Tr1 populations [16], which are reported to be induced by vitamin D3-treated dermal DCs, in contrast to FoxP3⁺ Tregs, which are induced by vitamin D3-treated epidermal LCs [95]. As MNAs provide deeper delivery of MC903 and antigen, we may

expect to see greater expansion of Tr1 populations than with epicutaneous application of antigen and MC903.

Delayed-type hypersensitivity (DTH) responses to OVA_{ETX} MNA challenge in sensitized mice were characterized by considerable edema at 48 hours (Figure 4-4A) and prolonged infiltration of leukocytes observed 48 and 96 hours post-challenge (Figure 4-4). This cellular response was characterized by a sustained influx of inflammatory monocytes, macrophages, and possibly eosinophils (Figure 4-4B-C), an early influx of neutrophils that decreased with time (Figure 4-4B), and an influx of CD4⁺ and CD8⁺ T cells that increased with time (Figure 4-4B) and included more CD4⁺ T cells, as expected for a response to extracellular protein antigen. Notably, prophylactic tolerization of naïve mice with OVA + MC903 MNA inhibited later sensitization with OVA_{ETX} MNA, as indicated by reduced DTH responses to subsequent OVA challenge (Figure 4-6). In fact, ear swelling in tolerized mice 24-48 hours post-challenge (Figure 4-6B) was reduced to levels seen in unsensitized mice (Figure 4-3B), suggesting that tolerization substantially inhibited the adaptive immune response. Although pre-treatment with OVA MNA led to faster resolution of DTH responses, compared to sensitized, intolerized mice, it failed to prevent the early phase ear swelling response at 24 hours (Figure 4-6B). Pre-treatment with MC903 MNA alone had minimal effect on OVA-specific DTH responses (Figure 4-6B), indicating that inhibition of OVA-sensitization by OVA + MC903 MNA is not merely a result of non-specific systemic immunosuppression by MC903. The reduced ear swelling response in OVA + MC903 tolerized mice was supported by histology and flow cytometry on skin at 96 hours, which both revealed substantial reductions in inflammatory infiltrates, compared to sensitized, intolerized controls (Figure 4-6C-D). Future experiments will be needed to characterize the specific inflammatory infiltrates at earlier time points in tolerized mice.

The therapeutic effects of prophylactic treatment with OVA + MC903 MNAs can be attributed to changes in cellular and humoral immune responses. Specifically, OVA ± MC903 MNAs reduced Th1 populations and enhanced Th2 populations, while OVA + MC903 MNA also reduced Tc1 populations and expanded Treg populations (measured post-challenge; Figure 4-7). Th2-skewing was also confirmed by analysis of humoral responses, which revealed higher serum levels of OVA-specific IgG1 in mice pre-treated with OVA ± MC903 MNA (Figure 4-8). In contrast, Th1-associated OVA-specific IgG2c levels were not affected by OVA ± MC903 MNA, though elevated levels were unexpectedly observed in mice pre-treated with MC903 MNA (Figure 4-8) or OVAp + MC903 MNA (data not shown). Importantly, the Th2-biased humoral responses were not accompanied by increases in OVA-specific IgE, a second Th2-associated isotype involved in type I hypersensitivities. While Th2-associated cytokines (IL-4 and IL-13) typically cause B cells to produce both IgG1 and IgE, the lack of IgE production is consistent with a prior report that intradermal injection of antigens promotes IgG1 production but diminishes IgE production [216]. These findings and literature precedent favor the use of MNAs for tolerance introduction, as IgE production and increased risk of type I hypersensitivity is more likely to be associated with epicutaneous introduction of protein antigens [216]. Ultimately, Th2-biasing by OVA ± MC903 MNA pre-treatment appears to contribute to faster resolution of DTH responses (Figure 4-6B), while OVA + MC903 MNA treatment also inhibits the early phase of the DTH response (Figure 4-6B), likely via enhanced Treg populations and further reduced Th1 and Tc1 populations (Figure 4-7). Such conclusions are supported by prior reports that adoptive transfer of OVA-specific Th1, but not Th2, cells results in strong DTH responses to OVA challenge [217]. Furthermore, as Tregs can inhibit neutrophil survival, production of inflammatory mediators [218], and recruitment to the skin (by blocking CXCL1/2 expression

[23]), Treg populations enhanced by OVA + MC903 MNA pre-treatment may be suppressing the early influx of pro-inflammatory neutrophils (Figure 4-4B), which are essential for elicitation of DTH responses [219].

In addition to preventing sensitization by prophylactic treatment with OVA + MC903 MNA, tolerization of previously sensitized mice was capable of suppressing DTH responses to subsequent allergen challenge (Figure 4-9). As with the prophylactic tolerization schedule, we observed both Th2-skewing, as indicated by an increase in serum anti-OVA IgG1 (Figure 4-10B), and a significant increase in Treg frequency in skin DLN post-challenge (Figure 4-10A); however, there were no discernable differences in Th1 or Tc1 populations with OVA + MC903 MNA treatment (Figure 4-10A). Since total polyclonal T cell populations may mask changes in antigen-specific T cell subsets, future studies may use peptide-MHC tetramer staining to identify OVA-specific T cell populations. Therapeutic tolerization, or hyposensitization, represents a more clinically relevant approach for individuals with pre-existing allergies, whereas prophylactic tolerization may be more suitable for strong sensitizing allergens that most people become allergic to upon contact (e.g. poison ivy), or for people with anticipated exposure to common occupational contact allergens (e.g. hairdressers exposed to *p*-phenylenediamine in hair dyes, or construction workers exposed to chromium in cement [220]). Notably, while previous studies have shown that sensitization is inhibited by epicutaneous exposure to allergen through UVB- or MC903-treated skin [81, 82, 84, 86], our results indicate that Allergen + MC903 MNAs can both prevent subsequent sensitization (at a different site) and tolerize previously sensitized mice.

Given the prophylactic and therapeutic effects of MC903 MNA in murine models of ACD, we investigated their effects on the skin microenvironment. MC903 MNA promoted a

more tolerogenic microenvironment for allergen introduction in murine skin by enhancing expression of anti-inflammatory IL10 and reducing expression of pro-inflammatory IL18 (Figure 4-11). Notably, co-delivery of DNCB and MC903 with MNAs inhibited expression of allergen-induced pro-inflammatory cytokines IL1B and TNF, as well as the NLRP3 inflammasome (Figure 4-12) [44]. While IL18 mRNA expression was reduced in DNCB + MC903 MNA-treated skin, relative to naïve skin, DNCB MNA did not enhance IL18 expression (Figure 4-12), as was previously reported with topical application of contact allergens to skin of Balb/c mice [221]. However, DNCB MNA may still enhance secretion of active IL-18 in skin of C57BL/6 mice by increasing post-translational processing of pro-IL-18 by the inflammasome [44]. Accordingly, future measurements of IL-18 protein in skin after DNCB MNA application would be of interest.

Experiments with human skin explants allowed us to extend these promising results in murine models to a human preclinical model. Quantitative analysis of RNA isolated from human skin explants after application of Blank MNAs or MC903 MNAs revealed both MNA-mediated effects (due to microtrauma from application) and MC903-mediated effects on human skin microenvironment. In particular, MNA application induced expression of several neutrophil recruiting CXC chemokines (especially CXCL3/5 Figure 4-13), which correlates with the early influx of neutrophils seen in murine skin 48 hours after application of Blank MNAs (Figure 4-4B). MC903 MNAs increased expression of several anti-inflammatory molecules (e.g. IL10, IL1RN, FOS) and reduced expression of pro-inflammatory factors (e.g. CCL13, CCR2, TLR7, IL18, IL22) (Figure 4-13). Increased expression of the suppressive cytokine IL-10 is a hallmark of vitamin D3-mediated immune responses [201, 222, 223], as are increased expression of the anti-inflammatory transcription factor FOS [224] and IL1RN, a gene encoding the IL-1 receptor

antagonist (a suppressor of pro-inflammatory IL-1 activity) [225]. Inhibited expression of CCL13, CCR2, TLRs, IL-18, and IL-22 have also been reported following treatment of skin and/or immune cells with vitamin D3, or related analogs [225-228]. Collectively, these MC903 MNA-mediated effects on human skin are consistent with a more tolerogenic microenvironment for allergen introduction.

In addition to altering the human skin microenvironment, MC903 MNAs selectively enhanced migration of CD14⁺ dermal DCs and reduced migration of CD1a⁺ dermal DCs from human skin explants, with no effects on migration of LCs (Figure 4-14). These results are consistent with a prior report that intradermal injection of 1,25-dihydroxyvitamin D3 with insulin syringes selectively increased migration of CD14⁺ dermal DCs from human skin explants [229]. Importantly, that study also demonstrated that Treg and Th1 induction by total migratory DCs were enhanced and inhibited, respectively, by intradermal vitamin D3 [229]. This finding is supported by several reports that describe CD14⁺ DCs as less mature and more tolerogenic than CD1a⁺ DCs, and capable of inducing Treg differentiation [229-233]. As cells migrating out of explants represent cells that would carry antigen to skin DLN *in vivo*, enhanced migration of more tolerogenic DCs could presumably promote Treg induction and allergen tolerance. Since vitamin D3 has been reported to enhance expression of CD14 on dermal DCs, epidermal LCs, blood DCs, and monocytes [95, 226, 233, 234], enhanced migration of CD14⁺ DCs could be the result of increased expression of CD14 by CD1a⁺ DCs and/or selective enhancement of CD14⁺ DC migration and CD1a⁺ DC retention in the skin [229]. Future studies will be needed to further characterize human migratory DC populations following MC903 MNA application and distinguish between these two possible mechanisms; however, the substantial upregulation of CD14 mRNA observed in the skin microenvironment after MC903 MNA application (Figure

4-13) suggests that the enhanced frequency of CD14⁺ DCs among migratory cells is at least partially attributable to the first mechanism. Changes in expression levels of co-stimulatory (CD80, CD83, CD86, CD40) and co-inhibitory (ILT3, ILT4, PD-L1) receptors in response to MC903 MNA treatment would also be of interest in future studies.

Together with the promising data showing both prophylactic and therapeutic induction of allergen tolerance in mice, demonstration of a more tolerogenic cutaneous microenvironment and migration of more tolerogenic DCs from human skin explant experiments support the potential for clinical translation of this approach. The ease of incorporating diverse types of allergens and prior FDA approval of MC903 for dermatological applications (plaque psoriasis) make this cutaneous microenvironment-modifying technology an exciting candidate for clinical translation. The path to clinical translation is also simplified by the fact that the MNAs are made of FDA-designated “Generally Recognized As Safe” (GRAS) materials (sodium carboxymethyl cellulose and trehalose), and are being used to deliver doxorubicin in an ongoing phase I clinical trial for cutaneous T-cell lymphoma ([NCT02192021](#)).

In conclusion, by providing tolerogenic context for allergen introduction using a vitamin D3 analog—thereby mimicking natural synthesis of vitamin D3 in the skin—MC903 MNAs were able to induce allergen tolerance—mediated at least in part by increases in Treg/Teff and Th2/Th1 ratios—in both prophylactic and therapeutic murine models of ACD. Experiments with human skin explants provide insight and correlation between the promising results in mice and humans and support the possibility for clinical translation. Ultimately, as with the TRI MPs in Chapter 3, this approach to allergen-specific tolerance induction may be applicable to a variety of T-cell-mediated inflammatory diseases, autoimmune diseases, and allograft rejection.

5.0 FUTURE WORK

The studies presented in Chapters 2-4 open a number of promising avenues for future exploration. In addition to some of the future experiments identified in the discussion sections of those chapters, the following areas could merit further investigation:

5.1 USING AGENT-POLYMER INTERACTIONS TO IMPROVE RATIONAL DESIGN OF CONTROLLED RELEASE SYSTEMS

In the future, our findings regarding release of positively charged agents from negatively charged polymer matrices (Chapter 2 [144]), may be incorporated into existing mathematical models of controlled release [101, 102] to improve their predictive capacity. Additionally, we expect this new understanding of how agent-polymer electrostatic interactions influence drug release kinetics will help to improve future rational design of controlled release formulations for a variety of therapeutic peptide, proteins, or charged small molecule drugs. Finally, novel approaches to negate agent-polymer matrix interactions and different types of polymers could require further measurements of electrostatic interactions and new models of the influence of these interactions on release from different types of matrices.

5.2 IMPROVING TRI MP FOR CLINICAL TRANSLATION

While TRI MPs described in Chapter 3 deliver bioactive factors and effectively suppress ACD in murine models [235], maximizing loading and reducing particle residence time (i.e. the time MPs remain in tissue after complete release) would be important for translational purposes. Greater loading and/or faster degrading MPs would allow the same amount of TRI factors to be delivered from a smaller and/or faster disappearing particle depot, and thereby minimize injection site irritation, facilitate scale-up for clinical translation [236], and make repeated injections easier if needed. Microfluidic-based synthesis of MPs may facilitate increased loading and easier scale-up of fabrication, as microfluidic systems can be run in parallel with similar control parameters to achieve production of larger quantities of particles [237]. Compared to traditional particle fabrication using a homogenizer, microfluidic chips can reduce shear (improve bioactivity), increase loading, and decrease particle polydispersity, eliminating MPs at the low end of the size distribution, which may make up a sizable fraction of total mass with very little drug encapsulation [238-240]. Alternatively, TRI factor loading could be increased in MPs fabricated with the single or double emulsion solvent evaporation methods used in Chapters 2 and 3 [93, 121, 144, 235] by increasing the amount of factor and/or reducing the total mass of polymer per batch. To achieve faster particle degradation, lower molecular weight PLGA and/or PEG-PLGA polymers could be used [99, 102, 144]. Since lower molecular weight polymers have greater densities of end-groups, ester-capped PLGA would be used, especially for TGF- β 1 MPs, to reduce the negative charge density shown in Chapter 2 to impede release of positively charged proteins, like TGF- β 1 [144].

5.3 EVALUATING TRI MP EFFICACY IN CHRONIC MODELS OF ACD

In Chapter 3, we demonstrated that TRI MPs provide sufficient tolerogenic context during allergen exposure to enhance Treg / Teff ratios and suppress subsequent DTH responses in an allergen-specific manner [235]. Given these promising results in acute models of hapten- and protein-mediated ACD, future studies may investigate the therapeutic potential TRI MPs in chronic hypersensitivity models, which more closely reflect the clinical presentation of ACD. Since ACD often involves repeated exposure to contact allergens over extended periods of time, determining the duration and durability of TRI MP-induced allergen tolerance would be advantageous for future clinical translation of this approach, and could be investigated in long-term and repeated-exposure models (summarized in Figure 5-1). Since long-term tolerance depends on enduring allergen-specific memory Tregs, persistence and stability of TRI MP-induced Tregs could be evaluated using congenic T cell adoptive transfer models and transgenic Foxp3 fate-mapping reporter mice [241, 242]. To identify and track allergen-specific Tregs at extended time points, wild-type (CD45.2⁺) conventional (FoxP3⁻) T cells could be adoptively transferred to congenic (CD45.1⁺) recipients prior to TRI MP and hapten sensitization. At extended time points, hapten-specific (CD45.2⁺) peripherally induced pTregs could be identified and quantified in skin and lymphatic tissues. Since reports have suggested that peripherally induced Tregs (e.g. those generated by TRI MP treatment) may retain some degree of plasticity [243, 244], stability of allergen-specific Tregs induced by TRI MP treatment could be evaluated using FoxP3 fate-mapping reporter mice [242]. Finally, for long-term studies, release assays for IL-2 and TGF- β 1 (as in Figure 3-1) would need to be extended beyond three weeks, and particles may need to be reformulated if bioactive cytokines are released after three weeks. Increasing

the overall PEG:PLGA ratio or blending the PEG-PLGA co-polymer with a lower molecular weight PLGA would help to achieve complete release within the first week [245].

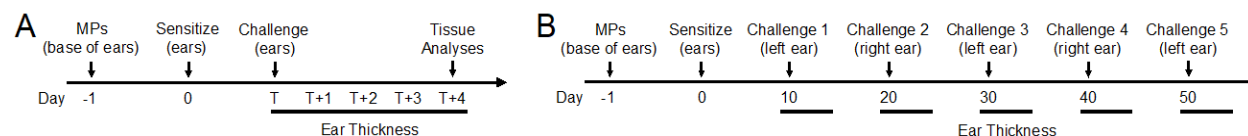


Figure 5-1. Timelines for future experiments to evaluate (A) duration and (B) durability of TRI MP-induced tolerance. Mice would be sensitized and challenge with the same allergen (e.g. DNFB) at the indicated times. In (A), “T” represents the time to first challenge, which would be greater than 10 days (prior studies from Chapter 3). As in acute models, DTH responses would be evaluated by ear swelling, cutaneous histology, and flow cytometry.

5.4 TESTING MC903 MNA IN MURINE MODELS OF HAPTEN-MEDIATED ACD

Since sensitization to haptens requires innate inflammatory responses [44], and co-delivery of DNCB and MC903 with MNAs inhibited cutaneous expression of DNCB-induced inflammatory cytokines and inflammasome (Figure 4-12), future studies should determine whether DNCB + MC903 MNA can tolerize mice to DNCB. Experiments involving prophylactic tolerization of naïve mice and therapeutic tolerization of previously sensitized mice would be similar to those with OVA + MC903 MNA, described in Chapter 4. Evaluating induction of tolerance to different types of chemical allergens would also help to demonstrate broad translational potential for thousands of potential chemical allergens [2], or alternatively, identify subsets of allergens that may be more or less compatible with this therapeutic approach. In particular, DNCB, nickel, and urushiol represent three different types of contact allergens that induce innate inflammatory responses through similar yet distinct mechanisms. DNCB induces production of damage associated molecular patterns (DAMPs) that activate TLR2 and TLR4, and release of ATP that

promotes inflammasome activation [44]. Metal allergens like nickel directly bind to and activate human TLR4 [174], while urushiol, a mixture of allergenic lipids in poison ivy, signals through the CD1a receptor on cutaneous APCs [246]. Accordingly, tolerization with Nickel + MC903 MNA, or Urushiol + MC903 MNA, could be tested in human TLR4 transgenic mice [174], or human CD1a transgenic mice [246], respectively.

5.5 EVALUATING HUMAN SKIN MICROENVIRONMENT RESPONSES TO ALLERGEN + MC903 MNA

The absence of pro-inflammatory stimuli (i.e. allergen) is a potential limitation of the experiments with human skin explants presented in Chapter 4. Changes to the cutaneous microenvironment in response to MC903 MNA were reported relative to untreated skin (Figure 4-13), with very low baseline expression of many pro-inflammatory cytokines or chemokines, which means that even 10-fold increases in expression may not be physiologically significant. Thus, future studies could examine human skin responses to MNAs containing allergen (e.g. DNCB, nickel, and/or urushiol) with or without MC903, as allergens alone should induce sufficient expression of pro-inflammatory factors to generate physiological responses. As in Chapter 4, RNA isolated from human skin explants would be analyzed by qRT-PCR arrays. Alternatively, analysis of additional target genes (e.g. expression of 249 inflammation-related genes by NanoString nCounter Gene Expression Assays), or whole transcriptome analysis by RNA-Seq could be used to further characterize cutaneous microenvironment responses to treatments. In addition to microenvironment evaluation, migrating cells would be harvested from human skin explants treated with Allergen \pm MC903 MNAs, and flow cytometry used to

assess subsets and inflammatory / tolerogenic phenotypes. The stimulatory capacity of migratory DCs could also be evaluated by allogeneic mixed leukocyte reactions (co-cultures of migratory DCs with naïve allogeneic T cells). Finally, assessment of differential responses to Allergen + MC903 MNA in explants from allergic and nonallergic individuals would be relevant to future clinical translation for prophylactic or therapeutic tolerization.

5.6 INVESTIGATING RESPONSES TO DIFFERENT MODES OF CUTANEOUS DELIVERY OF DIFFERENT TYPES OF ALLERGENS

Since allergens and MC903 have traditionally been introduced epicutaneously, and MNAs provide deeper delivery to epidermal and dermal layers of the skin, future studies are needed to investigate the influence of these distinct delivery routes on the subsets of skin-resident DCs targeted and modulation of their phenotype. Preliminary data suggest that MNAs deliver OVA protein to epidermal Langerhans cells (LCs), CD11b⁺ dermal DCs, and CD103⁺ dermal DCs (Figure 5-2). Furthermore, most OVA⁺ cells in DLN were CD11b⁺ dermal DCs, and few non-migratory lymphoid-resident CD8a⁺ DCs contained OVA (Figure 5-2). To compare delivery with MNAs to epicutaneous application, OVA-AF647 would be applied topically to tape-stripped skin and covered with an occlusive dressing. To extend these results to other types of allergens, fluorescent peptide or FITC (a model hapten) could be delivered with tip-loaded MNAs or applied epicutaneously. Compared to epicutaneous application, MNAs would be expected to provide greater delivery of proteins and peptides to dermal DCs; however, since low molecular weight haptens easily penetrate the skin, both modes of delivery for haptens may ultimately target similar populations of DCs. Finally, to determine the influence of cutaneous

microenvironment and antigen introduction method (i.e. epicutaneous vs. MNA) on the phenotype of DCs that access allergen, OVA-AF647 ± MC903 MNAs could be applied to murine or human skin, and the phenotype of OVA⁺ migratory DCs assessed by flow cytometry.

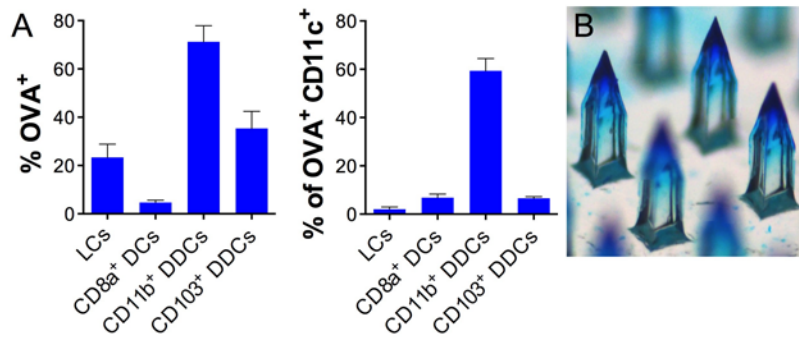


Figure 5-2. MNAs deliver OVA protein to different subsets of skin migratory DCs. (A) Flow cytometry analysis of DC subsets in skin DLN 24 hours after application of (B) tip-loaded Alexa Fluor 647-labeled OVA MNA to ears of mice (mean ± SD, N = 4).

6.0 CONCLUSIONS AND BROADER IMPLICATIONS

TRI MPs and MC903 MNAs effectively modify the skin and draining lymph node (DLN) microenvironments associated with allergen uptake by APCs and presentation to T cells, respectively. In doing so, these delivery systems mimic some of the natural mechanisms the body uses to induce differentiation of Tregs. Specifically, TRI MPs mimic the secretion of IL-2 and TGF- β 1 by tolerogenic DCs and other cells in the body, which provide key signals to naïve T cells, causing them to differentiate into Tregs [40, 88, 89]. Alternatively, delivery of MC903 into the skin with MNAs mimics cutaneous synthesis of 1,25-dihydroxyvitamin D3 in response to sunlight (UV), which helps maintain immunological homeostasis and peripheral tolerance to benign foreign and self antigens [90, 91]. By providing key signals with appropriate temporospatial context, these biomimetic delivery systems convey instructions that can be interpreted by the immune system [87], and result in allergen-specific tolerogenic responses, characterized by enhanced Treg induction and reduced differentiation of effector T cells.

Notably, our approaches to promote Treg differentiation and allergen tolerance using TRI MPs (Chapter 3) or MC903 MNAs (Chapter 4) may be broadly applicable to a variety of autoimmune diseases, inflammatory diseases, or transplant rejection. In many of these conditions, much like ACD, tissue destruction is mediated by pro-inflammatory effector T cells that recognize self antigens or alloantigens instead of allergens. Furthermore, as in ACD, Tregs are known to efficiently regulate such aberrant inflammation, and enhancing Treg populations

has been a common therapeutic goal in numerous murine and human studies [19, 247-251]. Accordingly, in our lab, Treg-inducing TRI MP are currently being used to restore immune homeostasis in murine models of dry eye disease, periodontal disease, type I diabetes, and vascularized composite allotransplantation (unpublished data). Finally, we also envision using MC903 MNA to treat autoimmune diseases, or prevent allograft rejection, by incorporating autoantigens, or alloantigens (e.g. donor splenocytes), instead of allergens.

BIBLIOGRAPHY

- [1] Peiser, M., Tralau, T., Heidler, J., Api, A.M., Arts, J.H., Basketter, D.A., English, J., Diepgen, T.L., Fuhlbrigge, R.C., Gaspari, A.A., Johansen, J.D., Karlberg, A.T., Kimber, I., Lepoittevin, J.P., Liebsch, M., Maibach, H.I., Martin, S.F., Merk, H.F., Platzek, T., Rustemeyer, T., Schnuch, A., Vandebriel, R.J., White, I.R., Luch, A. Allergic contact dermatitis: epidemiology, molecular mechanisms, in vitro methods and regulatory aspects. Current knowledge assembled at an international workshop at BfR, Germany. *Cell Mol Life Sci* (2012) 69: 763-781.
- [2] De Groot, A.C., Patch Testing: Test Concentrations and Vehicles for 4350 Chemicals, 3rd ed., Acdegroot Publishing, Wapserveen, Netherlands, 2008.
- [3] Kadyk, D.L., Hall, S., Belsito, D.V. Quality of life of patients with allergic contact dermatitis: an exploratory analysis by gender, ethnicity, age, and occupation. *Dermatitis* (2004) 15: 117-124.
- [4] Kadyk, D.L., McCarter, K., Achen, F., Belsito, D.V. Quality of life in patients with allergic contact dermatitis. *J Am Acad Dermatol* (2003) 49: 1037-1048.
- [5] Bickers, D.R., Lim, H.W., Margolis, D., Weinstock, M.A., Goodman, C., Faulkner, E., Gould, C., Gemmen, E., Dall, T., American Academy of Dermatology, A., Society for Investigative, D. The burden of skin diseases: 2004 a joint project of the American Academy of Dermatology Association and the Society for Investigative Dermatology. *J Am Acad Dermatol* (2006) 55: 490-500.
- [6] Pariser, D. Topical corticosteroids and topical calcineurin inhibitors in the treatment of atopic dermatitis: focus on percutaneous absorption. *Am J Ther* (2009) 16: 264-273.
- [7] Tuckermann, J.P., Kleiman, A., Moriggl, R., Spanbroek, R., Neumann, A., Illing, A., Clausen, B.E., Stride, B., Forster, I., Habenicht, A.J., Reichardt, H.M., Tronche, F., Schmid, W., Schutz, G. Macrophages and neutrophils are the targets for immune suppression by glucocorticoids in contact allergy. *J Clin Invest* (2007) 117: 1381-1390.
- [8] Simpson, E.L. Atopic dermatitis: a review of topical treatment options. *Curr Med Res Opin* (2010) 26: 633-640.
- [9] Kim, M., Jung, M., Hong, S.P., Jeon, H., Kim, M.J., Cho, M.Y., Lee, S.H., Man, M.Q., Elias, P.M., Choi, E.H. Topical calcineurin inhibitors compromise stratum corneum

- integrity, epidermal permeability and antimicrobial barrier function. *Exp Dermatol* (2010) 19: 501-510.
- [10] Kao, J.S., Fluhr, J.W., Man, M.-Q., Fowler, A.J., Hachem, J.-P., Crumrine, D., Ahn, S.K., Brown, B.E., Elias, P.M., Feingold, K.R. Short-term glucocorticoid treatment compromises both permeability barrier homeostasis and stratum corneum integrity: inhibition of epidermal lipid synthesis accounts for functional abnormalities. *J Invest Dermatol* (2003) 120: 456-464.
- [11] Lee, P.W., Elsaie, M.L., Jacob, S.E. Allergic contact dermatitis in children: common allergens and treatment: a review. *Curr Opin Pediatr* (2009) 21: 491-498.
- [12] Min, D.I., Monaco, A.P. Complications associated with immunosuppressive therapy and their management. *Pharmacotherapy* (1991) 11: 119S-125S.
- [13] Saary, J., Qureshi, R., Palda, V., DeKoven, J., Pratt, M., Skotnicki-Grant, S., Holness, L. A systematic review of contact dermatitis treatment and prevention. *J Am Acad Dermatol* (2005) 53: 845.
- [14] Vignali, D.A.A., Collison, L.W., Workman, C.J. How regulatory T cells work. *Nat Rev Immunol* (2008) 8: 523-532.
- [15] Sakaguchi, S., Yamaguchi, T., Nomura, T., Ono, M. Regulatory T cells and immune tolerance. *Cell* (2008) 133: 775-787.
- [16] Gagliani, N., Magnani, C.F., Huber, S., Gianolini, M.E., Pala, M., Licona-Limon, P., Guo, B.G.G., Herbert, D.R., Bulfone, A., Trentini, F., Di Serio, C., Bacchetta, R., Andreani, M., Brockmann, L., Gregori, S., Flavell, R.A., Roncarolo, M.G. Coexpression of CD49b and LAG-3 identifies human and mouse T regulatory type 1 cells. *Nat Med* (2013) 19: 739-+.
- [17] Zeng, H., Zhang, R., Jin, B., Chen, L. Type 1 regulatory T cells: a new mechanism of peripheral immune tolerance. *Cell Mol Immunol* (2015) 12: 566-571.
- [18] Sakaguchi, S. Naturally arising Foxp3-expressing CD25(+) CD4(+) regulatory T cells in immunological tolerance to self and non-self. *Nat Immunol* (2005) 6: 345-352.
- [19] Brusko, T.M., Putnam, A.L., Bluestone, J.A. Human regulatory T cells: role in autoimmune disease and therapeutic opportunities. *Immunol Rev* (2008) 223: 371-390.
- [20] Sakaguchi, S., Wing, K., Onishi, Y., Prieto-Martin, P., Yamaguchi, T. Regulatory T cells: how do they suppress immune responses? *Int Immunol* (2009) 21: 1105-1111.
- [21] Ring, S., Oliver, S.J., Cronstein, B.N., Enk, A.H., Mahnke, K. CD4(+)CD25(+) regulatory T cells suppress contact hypersensitivity reactions through a CD39, adenosine-dependent mechanism. *J Allergy Clin Immunol* (2009) 123: 1287-1296.

- [22] Ghiringhelli, F., Menard, C., Terme, M., Flament, C., Taieb, J., Chaput, N., Puig, P.E., Novault, S., Escudier, B., Vivier, E., Lecesne, A., Robert, C., Blay, J.Y., Bernard, J., Caillat-Zucman, S., Freitas, A., Tursz, T., Wagner-Ballon, O., Capron, C., Vainchenker, W., Martin, F., Zitvogel, L. CD4(+) CD25(+) regulatory T cells inhibit natural killer cell functions in a transforming growth factor-beta-dependent manner. *J Exp Med* (2005) 202: 1075-1085.
- [23] Richards, H., Williams, A., Jones, E., Hindley, J., Godkin, A., Simon, A.K., Gallimore, A. Novel role of regulatory T cells in limiting early neutrophil responses in skin. *Immunology* (2010) 131: 583-592.
- [24] Tubo, N.J., Jenkins, M.K. TCR signal quantity and quality in CD4+ T cell differentiation. *Trends Immunol* (2014) 35: 591-596.
- [25] Kim, C., Wilson, T., Fischer, K.F., Williams, M.A. Sustained Interactions between T Cell Receptors and Antigens Promote the Differentiation of CD4(+) Memory T Cells. *Immunity* (2013) 39: 508-520.
- [26] Appleman, L.J., Boussiotis, V.A. T cell anergy and costimulation. *Immunol Rev* (2003) 192: 161-180.
- [27] Lanzavecchia, A., Sallusto, F. Regulation of T cell immunity by dendritic cells. *Cell* (2001) 106: 263-266.
- [28] Wells, A.D., Walsh, M.C., Bluestone, J.A., Turka, L.A. Signaling through CD28 and CTLA-4 controls two distinct forms of T cell anergy. *J Clin Invest* (2001) 108: 895-903.
- [29] Jiang, S., Dong, C. A complex issue on CD4(+) T-cell subsets. *Immunol Rev* (2013) 252: 5-11.
- [30] Zhu, J., Paul, W.E. Heterogeneity and plasticity of T helper cells. *Cell Res* (2010) 20: 4-12.
- [31] Shevach, E.M., Thornton, A.M. tTregs, pTregs, and iTregs: similarities and differences. *Immunol Rev* (2014) 259: 88-102.
- [32] Mittrucker, H.W., Visekruna, A., Huber, M. Heterogeneity in the Differentiation and Function of CD8(+) T Cells. *Arch Immunol Ther Ex* (2014) 62: 449-458.
- [33] Chen, L., Flies, D.B. Molecular mechanisms of T cell co-stimulation and co-inhibition. *Nat Rev Immunol* (2013) 13: 227-242.
- [34] Pardoll, D.M. The blockade of immune checkpoints in cancer immunotherapy. *Nat Rev Cancer* (2012) 12: 252-264.
- [35] Steinman, R.M., Hawiger, D., Liu, K., Bonifaz, L., Bonnyay, D., Mahnke, K., Iyoda, T., Ravetch, J., Dhodapkar, M., Inaba, K., Nussenzweig, M. Dendritic cell function in vivo

- during the steady state: A role in peripheral tolerance. *Ann Ny Acad Sci* (2003) 987: 15-25.
- [36] Hackstein, H., Thomson, A.W. Dendritic cells: emerging pharmacological targets of immunosuppressive drugs. *Nat Rev Immunol* (2004) 4: 24-34.
- [37] Adorini, L., Giarratana, N., Penna, G. Pharmacological induction of tolerogenic dendritic cells and regulatory T cells. *Semin Immunol* (2004) 16: 127-134.
- [38] Kalantari, T., Kamali-Sarvestani, E., Ciric, B., Karimi, M.H., Kalantari, M., Faridar, A., Xu, H., Rostami, A. Generation of immunogenic and tolerogenic clinical-grade dendritic cells. *Immunol Res* (2011) 51: 153-160.
- [39] Hubo, M., Trinschek, B., Kryczanowsky, F., Tuettenberg, A., Steinbrink, K., Jonuleit, H. Costimulatory molecules on immunogenic versus tolerogenic human dendritic cells. *Front Immunol* (2013) 4.
- [40] Maldonado, R.A., von Andrian, U.H. How Tolerogenic Dendritic Cells Induce Regulatory T Cells. *Adv Immunol* (2010) 108: 111-165.
- [41] Manicassamy, S., Pulendran, B. Dendritic cell control of tolerogenic responses. *Immunol Rev* (2011) 241: 206-227.
- [42] Kushwah, R., Hu, J. Role of dendritic cells in the induction of regulatory T cells. *Cell Biosci* (2011) 1.
- [43] Morelli, A.E., Thomson, A.W. Tolerogenic dendritic cells and the quest for transplant tolerance. *Nat Rev Immunol* (2007) 7: 610-621.
- [44] Kaplan, D.H., Igyarto, B.Z., Gaspari, A.A. Early immune events in the induction of allergic contact dermatitis. *Nat Rev Immunol* (2012) 12: 114-124.
- [45] Honda, T., Egawa, G., Grabbe, S., Kabashima, K. Update of immune events in the murine contact hypersensitivity model: toward the understanding of allergic contact dermatitis. *J Invest Dermatol* (2013) 133: 303-315.
- [46] Ishizaki, K., Yamada, A., Yoh, K., Nakano, T., Shimohata, H., Maeda, A., Fujioka, Y., Morito, N., Kawachi, Y., Shibuya, K., Otsuka, F., Shibuya, A., Takahashi, S. Th1 and type 1 cytotoxic T cells dominate responses in T-bet overexpression transgenic mice that develop contact dermatitis. *J Immunol* (2007) 178: 605-612.
- [47] Girolomoni, G., Gisondi, P., Ottaviani, C., Cavani, A. Immunoregulation of allergic contact dermatitis. *J Dermatol* (2004) 31: 264-270.
- [48] Lehtimäki, S., Savinko, T., Lahl, K., Sparwasser, T., Wolff, H., Lauerma, A., Alenius, H., Fyhrquist, N. The temporal and spatial dynamics of Foxp3⁺ Treg cell-mediated suppression during contact hypersensitivity responses in a murine model. *J Invest Dermatol* (2012) 132: 2744-2751.

- [49] Ring, S., Schafer, S.C., Mahnke, K., Lehr, H.A., Enk, A.H. CD4(+)CD25(+) regulatory T cells suppress contact hypersensitivity reactions by blocking influx of effector T cells into inflamed tissue. *Eur J Immunol* (2006) 36: 2981-2992.
- [50] Gocinski, B.L., Tigelaar, R.E. Roles of CD4+ and CD8+ T cells in murine contact sensitivity revealed by in vivo monoclonal antibody depletion. *J Immunol* (1990) 144: 4121-4128.
- [51] Xu, H., DiIulio, N.A., Fairchild, R.L. T cell populations primed by hapten sensitization in contact sensitivity are distinguished by polarized patterns of cytokine production: interferon gamma-producing (Tc1) effector CD8+ T cells and interleukin (Il) 4/Il-10-producing (Th2) negative regulatory CD4+ T cells. *J Exp Med* (1996) 183: 1001-1012.
- [52] Ring, S., Thome, M., Pretsch, L., Enk, A.H., Mahnke, K. Expanded murine regulatory T cells: analysis of phenotype and function in contact hypersensitivity reactions. *J Immunol Methods* (2007) 326: 10-21.
- [53] Hippen, K.L., Merkel, S.C., Schirm, D.K., Sieben, C.M., Sumstad, D., Kadidlo, D.M., McKenna, D.H., Bromberg, J.S., Levine, B.L., Riley, J.L., June, C.H., Scheinberg, P., Douek, D.C., Miller, J.S., Wagner, J.E., Blazar, B.R. Massive ex vivo expansion of human natural regulatory T cells (Tregs) with minimal loss of in vivo functional activity. *Sci Transl Med* (2011) 3: 83ra41.
- [54] Roncarolo, M.G., Battaglia, M. Regulatory T-cell immunotherapy for tolerance to self antigens and alloantigens in humans. *Nat Rev Immunol* (2007) 7: 585-598.
- [55] Trzonkowski, P., Bacchetta, R., Battaglia, M., Berglund, D., Bohnenkamp, H.R., ten Brinke, A., Bushell, A., Cools, N., Geissler, E.K., Gregori, S., Marieke van Ham, S., Hilkens, C., Hutchinson, J.A., Lombardi, G., Madrigal, J.A., Marek-Trzonkowska, N., Martinez-Caceres, E.M., Roncarolo, M.G., Sanchez-Ramon, S., Saudemont, A., Sawitzki, B. Hurdles in therapy with regulatory T cells. *Sci Transl Med* (2015) 7: 304ps318.
- [56] Kontos, S., Grimm, A.J., Hubbell, J.A. Engineering antigen-specific immunological tolerance. *Curr Opin Immunol* (2015) 35: 80-88.
- [57] Miyara, M., Wing, K., Sakaguchi, S. Therapeutic approaches to allergy and autoimmunity based on FoxP3+ regulatory T-cell activation and expansion. *J Allergy Clin Immunol* (2009) 123: 749-755.
- [58] Matsuoka, K., Koreth, J., Kim, H.T., Bascug, G., McDonough, S., Kawano, Y., Murase, K., Cutler, C., Ho, V.T., Alyea, E.P., Armand, P., Blazar, B.R., Antin, J.H., Soiffer, R.J., Ritz, J. Low-Dose Interleukin-2 Therapy Restores Regulatory T Cell Homeostasis in Patients with Chronic Graft-Versus-Host Disease. *Sci Transl Med* (2013) 5.
- [59] Deal watch: Boosting TRegs to target autoimmune disease. *Nat Rev Drug Discov* (2011) 10: 566.

- [60] Helling, B., Konig, M., Dalken, B., Engling, A., Kromer, W., Heim, K., Wallmeier, H., Haas, J., Wildemann, B., Fritz, B., Jonuleit, H., Kubach, J., Dingermann, T., Radeke, H.H., Osterroth, F., Uherek, C., Czeloth, N., Schuttrumpf, J. A specific CD4 epitope bound by tregalizumab mediates activation of regulatory T cells by a unique signaling pathway. *Immunol Cell Biol* (2014).
- [61] Beyersdorf, N., Gaupp, S., Balbach, K., Schmidt, J., Toyka, K.V., Lin, C.H., Hanke, T., Hunig, T., Kerkau, T., Gold, R. Selective targeting of regulatory T cells with CD28 superagonists allows effective therapy of experimental autoimmune encephalomyelitis. *J Exp Med* (2005) 202: 445-455.
- [62] Suntharalingam, G., Perry, M.R., Ward, S., Brett, S.J., Castello-Cortes, A., Brunner, M.D., Panoskaltsis, N. Cytokine storm in a phase 1 trial of the anti-CD28 monoclonal antibody TGN1412. *N Engl J Med* (2006) 355: 1018-1028.
- [63] Schreiber, T.H., Wolf, D., Tsai, M.S., Chirinos, J., Deyev, V.V., Gonzalez, L., Malek, T.R., Levy, R.B., Podack, E.R. Therapeutic Treg expansion in mice by TNFRSF25 prevents allergic lung inflammation. *J Clin Invest* (2010) 120: 3629-3640.
- [64] Long, S.A., Rieck, M., Sanda, S., Bollyky, J.B., Samuels, P.L., Goland, R., Ahmann, A., Rabinovitch, A., Aggarwal, S., Phippard, D., Turka, L.A., Ehlers, M.R., Bianchine, P.J., Boyle, K.D., Adah, S.A., Bluestone, J.A., Buckner, J.H., Greenbaum, C.J., Tolerance, D.T.I. Rapamycin/IL-2 Combination Therapy in Patients With Type 1 Diabetes Augments Tregs Yet Transiently Impairs beta-cell Function. *Diabetes* (2012) 61: 2340-2348.
- [65] Wilson, M.S., Pesce, J.T., Ramalingam, T.R., Thompson, R.W., Cheever, A., Wynn, T.A. Suppression of Murine Allergic Airway Disease by IL-2:Anti-IL-2 Monoclonal Antibody-Induced Regulatory T Cells. *J Immunol* (2008) 181: 6942-6954.
- [66] Webster, K.E., Walters, S., Kohler, R.E., Mrkvan, T., Boyman, O., Surh, C.D., Grey, S.T., Sprent, J. In vivo expansion of T reg cells with IL-2-mAb complexes: induction of resistance to EAE and long-term acceptance of islet allografts without immunosuppression. *J Exp Med* (2009) 206: 751-760.
- [67] El Beidaq, A., Link, C.W., Hofmann, K., Frehse, B., Hartmann, K., Bieber, K., Martin, S.F., Ludwig, R.J., Manz, R.A. In Vivo Expansion of Endogenous Regulatory T Cell Populations Induces Long-Term Suppression of Contact Hypersensitivity. *J Immunol* (2016) 197: 1567-1576.
- [68] Letourneau, S., van Leeuwen, E.M.M., Krieg, C., Martin, C., Pantaleo, G., Sprent, J., Surh, C.D., Boyman, O. IL-2/anti-IL-2 antibody complexes show strong biological activity by avoiding interaction with IL-2 receptor alpha subunit CD25. *Proc Nat Acad Sci USA* (2010) 107: 2171-2176.
- [69] McDermott, D.F., Regan, M.M., Clark, J.I., Flaherty, L.E., Weiss, G.R., Logan, T.F., Kirkwood, J.M., Gordon, M.S., Sosman, J.A., Ernstoff, M.S., Tretter, C.P.G., Urba, W.J., Smith, J.W., Margolin, K.A., Mier, J.W., Gollob, J.A., Dutcher, J.P., Atkins, M.B.

- Randomized phase III trial of high-dose interleukin-2 versus subcutaneous interleukin-2 and interferon in patients with metastatic renal cell carcinoma. *J Clin Oncol* (2005) 23: 133-141.
- [70] Clemente-Casares, X., Blanco, J., Ambalavanan, P., Yamanouchi, J., Singha, S., Fandos, C., Tsai, S., Wang, J., Garabatos, N., Izquierdo, C., Agrawal, S., Keough, M.B., Yong, V.W., James, E., Moore, A., Yang, Y., Stratmann, T., Serra, P., Santamaria, P. Expanding antigen-specific regulatory networks to treat autoimmunity. *Nature* (2016) 530: 434-440.
- [71] Yeste, A., Nadeau, M., Burns, E.J., Weiner, H.L., Quintana, F.J. Nanoparticle-mediated codelivery of myelin antigen and a tolerogenic small molecule suppresses experimental autoimmune encephalomyelitis. *Proc Natl Acad Sci USA* (2012) 109: 11270-11275.
- [72] Getts, D.R., Martin, A.J., McCarthy, D.P., Terry, R.L., Hunter, Z.N., Yap, W.T., Getts, M.T., Pleiss, M., Luo, X.R., King, N.J.C., Shea, L.D., Miller, S.D. Microparticles bearing encephalitogenic peptides induce T-cell tolerance and ameliorate experimental autoimmune encephalomyelitis. *Nat Biotechnol* (2012) 30: 1217-1224.
- [73] Maldonado, R.A., LaMothe, R.A., Ferrari, J.D., Zhang, A.H., Rossi, R.J., Kolte, P.N., Griset, A.P., O'Neil, C., Altreuter, D.H., Browning, E., Johnston, L., Farokhzad, O.C., Langer, R., Scott, D.W., von Andrian, U.H., Kishimoto, T.K. Polymeric synthetic nanoparticles for the induction of antigen-specific immunological tolerance. *Proc Nat Acad Sci USA* (2015) 112: E156-E165.
- [74] Kishimoto, T.K., Ferrari, J.D., LaMothe, R.A., Kolte, P.N., Griset, A.P., O'Neil, C., Chan, V., Browning, E., Chalishazar, A., Kuhlman, W., Fu, F.N., Viseux, N., Altreuter, D.H., Johnston, L., Maldonado, R.A. Improving the efficacy and safety of biologic drugs with tolerogenic nanoparticles. *Nat Nanotechnol* (2016) 11: 890-899.
- [75] Tostanoski, L.H., Chiu, Y.C., Gammon, J.M., Simon, T., Andorko, J.I., Bromberg, J.S., Jewell, C.M. Reprogramming the Local Lymph Node Microenvironment Promotes Tolerance that Is Systemic and Antigen Specific. *Cell Rep* (2016) 16: 2940-2952.
- [76] Akdis, M., Akdis, C.A. Therapeutic manipulation of immune tolerance in allergic disease. *Nat Rev Drug Discov* (2009) 8: 645-660.
- [77] Watanabe, H., Gehrke, S., Contassot, E., Roques, S., Tschopp, J., Friedmann, P.S., French, L.E., Gaide, O. Danger signaling through the inflammasome acts as a master switch between tolerance and sensitization. *J Immunol* (2008) 180: 5826-5832.
- [78] Steinbrink, K., Sorg, C., Macher, E. Low zone tolerance to contact allergens in mice: a functional role for CD8+ T helper type 2 cells. *J Exp Med* (1996) 183: 759-768.
- [79] Steinbrink, K., Kolde, G., Sorg, C., Macher, E. Induction of low zone tolerance to contact allergens in mice does not require functional Langerhans cells. *J Invest Dermatol* (1996) 107: 243-247.

- [80] van Hoogstraten, I.M., von Blomberg, B.M., Boden, D., Kraal, G., Scheper, R.J. Non-sensitizing epicutaneous skin tests prevent subsequent induction of immune tolerance. *J Invest Dermatol* (1994) 102: 80-83.
- [81] Ghoreishi, M., Dutz, J.P. Tolerance induction by transcutaneous immunization through ultraviolet-irradiated skin is transferable through CD4+CD25+ T regulatory cells and is dependent on host-derived IL-10. *J Immunol* (2006) 176: 2635-2644.
- [82] Schwarz, A., Beissert, S., Grosse-Heitmeyer, K., Gunzer, M., Bluestone, J.A., Grabbe, S., Schwarz, T. Evidence for functional relevance of CTLA-4 in ultraviolet-radiation-induced tolerance. *J Immunol* (2000) 165: 1824-1831.
- [83] Hart, P.H., Gorman, S., Finlay-Jones, J.J. Modulation of the immune system by UV radiation: more than just the effects of vitamin D? *Nat Rev Immunol* (2011) 11: 584-596.
- [84] Schwarz, A., Navid, F., Sparwasser, T., Clausen, B.E., Schwarz, T. 1,25-dihydroxyvitamin D exerts similar immunosuppressive effects as UVR but is dispensable for local UVR-induced immunosuppression. *J Invest Dermatol* (2012) 132: 2762-2769.
- [85] Gorman, S., Kuritzky, L.A., Judge, M.A., Dixon, K.M., McGlade, J.P., Mason, R.S., Finlay-Jones, J.J., Hart, P.H. Topically applied 1,25-dihydroxyvitamin D3 enhances the suppressive activity of CD4+CD25+ cells in the draining lymph nodes. *J Immunol* (2007) 179: 6273-6283.
- [86] Ghoreishi, M., Bach, P., Obst, J., Komba, M., Fleet, J.C., Dutz, J.P. Expansion of antigen-specific regulatory T cells with the topical vitamin d analog calcipotriol. *J Immunol* (2009) 182: 6071-6078.
- [87] Balmert, S.C., Little, S.R. Biomimetic delivery with micro- and nanoparticles. *Adv Mater* (2012) 24: 3757-3778.
- [88] Horwitz, D.A., Zheng, S.G., Wang, J., Gray, J.D. Critical role of IL-2 and TGF-beta in generation, function and stabilization of Foxp3(+)CD4(+) Treg. *Eur J Immunol* (2008) 38: 912-915.
- [89] Yamazaki, S., Dudziak, D., Heidkamp, G.F., Fiorese, C., Bonito, A.J., Inaba, K., Nussenzweig, M.C., Steinman, R.M. CD8(+)CD205(+) Splenic Dendritic Cells Are Specialized to Induce Foxp3(+) Regulatory T Cells. *J Immunol* (2008) 181: 6923-6933.
- [90] Scott, J.F., Das, L.M., Ahsanuddin, S., Qiu, Y.Q., Binko, A.M., Traylor, Z.P., Debanne, S.M., Cooper, K.D., Boxer, R., Lu, K.Q. Oral Vitamin D Rapidly Attenuates Inflammation from Sunburn: An Interventional Study. *J Invest Dermatol* (2017) 137: 2078-2086.
- [91] Peelen, E., Knippenberg, S., Muris, A.H., Thewissen, M., Smolders, J., Tervaert, J.W.C., Hupperts, R., Damoiseaux, J. Effects of vitamin D on the peripheral adaptive immune system: A review. *Autoimmun Rev* (2011) 10: 733-743.

- [92] Battaglia, M., Stabilini, A., Roncarolo, M.G. Rapamycin selectively expands CD4+CD25+FoxP3+ regulatory T cells. *Blood* (2005) 105: 4743-4748.
- [93] Jhunjunwala, S., Balmert, S.C., Raimondi, G., Dons, E., Nichols, E.E., Thomson, A.W., Little, S.R. Controlled release formulations of IL-2, TGF-beta1 and rapamycin for the induction of regulatory T cells. *J Control Release* (2012) 159: 78-84.
- [94] Jhunjunwala, S., Chen, L.C., Nichols, E.E., Thomson, A.W., Raimondi, G., Little, S.R. All-trans retinoic acid and rapamycin synergize with transforming growth factor-beta 1 to induce regulatory T cells but confer different migratory capacities. *J Leukoc Biol* (2013) 94: 981-989.
- [95] van der Aar, A.M.G., Sibiryak, D.S., Bakdash, G., van Capel, T.M.M., van der Kleij, H.P.M., Opstelten, D.J.E., Teunissen, M.B.M., Kapsenberg, M.L., de Jong, E.C. Vitamin D3 targets epidermal and dermal dendritic cells for induction of distinct regulatory T cells. *J Allergy Clin Immunol* (2011) 127: 1532-1540.
- [96] Korkmaz, E., Friedrich, E.E., Ramadan, M.H., Erdos, G., Mathers, A.R., Ozdoganlar, O.B., Washburn, N.R., Faló, L.D. Therapeutic intradermal delivery of tumor necrosis factor-alpha antibodies using tip-loaded dissolvable microneedle arrays. *Acta Biomater* (2015) 24: 96-105.
- [97] Korkmaz, E., Friedrich, E.E., Ramadan, M.H., Erdos, G., Mathers, A.R., Ozdoganlar, O.B., Washburn, N.R., Faló, L.D. Tip-Loaded Dissolvable Microneedle Arrays Effectively Deliver Polymer-Conjugated Antibody Inhibitors of Tumor-Necrosis-Factor-Alpha Into Human Skin. *J Pharm Sci* (2016) 105: 3453-3457.
- [98] Bediz, B., Korkmaz, E., Khilwani, R., Donahue, C., Erdos, G., Faló, L.D., Ozdoganlar, O.B. Dissolvable Microneedle Arrays for Intradermal Delivery of Biologics: Fabrication and Application. *Pharm Res* (2014) 31: 117-135.
- [99] Rothstein, S.N., Little, S.R. A "tool box" for rational design of degradable controlled release formulations. *J Mater Chem* (2011) 21: 29-39.
- [100] Ford Versypt, A.N., Pack, D.W., Braatz, R.D. Mathematical modeling of drug delivery from autocatalytically degradable PLGA microspheres - A review. *J Control Release* (2013) 165: 29-37.
- [101] Rothstein, S.N., Little, S.R., Federspiel, W.J. A simple model framework for the prediction of controlled release from bulk eroding polymer matrices. *J Mater Chem* (2008) 18: 1873-1880.
- [102] Rothstein, S.N., Federspiel, W.J., Little, S.R. A unified mathematical model for the prediction of controlled release from surface and bulk eroding polymer matrices. *Biomaterials* (2009) 30: 1657-1664.
- [103] BCC Research. Global Markets and Manufacturing Technologies for Protein Drugs. *Global Markets and Manufacturing Technologies for Protein Drugs* (2013).

- [104] Kaspar, A.A., Reichert, J.M. Future directions for peptide therapeutics development. *Drug discovery today* (2013) 18: 807-817.
- [105] Osterberg, L., Blaschke, T. Adherence to medication. *N Engl J Med* (2005) 353: 487-497.
- [106] National Heart Lung and Blood Institute, *NHLBI Fact Book, Fiscal Year 2012*. Bethesda, MD: National Institutes of Health; 2013.
- [107] Ford Versypt, A.N., Pack, D.W., Braatz, R.D. Mathematical modeling of drug delivery from autocatalytically degradable PLGA microspheres--a review. *J Control Release* (2013) 165: 29-37.
- [108] Fredenberg, S., Wahlgren, M., Reslow, M., Axelsson, A. The mechanisms of drug release in poly(lactic-co-glycolic acid)-based drug delivery systems—A review. *Int J Pharm* (2011) 415: 34-52.
- [109] Makadia, H.K., Siegel, S.J. Poly Lactic-co-Glycolic Acid (PLGA) as Biodegradable Controlled Drug Delivery Carrier. *Polymers-Basel* (2011) 3: 1377-1397.
- [110] Mundargi, R.C., Babu, V.R., Rangaswamy, V., Patel, P., Aminabhavi, T.M. Nano/micro technologies for delivering macromolecular therapeutics using poly(D,L-lactide-co-glycolide) and its derivatives. *J Control Release* (2008) 125: 193-209.
- [111] Sophocleous, A.M., Zhang, Y., Schwendeman, S.P. A new class of inhibitors of peptide sorption and acylation in PLGA. *J Control Release* (2009) 137: 179-184.
- [112] Gaspar, M.M., Blanco, D., Cruz, M.E., Alonso, M.J. Formulation of l-asparaginase-loaded poly(lactide-co-glycolide) nanoparticles: influence of polymer properties on enzyme loading, activity and in vitro release. *J Control Release* (1998) 52: 53-62.
- [113] Blanco, M.D., Alonso, M.J. Development and characterization of protein-loaded poly(lactide-co-glycolide) nanospheres. *Eur J Pharm Biopharm* (1997) 43: 287-294.
- [114] Sophocleous, A.M., Desai, K.G., Mazzara, J.M., Tong, L., Cheng, J.X., Olsen, K.F., Schwendeman, S.P. The nature of peptide interactions with acid end-group PLGAs and facile aqueous-based microencapsulation of therapeutic peptides. *J Control Release* (2013) 172: 662-670.
- [115] Lucke, A., Kiermaier, J., Gopferich, A. Peptide acylation by poly(alpha-hydroxy esters). *Pharm Res* (2002) 19: 175-181.
- [116] Ghassemi, A.H., van Steenberg, M.J., Barendregt, A., Talsma, H., Kok, R.J., van Nostrum, C.F., Crommelin, D.J., Hennink, W.E. Controlled release of octreotide and assessment of peptide acylation from poly(D,L-lactide-co-hydroxymethyl glycolide) compared to PLGA microspheres. *Pharm Res* (2012) 29: 110-120.
- [117] Zhang, Y., Schwendeman, S.P. Minimizing acylation of peptides in PLGA microspheres. *J Control Release* (2012) 162: 119-126.

- [118] Sen, M., Thomas, S.M., Kim, S., Yeh, J.I., Ferris, R.L., Johnson, J.T., Duvvuri, U., Lee, J., Sahu, N., Joyce, S., Freilino, M.L., Shi, H., Li, C., Ly, D., Rapireddy, S., Etter, J.P., Li, P.K., Wang, L., Chiosea, S., Seethala, R.R., Gooding, W.E., Chen, X., Kaminski, N., Pandit, K., Johnson, D.E., Grandis, J.R. First-in-human trial of a STAT3 decoy oligonucleotide in head and neck tumors: implications for cancer therapy. *Cancer Discov* (2012) 2: 694-705.
- [119] Lehninger, A.L., Principles of biochemistry, Worth Publishers, New York, 1982.
- [120] Jhunjhunwala, S., Raimondi, G., Glowacki, A.J., Hall, S.J., Maskarinec, D., Thorne, S.H., Thomson, A.W., Little, S.R. Bioinspired Controlled Release of CCL22 Recruits Regulatory T Cells In Vivo. *Adv Mater* (2012) 24: 4735-4738.
- [121] Jhunjhunwala, S., Balmert, S.C., Raimondi, G., Dons, E., Nichols, E.E., Thomson, A.W., Little, S.R. Controlled release formulations of IL-2, TGF- β 1 and rapamycin for the induction of regulatory T cells. *J Control Release* (2012) 159: 78-84.
- [122] Little, S.R., Lynn, D.M., Puram, S.V., Langer, R. Formulation and characterization of poly (β amino ester) microparticles for genetic vaccine delivery. *J Control Release* (2005) 107: 449-462.
- [123] Shenderova, A., Burke, T.G., Schwendeman, S.P. The acidic microclimate in poly(lactide-co-glycolide) microspheres stabilizes camptothecins. *Pharm Res* (1999) 16: 241-248.
- [124] Tracy, M.A., Ward, K.L., Firouzabadian, L., Wang, Y., Dong, N., Qian, R., Zhang, Y. Factors affecting the degradation rate of poly(lactide-co-glycolide) microspheres in vivo and in vitro. *Biomaterials* (1999) 20: 1057-1062.
- [125] Fu, K., Pack, D.W., Klibanov, A.M., Langer, R. Visual evidence of acidic environment within degrading poly(lactic-co-glycolic acid) (PLGA) microspheres. *Pharm Res* (2000) 17: 100-106.
- [126] Yeo, Y., Park, K. Control of encapsulation efficiency and initial burst in polymeric microparticle systems. *Arch Pharm Res* (2004) 27: 1-12.
- [127] Herrmann, J., Bodmeier, R. The Effect of Particle Microstructure on the Somatostatin Release from Poly(Lactide) Microspheres Prepared by a W/O/W Solvent Evaporation Method. *J Control Release* (1995) 36: 63-71.
- [128] Rothstein, S.N., Donahue, C., Falo, L.D., Little, S.R. In silico programming of degradable microparticles to hide and then reveal immunogenic payloads in vivo. *J Mater Chem B* (2014) 2: 6183-6187.
- [129] Schrier, J.A., DeLuca, P.P. Porous bone morphogenetic protein-2 microspheres: polymer binding and in vitro release. *AAPS PharmSciTech* (2001) 2: 66-72.

- [130] Tayalia, P., Mooney, D.J. Controlled growth factor delivery for tissue engineering. *Adv Mater* (2009) 21: 3269-3285.
- [131] Allemann, E., Leroux, J., Gurny, R. Polymeric nano- and microparticles for the oral delivery of peptides and peptidomimetics. *Adv Drug Deliv Rev* (1998) 34: 171-189.
- [132] Yang, S.C., Bhide, M., Crispe, I.N., Pierce, R.H., Murthy, N. Polyketal copolymers: a new acid-sensitive delivery vehicle for treating acute inflammatory diseases. *Bioconjugate Chem* (2008) 19: 1164-1169.
- [133] Allcock, H.R., Morozowich, N.L. Bioerodible polyphosphazenes and their medical potential. *Polym Chem-Uk* (2012) 3: 578-590.
- [134] Lee, E.S., Park, K.H., Kang, D., Park, I.S., Min, H.Y., Lee, D.H., Kim, S., Kim, J.H., Na, K. Protein complexed with chondroitin sulfate in poly(lactide-co-glycolide) microspheres. *Biomaterials* (2007) 28: 2754-2762.
- [135] Lundblad, R.L., Chemical reagents for protein modification, Fourth edition. ed., CRC Press, Boca Raton, 2013.
- [136] Jamison, J.A., Bryant, E.L., Kadali, S.B., Wong, M.S., Colvin, V.L., Matthews, K.S., Calabretta, M.K. Altering protein surface charge with chemical modification modulates protein-gold nanoparticle aggregation. *J Nanopart Res* (2011) 13: 625-636.
- [137] Na, D.H., DeLuca, P.P. PEGylation of octreotide: I. Separation of positional isomers and stability against acylation by poly(D,L-lactide-co-glycolide). *Pharm Res* (2005) 22: 736-742.
- [138] Liu, Y., Schwendeman, S.P. Mapping microclimate pH distribution inside protein-encapsulated PLGA microspheres using confocal laser scanning microscopy. *Mol Pharm* (2012) 9: 1342-1350.
- [139] Liu, Y., Ghassemi, A.H., Hennink, W.E., Schwendeman, S.P. The microclimate pH in poly(D,L-lactide-co-hydroxymethyl glycolide) microspheres during biodegradation. *Biomaterials* (2012) 33: 7584-7593.
- [140] Park, T.G. Degradation of poly(D,L-lactic acid) microspheres: effect of molecular weight. *J Control Release* (1994) 30: 161-173.
- [141] Glowacki, A.J., Yoshizawa, S., Jhunjhunwala, S., Vieira, A.E., Garlet, G.P., Sfeir, C., Little, S.R. Prevention of inflammation-mediated bone loss in murine and canine periodontal disease via recruitment of regulatory lymphocytes. *Proc Nat Acad Sci USA* (2013) 110: 18525-18530.
- [142] Wang, Y., Irvine, D.J. Engineering chemoattractant gradients using chemokine-releasing polysaccharide microspheres. *Biomaterials* (2011) 32: 4903-4913.

- [143] Lee, J., Oh, Y.J., Lee, S.K., Lee, K.Y. Facile control of porous structures of polymer microspheres using an osmotic agent for pulmonary delivery. *Journal of controlled release : official journal of the Controlled Release Society* (2010) 146: 61-67.
- [144] Balmert, S.C., Zmolek, A.C., Glowacki, A.J., Knab, T.D., Rothstein, S.N., Wokpetah, J.M., Fedorchak, M.V., Little, S.R. Positive Charge of "Sticky" Peptides and Proteins Impedes Release From Negatively Charged PLGA Matrices. *J Mater Chem B Mater Biol Med* (2015) 3: 4723-4734.
- [145] Jhunjhunwala, S., Raimondi, G., Thomson, A.W., Little, S.R. Delivery of rapamycin to dendritic cells using degradable microparticles. *J Control Release* (2009) 133: 191-197.
- [146] Saez, V., Ramon, J.A., Caballero, L., Aldana, R., Cruz, E., Peniche, C., Paez, R. Extraction of PLGA-microencapsulated proteins using a two-immiscible liquid phases system containing surfactants. *Pharm Res* (2013) 30: 606-615.
- [147] Tsang, M.L., Zhou, L., Zheng, B.L., Wenker, J., Fransen, G., Humphrey, J., Smith, J.M., O'Connor-McCourt, M., Lucas, R., Weatherbee, J.A. Characterization of recombinant soluble human transforming growth factor-beta receptor type II (rhTGF-beta sRII). *Cytokine* (1995) 7: 389-397.
- [148] Vihola, H., Laukkanen, A., Valtola, L., Tenhu, H., Hirvonen, J. Cytotoxicity of thermosensitive polymers poly(N-isopropylacrylamide), poly(N-vinylcaprolactam) and amphiphilically modified poly(N-vinylcaprolactam). *Biomaterials* (2005) 26: 3055-3064.
- [149] Buske, J., Konig, C., Bassarab, S., Lamprecht, A., Muhlau, S., Wagner, K.G. Influence of PEG in PEG-PLGA microspheres on particle properties and protein release. *Eur J Pharm Biopharm* (2012) 81: 57-63.
- [150] Pisani, E., Ringard, C., Nicolas, V., Raphael, E., Rosilio, V., Moine, L., Fattal, E., Tsapis, N. Tuning microcapsules surface morphology using blends of homo- and copolymers of PLGA and PLGA-PEG. *Soft Matter* (2009) 5: 3054-3060.
- [151] Zheng, S.G., Wang, J., Wang, P., Gray, J.D., Horwitz, D.A. IL-2 is essential for TGF-beta to convert naive CD4+CD25- cells to CD25+Foxp3+ regulatory T cells and for expansion of these cells. *J Immunol* (2007) 178: 2018-2027.
- [152] Lewis, J.S., Roche, C., Zhang, Y., Brusko, T.M., Wasserfall, C.H., Atkinson, M., Clare-Salzler, M.J., Keselowsky, B.G. Combinatorial delivery of immunosuppressive factors to dendritic cells using dual-sized microspheres. *J Mater Chem B Mater Biol Med* (2014) 2: 2562-2574.
- [153] Turnquist, H.R., Raimondi, G., Zahorchak, A.F., Fischer, R.T., Wang, Z., Thomson, A.W. Rapamycin-conditioned dendritic cells are poor stimulators of allogeneic CD4+ T cells, but enrich for antigen-specific Foxp3+ T regulatory cells and promote organ transplant tolerance. *J Immunol* (2007) 178: 7018-7031.

- [154] Yamaguchi, Y., Tsumura, H., Miwa, M., Inaba, K. Contrasting effects of TGF-beta 1 and TNF-alpha on the development of dendritic cells from progenitors in mouse bone marrow. *Stem Cells* (1997) 15: 144-153.
- [155] Brinster, N.K. Dermatopathology for the Surgical Pathologist A Pattern-based Approach to the Diagnosis of Inflammatory Skin Disorders (Part II). *Adv Anat Pathol* (2008) 15: 350-369.
- [156] Akiba, H., Ducluzeau, M.T., Nicolas, J.F. Interferon-gamma production in skin during contact hypersensitivity. No contribution from keratinocytes. *J Invest Dermatol* (2001) 117: 163-163.
- [157] Stephens, G.L., McHugh, R.S., Whitters, M.J., Young, D.A., Luxenberg, D., Carreno, B.M., Collins, M., Shevach, E.M. Engagement of glucocorticoid-induced TNFR family-related receptor on effector T cells by its ligand mediates resistance to suppression by CD4+ CD25+ T cells. *J Immunol* (2004) 173: 5008-5020.
- [158] Lahl, K., Loddenkemper, C., Drouin, C., Freyer, J., Arnason, J., Eberl, G., Hamann, A., Wagner, H., Huehn, J., Sparwasser, T. Selective depletion of Foxp3+ regulatory T cells induces a scurfy-like disease. *J Exp Med* (2007) 204: 57-63.
- [159] Hirosue, S., Kourtis, I.C., van der Vlies, A.J., Hubbell, J.A., Swartz, M.A. Antigen delivery to dendritic cells by poly(propylene sulfide) nanoparticles with disulfide conjugated peptides: Cross-presentation and T cell activation. *Vaccine* (2010) 28: 7897-7906.
- [160] Reddy, S.T., van der Vlies, A.J., Simeoni, E., Angeli, V., Randolph, G.J., O'Neil, C.P., Lee, L.K., Swartz, M.A., Hubbell, J.A. Exploiting lymphatic transport and complement activation in nanoparticle vaccines. *Nat Biotechnol* (2007) 25: 1159-1164.
- [161] St John, A.L., Chan, C.Y., Staats, H.F., Leong, K.W., Abraham, S.N. Synthetic mast-cell granules as adjuvants to promote and polarize immunity in lymph nodes. *Nat Mater* (2012) 11: 250-257.
- [162] Manolova, V., Flace, A., Bauer, M., Schwarz, K., Saudan, P., Bachmann, M.F. Nanoparticles target distinct dendritic cell populations according to their size. *Eur J Immunol* (2008) 38: 1404-1413.
- [163] Fedorchak, M.V., Conner, I.P., Schuman, J.S., Cugini, A., Little, S.R. Long Term Glaucoma Drug Delivery Using a Topically Retained Gel/Microsphere Eye Drop. *Sci Rep* (2017) 7: 8639.
- [164] Comas, M., Toshkov, I., Kuropatwinski, K.K., Chernova, O.B., Polinsky, A., Blagosklonny, M.V., Gudkov, A.V., Antoch, M.P. New nanof ormulation of rapamycin Rapatar extends lifespan in homozygous p53(-/-) mice by delaying carcinogenesis. *Aging-US* (2012) 4: 715-722.

- [165] Wakefield, L.M., Winokur, T.S., Hollands, R.S., Christopherson, K., Levinson, A.D., Sporn, M.B. Recombinant Latent Transforming Growth Factor-Beta-1 Has a Longer Plasma Half-Life in Rats Than Active Transforming Growth Factor-Beta-1, and a Different Tissue Distribution. *J Clin Invest* (1990) 86: 1976-1984.
- [166] Koehl, G.E., Andrassy, J., Guba, M., Richter, S., Kroemer, A., Scherer, M.N., Steinbauer, M., Graeb, C., Schlitt, H.J., Jauch, K.W., Geissler, E.K. Rapamycin protects allografts from rejection while simultaneously attacking tumors in immunosuppressed mice. *Transplantation* (2004) 77: 1319-1326.
- [167] Grinberg-Bleyer, Y., Baeyens, A., You, S., Elhage, R., Fourcade, G., Gregoire, S., Cagnard, N., Carpentier, W., Tang, Q.Z., Bluestone, J., Chatenoud, L., Klatzmann, D., Salomon, B.L., Piaggio, E. IL-2 reverses established type 1 diabetes in NOD mice by a local effect on pancreatic regulatory T cells. *J Exp Med* (2010) 207: 1871-1878.
- [168] Niedbala, W., Cai, B.L., Liu, H.Y., Pitman, N., Chang, L., Liew, F.Y. Nitric oxide induces CD4+ CD25+ Foxp3- regulatory T cells from CD4+ CD25- T cells via p53, IL-2, and OX40. *Proc Nat Acad Sci USA* (2007) 104: 15478-15483.
- [169] Duan, W., So, T., Mehta, A.K., Choi, H., Croft, M. Inducible CD4+ LAP+ Foxp3- Regulatory T Cells Suppress Allergic Inflammation. *J Immunol* (2011) 187: 6499-6507.
- [170] White, L.J., Kirby, G.T., Cox, H.C., Qodratnama, R., Qutachi, O., Rose, F.R., Shakesheff, K.M. Accelerating protein release from microparticles for regenerative medicine applications. *Mater Sci Eng C Mater Biol Appl* (2013) 33: 2578-2583.
- [171] Turner, M.S., Kane, L.P., Morel, P.A. Dominant role of antigen dose in CD4+Foxp3+ regulatory T cell induction and expansion. *J Immunol* (2009) 183: 4895-4903.
- [172] Yang, J., Brook, M.O., Carvalho-Gaspar, M., Zhang, J., Ramon, H.E., Sayegh, M.H., Wood, K.J., Turka, L.A., Jones, N.D. Allograft rejection mediated by memory T cells is resistant to regulation. *Proc Nat Acad Sci USA* (2007) 104: 19954-19959.
- [173] Gittler, J.K., Krueger, J.G., Guttman-Yassky, E. Atopic dermatitis results in intrinsic barrier and immune abnormalities: implications for contact dermatitis. *J Allergy Clin Immunol* (2013) 131: 300-313.
- [174] Schmidt, M., Raghavan, B., Muller, V., Vogl, T., Fejer, G., Tchaptchet, S., Keck, S., Kalis, C., Nielsen, P.J., Galanos, C., Roth, J., Skerra, A., Martin, S.F., Freudenberg, M.A., Goebeler, M. Crucial role for human Toll-like receptor 4 in the development of contact allergy to nickel. *Nat Immunol* (2010) 11: 814-819.
- [175] Oblak, A., Pohar, J., Jerala, R. MD-2 determinants of nickel and cobalt-mediated activation of human TLR4. *PLoS One* (2015) 10: e0120583.
- [176] Trompette, A., Divanovic, S., Visintin, A., Blanchard, C., Hegde, R.S., Madan, R., Thorne, P.S., Wills-Karp, M., Gioannini, T.L., Weiss, J.P., Karp, C.L. Allergenicity

- resulting from functional mimicry of a Toll-like receptor complex protein. *Nature* (2009) 457: 585-588.
- [177] Weber, F.C., Esser, P.R., Muller, T., Ganesan, J., Pellegatti, P., Simon, M.M., Zeiser, R., Idzko, M., Jakob, T., Martin, S.F. Lack of the purinergic receptor P2X(7) results in resistance to contact hypersensitivity. *J Exp Med* (2010) 207: 2609-2619.
- [178] Martin, S.F., Dudda, J.C., Bachtanian, E., Lembo, A., Liller, S., Durr, C., Heimesaat, M.M., Bereswill, S., Fejer, G., Vassileva, R., Jakob, T., Freudenberg, N., Termeer, C.C., Johner, C., Galanos, C., Freudenberg, M.A. Toll-like receptor and IL-12 signaling control susceptibility to contact hypersensitivity. *J Exp Med* (2008) 205: 2151-2162.
- [179] Esser, P.R., Wolffe, U., Durr, C., von Loewenich, F.D., Schempp, C.M., Freudenberg, M.A., Jakob, T., Martin, S.F. Contact sensitizers induce skin inflammation via ROS production and hyaluronic acid degradation. *PLoS One* (2012) 7: e41340.
- [180] Agner, T., Johansen, J.D., Overgaard, L., Volund, A., Basketter, D., Menne, T. Combined effects of irritants and allergens. Synergistic effects of nickel and sodium lauryl sulfate in nickel-sensitized individuals. *Contact Dermatitis* (2002) 47: 21-26.
- [181] Bonefeld, C.M., Nielsen, M.M., Rubin, I.M., Vennegaard, M.T., Dabelsteen, S., Gimenez-Arnau, E., Lepoittevin, J.P., Geisler, C., Johansen, J.D. Enhanced sensitization and elicitation responses caused by mixtures of common fragrance allergens. *Contact Dermatitis* (2011) 65: 336-342.
- [182] Bonefeld, C.M., Nielsen, M.M., Vennegaard, M.T., Johansen, J.D., Geisler, C., Thyssen, J.P. Nickel acts as an adjuvant during cobalt sensitization. *Exp Dermatol* (2015) 24: 229-231.
- [183] Bonefeld, C.M., Geisler, C., Gimenez-Arnau, E., Lepoittevin, J.P., Uter, W., Johansen, J.D. Immunological, chemical and clinical aspects of exposure to mixtures of contact allergens. *Contact Dermatitis* (2017) 77: 133-142.
- [184] Kinbara, M., Sato, N., Kuroishi, T., Takano-Yamamoto, T., Sugawara, S., Endo, Y. Allergy-inducing nickel concentration is lowered by lipopolysaccharide at both the sensitization and elicitation steps in a murine model. *Br J Dermatol* (2011) 164: 356-362.
- [185] Sato, N., Kinbara, M., Kuroishi, T., Kimura, K., Iwakura, Y., Ohtsu, H., Sugawara, S., Endo, Y. Lipopolysaccharide promotes and augments metal allergies in mice, dependent on innate immunity and histidine decarboxylase. *Clin Exp Allergy* (2007) 37: 743-751.
- [186] van Hoogstraten, I.M., Boden, D., von Blomberg, M.E., Kraal, G., Scheper, R.J. Persistent immune tolerance to nickel and chromium by oral administration prior to cutaneous sensitization. *J Invest Dermatol* (1992) 99: 608-616.
- [187] Ikeda, Y., Yasuno, H., Sato, A., Kawai, K. Oral and epicutaneous desensitization in urushiol contact dermatitis in guinea pigs sensitized by 2 methods of different sensitizing potency. *Contact Dermatitis* (1998) 39: 286-292.

- [188] Desvignes, C., Etchart, N., Kehren, J., Akiba, I., Nicolas, J.F., Kaiserlian, D. Oral administration of hapten inhibits in vivo induction of specific cytotoxic CD8+ T cells mediating tissue inflammation: a role for regulatory CD4+ T cells. *J Immunol* (2000) 164: 2515-2522.
- [189] Ishii, N., Moriguchi, N., Nakajima, H., Tanaka, S., Amemiya, F. Nickel sulfate-specific suppressor T cells induced by nickel sulfate in drinking water. *J Dermatol Sci* (1993) 6: 159-164.
- [190] Wu, X., Roelofs-Haarhuis, K., Zhang, J., Nowak, M., Layland, L., Jermann, E., Gleichmann, E. Dose dependence of oral tolerance to nickel. *Int Immunol* (2007) 19: 965-975.
- [191] Van Hoogstraten, I.M., Boos, C., Boden, D., Von Blomberg, M.E., Scheper, R.J., Kraal, G. Oral induction of tolerance to nickel sensitization in mice. *J Invest Dermatol* (1993) 101: 26-31.
- [192] Faria, A.M., Weiner, H.L. Oral tolerance. *Immunol Rev* (2005) 206: 232-259.
- [193] Mayer, L., Shao, L. Therapeutic potential of oral tolerance. *Nat Rev Immunol* (2004) 4: 407-419.
- [194] van Loveren, H., Cockshott, A., Gebel, T., Gundert-Remy, U., de Jong, W.H., Matheson, J., McGarry, H., Musset, L., Selgrade, M.K., Vickers, C. Skin sensitization in chemical risk assessment: Report of a WHO/IPCS international workshop focusing on dose-response assessment. *Regul Toxicol Pharm* (2008) 50: 155-162.
- [195] Spiewak, R. Immunotherapy of allergic contact dermatitis. *Immunotherapy* (2011) 3: 979-996.
- [196] Kligman, A.M. Hyposensitization against Rhus dermatitis. *AMA Arch Derm* (1958) 78: 47-72.
- [197] Ye, Y.L., Chuang, Y.H., Chiang, B.L. Strategies of mucosal immunotherapy for allergic diseases. *Cell Mol Immunol* (2011) 8: 453-461.
- [198] Schwarz, A., Maeda, A., Kernebeck, K., van Steeg, H., Beissert, S., Schwarz, T. Prevention of UV radiation-induced immunosuppression by IL-12 is dependent on DNA repair. *J Exp Med* (2005) 201: 173-179.
- [199] Schwarz, T. 25 years of UV-induced immunosuppression mediated by T cells-from disregarded T suppressor cells to highly respected regulatory T cells. *Photochem Photobiol* (2008) 84: 10-18.
- [200] Peelen, E., Knippenberg, S., Muris, A.H., Thewissen, M., Smolders, J., Tervaert, J.W., Hupperts, R., Damoiseaux, J. Effects of vitamin D on the peripheral adaptive immune system: a review. *Autoimmun Rev* (2011) 10: 733-743.

- [201] Barragan, M., Good, M., Kolls, J.K. Regulation of Dendritic Cell Function by Vitamin D. *Nutrients* (2015) 7: 8127-8151.
- [202] Baeke, F., Takiishi, T., Korf, H., Gysemans, C., Mathieu, C. Vitamin D: modulator of the immune system. *Curr Opin Pharmacol* (2010) 10: 482-496.
- [203] Korkmaz, E., Friedrich, E.E., Ramadan, M.H., Erdos, G., Mathers, A.R., Burak Ozdoganlar, O., Washburn, N.R., Faló, L.D., Jr. Therapeutic intradermal delivery of tumor necrosis factor-alpha antibodies using tip-loaded dissolvable microneedle arrays. *Acta Biomater* (2015) 24: 96-105.
- [204] Sen, D., Forrest, L., Kepler, T.B., Parker, I., Cahalan, M.D. Selective and site-specific mobilization of dermal dendritic cells and Langerhans cells by Th1-and Th2-polarizing adjuvants. *Proc Nat Acad Sci USA* (2010) 107: 8334-8339.
- [205] Peters, M., Dudziak, K., Stiehm, M., Bufe, A. T-cell polarization depends on concentration of the danger signal used to activate dendritic cells. *Immunol Cell Biol* (2010) 88: 537-544.
- [206] Eisenbarth, S.C., Piggott, D.A., Huleatt, J.W., Visintin, I., Herrick, C.A., Bottomly, K. Lipopolysaccharide-enhanced, toll-like receptor 4-dependent T helper cell type 2 responses to inhaled antigen. *J Exp Med* (2002) 196: 1645-1651.
- [207] Dupasquier, M., Stoitzner, P., van Oudenaren, A., Romani, N., Leenen, P.J. Macrophages and dendritic cells constitute a major subpopulation of cells in the mouse dermis. *J Invest Dermatol* (2004) 123: 876-879.
- [208] Kang, K.F., Hammerberg, C., Meunier, L., Cooper, K.D. Cd11b(+) Macrophages That Infiltrate Human Epidermis after in-Vivo Ultraviolet Exposure Potently Produce Il-10 and Represent the Major Secretory Source of Epidermal Il-10 Protein. *J Immunol* (1994) 153: 5256-5264.
- [209] Klechevsky, E., Morita, R., Liu, M., Cao, Y., Coquery, S., Thompson-Snipes, L., Briere, F., Chaussabel, D., Zurawski, G., Palucka, A.K., Reiter, Y., Banchereau, J., Ueno, H. Functional specializations of human epidermal Langerhans cells and CD14+ dermal dendritic cells. *Immunity* (2008) 29: 497-510.
- [210] Buechler, C., Ritter, M., Orso, E., Langmann, T., Klucken, J., Schmitz, G. Regulation of scavenger receptor CD163 expression in human monocytes and macrophages by pro- and antiinflammatory stimuli. *J Leukoc Biol* (2000) 67: 97-103.
- [211] Ochoa, M.T., Loncaric, A., Krutzik, S.R., Becker, T.C., Modlin, R.L. "Dermal dendritic cells" comprise two distinct populations: CD1+ dendritic cells and CD209+ macrophages. *J Invest Dermatol* (2008) 128: 2225-2231.
- [212] Kim, Y.C., Park, J.H., Prausnitz, M.R. Microneedles for drug and vaccine delivery. *Adv Drug Deliv Rev* (2012) 64: 1547-1568.

- [213] Leone, M., Monkare, J., Bouwstra, J.A., Kersten, G. Dissolving Microneedle Patches for Dermal Vaccination. *Pharm Res* (2017).
- [214] Prausnitz, M.R. Engineering Microneedle Patches for Vaccination and Drug Delivery to Skin. *Annu Rev Chem Biomol Eng* (2017) 8: 177-200.
- [215] Zhao, X., Birchall, J.C., Coulman, S.A., Tatovic, D., Singh, R.K., Wen, L., Wong, F.S., Dayan, C.M., Hanna, S.J. Microneedle delivery of autoantigen for immunotherapy in type 1 diabetes. *J Control Release* (2016) 223: 178-187.
- [216] Yasuda, T., Ura, T., Taniguchi, M., Yoshida, H. Intradermal Delivery of Antigens Enhances Specific IgG and Diminishes IgE Production: Potential Use for Vaccination and Allergy Immunotherapy. *PLoS One* (2016) 11: e0167952.
- [217] Ohta, A., Sato, N., Yahata, T., Ohmi, Y., Santa, K., Sato, T., Tashiro, H., Habu, S., Nishimura, T. Manipulation of Th1/Th2 balance in vivo by adoptive transfer of antigen-specific Th1 or Th2 cells. *J Immunol Methods* (1997) 209: 85-92.
- [218] Lewkowicz, P., Lewkowicz, N., Sasiak, A., Tchorzewski, H. Lipopolysaccharide-activated CD4⁺CD25⁺ T regulatory cells inhibit neutrophil function and promote their apoptosis and death. *J Immunol* (2006) 177: 7155-7163.
- [219] Weber, F.C., Nemeth, T., Csepregi, J.Z., Dudeck, A., Roers, A., Ozsvari, B., Oswald, E., Puskas, L.G., Jakob, T., Mocsai, A., Martin, S.F. Neutrophils are required for both the sensitization and elicitation phase of contact hypersensitivity. *J Exp Med* (2015) 212: 15-22.
- [220] Sasseville, D. Occupational contact dermatitis. *Allergy Asthma Clin Immunol* (2008) 4: 59-65.
- [221] Stoll, S., Muller, G., Kurimoto, M., Saloga, J., Tanimoto, T., Yamauchi, H., Okamura, H., Knop, J., Enk, A.H. Production of IL-18 (IFN-gamma-inducing factor) messenger RNA and functional protein by murine keratinocytes. *J Immunol* (1997) 159: 298-302.
- [222] Kang, S., Yi, S., Griffiths, C.E.M., Fancher, L., Hamilton, T.A., Choi, J.H. Calcipotriene-induced improvement in psoriasis is associated with reduced interleukin-8 and increased interleukin-10 levels within lesions. *Br J Dermatol* (1998) 138: 77-83.
- [223] Penna, G., Adorini, L. 1 Alpha,25-dihydroxyvitamin D3 inhibits differentiation, maturation, activation, and survival of dendritic cells leading to impaired alloreactive T cell activation. *J Immunol* (2000) 164: 2405-2411.
- [224] Ray, N., Kuwahara, M., Takada, Y., Maruyama, K., Kawaguchi, T., Tsubone, H., Ishikawa, H., Matsuo, K. c-Fos suppresses systemic inflammatory response to endotoxin. *Int Immunol* (2006) 18: 671-677.

- [225] Kong, J., Grando, S.A., Li, Y.C. Regulation of IL-1 family cytokines IL-1 α , IL-1 receptor antagonist, and IL-18 by 1,25-dihydroxyvitamin D₃ in primary keratinocytes. *J Immunol* (2006) 176: 3780-3787.
- [226] Sadeghi, K., Wessner, B., Laggner, U., Ploder, M., Tamandl, D., Friedl, J., Zugel, U., Steinmeyer, A., Pollak, A., Roth, E., Boltz-Nitulescu, G., Spittler, A. Vitamin D₃ down-regulates monocyte TLR expression and triggers hyporesponsiveness to pathogen-associated molecular patterns. *Eur J Immunol* (2006) 36: 361-370.
- [227] Palmer, M.T., Lee, Y.K., Maynard, C.L., Oliver, J.R., Bikle, D.D., Jetten, A.M., Weaver, C.T. Lineage-specific Effects of 1,25-Dihydroxyvitamin D-3 on the Development of Effector CD4 T Cells. *J Biol Chem* (2011) 286: 997-1004.
- [228] Riek, A.E., Oh, J., Darwech, I., Moynihan, C.E., Bruchas, R.R., Bernal-Mizrachi, C. 25(OH) vitamin D suppresses macrophage adhesion and migration by downregulation of ER stress and scavenger receptor A1 in type 2 diabetes. *J Steroid Biochem* (2014) 144: 172-179.
- [229] Bakdash, G., Schneider, L.P., van Capel, T.M., Kapsenberg, M.L., Teunissen, M.B., de Jong, E.C. Intradermal application of vitamin D₃ increases migration of CD14⁺ dermal dendritic cells and promotes the development of Foxp3⁺ regulatory T cells. *Hum Vaccin Immunother* (2013) 9: 250-258.
- [230] Klechevsky, E., Morita, R., Liu, M.C., Cao, Y.Y., Coquery, S., Thompson-Snipes, L., Briere, F., Chaussabel, D., Zurawski, G., Palucka, A.K., Reiter, Y., Banchereau, J., Ueno, H. Functional specializations of human epidermal langerhans cells and CD14(+) dermal dendritic cells. *Immunity* (2008) 29: 497-510.
- [231] Morelli, A.E., Rubin, J.P., Erdos, G., Tkacheva, O.A., Mathers, A.R., Zahorchak, A.F., Thomson, A.W., Falo, L.D., Larregina, A.T. CD4(+) T cell responses elicited by different subsets of human skin migratory dendritic cells. *J Immunol* (2005) 175: 7905-7915.
- [232] Angel, C.E., Lala, A., Chen, C.J.J., Edgar, S.G., Ostrovsky, L.L., Dunbar, P.R. CD14(+) antigen-presenting cells in human dermis are less mature than their CD1a(+) counterparts. *Int Immunol* (2007) 19: 1271-1279.
- [233] Chu, C.C., Ali, N., Karagiannis, P., Di Meglio, P., Skowera, A., Napolitano, L., Barinaga, G., Grys, K., Sharif-Paghaleh, E., Karagiannis, S.N., Peakman, M., Lombardi, G., Nestle, F.O. Resident CD141 (BDCA3)(+) dendritic cells in human skin produce IL-10 and induce regulatory T cells that suppress skin inflammation. *J Exp Med* (2012) 209: 935-945.
- [234] Zhang, D.E., Hetherington, C.J., Gonzalez, D.A., Chen, H.M., Tenen, D.G. Regulation of CD14 expression during monocytic differentiation induced with 1 α ,25-dihydroxyvitamin D₃. *J Immunol* (1994) 153: 3276-3284.

- [235] Balmert, S.C., Donahue, C., Vu, J.R., Erdos, G., Falo, L.D., Jr., Little, S.R. In vivo induction of regulatory T cells promotes allergen tolerance and suppresses allergic contact dermatitis. *J Control Release* (2017) 261: 223-233.
- [236] Sharma, V., McNeill, J.H. To scale or not to scale: the principles of dose extrapolation. *Br J Pharmacol* (2009) 157: 907-921.
- [237] Lim, J.M., Bertrand, N., Valencia, P.M., Rhee, M., Langer, R., Jon, S., Farokhzad, O.C., Karnik, R. Parallel microfluidic synthesis of size-tunable polymeric nanoparticles using 3D flow focusing towards in vivo study. *Nanomed-Nanotechnol* (2014) 10: 401-409.
- [238] Xu, Q.B., Hashimoto, M., Dang, T.T., Hoare, T., Kohane, D.S., Whitesides, G.M., Langer, R., Anderson, D.G. Preparation of Monodisperse Biodegradable Polymer Microparticles Using a Microfluidic Flow-Focusing Device for Controlled Drug Delivery. *Small* (2009) 5: 1575-1581.
- [239] Duncanson, W.J., Lin, T., Abate, A.R., Seiffert, S., Shah, R.K., Weitz, D.A. Microfluidic synthesis of advanced microparticles for encapsulation and controlled release. *Lab Chip* (2012) 12: 2135-2145.
- [240] Dendukuri, D., Doyle, P.S. The Synthesis and Assembly of Polymeric Microparticles Using Microfluidics. *Adv Mater* (2009) 21: 4071-4086.
- [241] Rubtsov, Y.P., Niec, R.E., Josefowicz, S., Li, L., Darce, J., Mathis, D., Benoist, C., Rudensky, A.Y. Stability of the regulatory T cell lineage in vivo. *Science* (2010) 329: 1667-1671.
- [242] Miyao, T., Floess, S., Setoguchi, R., Luche, H., Fehling, H.J., Waldmann, H., Huehn, J., Hori, S. Plasticity of Foxp3(+) T cells reflects promiscuous Foxp3 expression in conventional T cells but not reprogramming of regulatory T cells. *Immunity* (2012) 36: 262-275.
- [243] Sawant, D.V., Vignali, D.A.A. Once a Treg, always a Treg? *Immunol Rev* (2014) 259: 173-191.
- [244] Komatsu, N., Mariotti-Ferrandiz, M.E., Wang, Y., Malissen, B., Waldmann, H., Hori, S. Heterogeneity of natural Foxp3+ T cells: a committed regulatory T-cell lineage and an uncommitted minor population retaining plasticity. *Proc Natl Acad Sci USA* (2009) 106: 1903-1908.
- [245] White, L.J., Kirby, G.T.S., Cox, H.C., Qodratnama, R., Qutachi, O., Rose, F.R.A.J., Shakesheff, K.M. Accelerating protein release from microparticles for regenerative medicine applications. *Materials Science & Engineering C-Materials for Biological Applications* (2013) 33: 2578-2583.
- [246] Kim, J.H., Hu, Y., Yongqing, T., Kim, J., Hughes, V.A., Le Nours, J., Marquez, E.A., Purcell, A.W., Wan, Q., Sugita, M., Rossjohn, J., Winau, F. CD1a on Langerhans cells controls inflammatory skin disease. *Nat Immunol* (2016) 17: 1159-1166.

- [247] Tang, Q., Henriksen, K.J., Bi, M., Finger, E.B., Szot, G., Ye, J., Masteller, E.L., McDevitt, H., Bonyhadi, M., Bluestone, J.A. In vitro-expanded antigen-specific regulatory T cells suppress autoimmune diabetes. *J Exp Med* (2004) 199: 1455-1465.
- [248] Wing, K., Sakaguchi, S. Regulatory T cells exert checks and balances on self tolerance and autoimmunity. *Nat Immunol* (2010) 11: 7-13.
- [249] Di Ianni, M., Falzetti, F., Carotti, A., Terenzi, A., Castellino, F., Bonifacio, E., Del Papa, B., Zei, T., Ostini, R.I., Cecchini, D., Aloisi, T., Perruccio, K., Ruggeri, L., Balucani, C., Pierini, A., Sportoletti, P., Aristei, C., Falini, B., Reisner, Y., Velardi, A., Aversa, F., Martelli, M.F. Tregs prevent GVHD and promote immune reconstitution in HLA-haploidentical transplantation. *Blood* (2011) 117: 3921-3928.
- [250] Taams, L.S., Palmer, D.B., Akbar, A.N., Robinson, D.S., Brown, Z., Hawrylowicz, C.M. Regulatory T cells in human disease and their potential for therapeutic manipulation. *Immunology* (2006) 118: 1-9.
- [251] Joffre, O., Santolaria, T., Calise, D., Al Saati, T., Hudrisier, D., Romagnoli, P., van Meerwijk, J.P.M. Prevention of acute and chronic allograft rejection with CD4(+)CD25(+)Foxp3(+) regulatory T lymphocytes. *Nat Med* (2008) 14: 88-92.